

# 博士論文

## **Dampening mechanism of fluid flow under shear in different physical phenomena - analytical and experimental approach**

(異なる物理現象における剪断下の流体の流れの減衰メカニズム-分析的および実験的アプローチ)

ガダム プルタヴィ ラジ (37-177179)

## ACKNOWLEDGEMENTS

Pursuing Ph. D has been really a life changing experience for me. During my journey, many people have been very much supportive and encouraging without which I would not have been able to achieve it.

Firstly, I would like to thank to my PhD advisor, Professor Toshiharu KISHI, for supporting me during these past three years. I am very honored to learn from his precious research experiences and vision during my studies at The University of Tokyo. I would like to thank sensei for encouraging my research and for allowing me to grow as a researcher. I will never be able to forget the support and confidence imbibed in me by sensei during my unprogressive days. Sensei provided me with the freedom to explore what I am interested in and encouraged me to spend allotted time very efficiently. Thanks to sensei's well-balanced freedom and attentiveness, due to which I was able to complete my PhD thesis. I am very much grateful to have KISHI sensei as my advisor.

I also must thank the members of my PhD committee, Professor Tetsuya Ishida, Assistant Professor Takahashi, and Associate professor Yuya Sakai for their helpful research advices and suggestions in general.

I am also very grateful to Kamada Sensei for his scientific advice and knowledge and many insightful discussions and suggestions. He is my primary resource for getting my questions answered and was instrumental in helping me in completing my thesis. I would like to convey my regards to him as he patiently helped throughout my research work during my experimental and theoretical work. I am very thankful to him for giving me dedicated time and strength even in conducting small simple experiments which I had to perform in the lab. I could not have imagined my research life without him. He was also very helpful in getting over the problems encountered in my daily life. I am indebted to him for making my research life better and happy. I must mention Kayondo San for his input during my research work.

I am thankful to my JICA-Friendship scholarship coordinators Kotaro sensei, Ando San, Chikako san for providing me an opportunity to study in The University Tokyo.

I am grateful to each person whom I have met in my journey of PhD, for making my life in Tokyo a memorable one. I do not know how to convey my regards to every person who have supported me and encouraged me in completing my PhD.

Finally, I especially thank my mom, dad, sister, and brother. My hard-working parents have sacrificed their lives for my sister and myself and provided unconditional love and care. I would not have made it this far without them. My sister has been my best friend and thank her for all her advice and support. She was very strong in hard times and been the motivator to be able to receive things in easier way.

Thank you, God, for letting me finish my degree with perfection.

## 論文の内容の要旨

### Thesis Summary

Dampening mechanism of fluid flow under shear in different physical phenomena - Analytical and experimental approach (異なる物理現象における剪断下の流体の流れの減衰メカニズム-分析的および実験的アプローチ)

### Gaddam Pruthvi Raj

Shear flow in a fluid can be induced by a pressure difference or the shear stress over a distance in a thin-walled structure. Fluids at rest do not resist any applied shear force and they deform continuously under the shear forces; however small they are. The applied shear stress is a function of the rate of shear strain in the case of fluids. The resistance to the shear force appears only when the fluid is under motion. This property of the fluid to resist the growth of shear deformation is called viscosity. Viscosity is caused due to the interchange of momentum between the layers of fluid moving with different velocities due to the random motions. Examples of shear flows occurring in the fluid are Couette flow (by applied shear force), flow in pipes (pressure-driven flow). Here, we are considering the shear flow of water in the microchannel to study the water flow rate reduction mechanism based on experimental work and understand the shear rate mechanism in Non-Newtonian flows based on analytical analysis of velocity profiles obtained in Couette flows.

Flows in microchannel devices differ from their macroscopic counterparts for two reasons: the small scale makes molecular effects such as wall slip more important, and it amplifies the magnitudes of certain ordinary continuum effects to extreme levels. Fluids that are Newtonian at ordinary rates of shear can become non-Newtonian at very high rates at the microscale level. Several experiments have shown general agreement with the macroscale theoretical predictions for the flow of a Newtonian fluid in at least certain parameter ranges in circular microtubes and rectangular microchannels. Good agreement between conventional Poiseuille theory and experimental results has been reported for other microscale flows including square microtubes with a diameter or hydraulic diameter of 15 to 150 microns and Reynolds numbers of 8–2300 [Judy et al., 2002]; and rectangular channels with hydraulic diameters from 244–974 microns [Liu and Garimella, 2004].

Water flow in narrow gaps is the most intriguing study in recent times, especially when there is a presence of two different phases, due to the observations of interesting mechanisms. For example, two-phase flow patterns of air and water flow in microchannels studied based on surface contamination and wettability between tube wall and fluids, show different flow patterns. If the wettability of the surface increases the apparent viscosity also increases and deviates more from theory and experimental. Moreover, the effect of the wettability decreases with an increase in hydraulic diameter. However, in some cases, a significant change in the flow behavior of

microchannels is not observed as the flows are unpredictable because of the variations in viscosity, size effect, surface roughness. Interface wettability has a different effect on the apparent viscosity and liquid flow in smooth microchannels.

The flow rate of the fluid in microchannels is least focused by researchers. Initial investigation on the effect of water flow rate due to slip was carried out by Chang-Hwan Choi et al. (2003). The water flow experiences drag resistance due to friction of the solid surfaces and no-slip boundary conditions. The drag force reduces the water flow rate because of the adhesion between the surface and the water in hydrophilic surfaces. However, some micro and nano air bubbles help in reducing the friction on the hydrophobic wall surfaces mentioned by Hajime Tanaka et al. (2020). This kind of phenomenon is most utilized in ship propulsion, in which microbubbles are formed due to cavitation near the propeller and helps in moving forward. In this case, the micro air bubbles are continuously formed and destroyed due to the water flow near the propeller surface. The air bubbles in the propulsion have very little lifetime but help in propulsion. In the current research, air bubbles are held at the crevices (bubble forming locations) to know its effect on the water flow rate over time in microchannels. The air-water interface is responsible for the water braking effect is confirmed based on the findings of Kayondo et al. (2017). The water flow rate is reduced due to the interface effect. If the supersaturated water is used the air bubbles grow larger and block the entire microchannel resulting in the water blocking effect.

The effect of large air bubbles blocking the entire path, by reducing the flow area, of the microchannel can be easily and clearly understood. The water braking effect is novel and difficult to interpret. The presence of small micro air bubbles in the path of the water flow takes time to show its effect on the water flow rate. By conducting continuous observations and water flow measurements, the water flow reduction is observed continuously. The formation of small size micro and nano air bubbles on crevices are responsible for the water flow reduction. This is experimentally observed by a microscope and analytically understood. The braking effect of the air-water interface, formed by the small micro air bubbles, is responsible for the water flow reduction. Thus, the Newtonian fluid like water behaves differently in micro scales in the presence of the air-water interface. Water flow tests are also conducted to know the condition for water flow reduction by using a different type of water, varying the type of surface, changing the number of crevices present to know their dependency on the water flow rate. Bubble formation was observed on both hydrophobic and hydrophilic surfaces, but the water flow reduction was observed in the case of the hydrophilic surface when equilibrated water is used. This water flow reduction was observed even when there were no visible air bubbles. The probable formation of air bubbles on the surface of the microchannel leads to a reduction in the water flow rate. The flow behavior of water near the interface is indifferent and is responsible for the water flow reduction.

The flow behavior of ‘complex fluids’ which includes all types of materials like pastes, emulsions, colloids, suspensions, and anatomy like plasma, blood, etc. is of practical and fundamental interest. The flow field of these fluids is responsible for the structural, rheological behavior of the material and in deciding the type, usage of material. A flow curve is determined by applying a shear rate to the materials by different viscometric flows like Couette flow, parallel disks flow, cone-plate flow. A flow curve (shear stress vs shear strain graph) generally represents

the rheological behavior of the fluid. The main properties of shear flow of fluids include viscosity, shear rate, and shear stress, which help determine the flow behavior.

In rheology, apart from knowing the shear stress and viscosity to understand the flow behavior, velocity profile also plays a prominent role in deriving the constitutive laws. Many researchers have focused on the velocity profiles of the material in Couette flow due to the observation of viscosity bifurcation near the critical stress. The velocity profiles are obtained by using techniques MRI, NMR studies by considering the Couette flow. Most of the materials like emulsions, foams, cornstarch, and cement paste exhibit different behavior at low and high shear rates in Couette flow as suggested in the literature. At low shear rates, the materials get localized near the rotor but for high shear rates, we can observe sheared and un-sheared zones visualizing the two different regions in the velocity profile observed by Cussot et al. (2002). The profile closer to the moving cylinder has a constant slope and far away the profile has zero slopes. The Power-law model can be fitted easily for low shear rate velocity profiles and are validated with the shear flow curves.

Based on the obtained velocity profiles, individual material behavior like the colloidal formation, jamming of fluids locally and others were discussed. Many different shear flow equations were used to define the shear flow as well as velocity behavior. These equations could not exactly define the velocity behavior and regularity of flow of the material in Couette flow. In this study, various velocity profiles of different materials and different RPM values are considered to understand the shear rate mechanism and the flow regularity of the fluid in Couette flow. Partially sheared Couette flows are only considered to avoid the boundary effects, to consider the actual fluid behavior of the material. The velocity profiles of these flows are considered and analytically analyzed using theoretical cubic and quadratic equations to find the regularity of the fluids in Couette flows.

The analysis of the velocity profiles is started by separating the Newtonian and Non-Newtonian regions. Initially, the Newtonian velocity equation is applied to a limited portion of velocity profiles always starting from the rotor end and the corresponding residual is calculated. The region has the least residual variance is considered as the Newtonian region. In some profiles, the Newtonian region is not identified. So, the whole sheared region is considered a Non-Newtonian profile region. These Non-Newtonian profiles are either fitted by the quadratic equation or the cubic equation based on their behavior. Almost 50 velocity profiles have been analyzed and they can be either fitted with the quadratic or cubic equation. This piecewise analysis of the velocity profile shows either a linear or non-linear rate of reduction in the shear rate. The type of material behavior is distinguished based on the shift of the velocity profiles, the material parameter  $\alpha$ , and the extent of the Newtonian region present.

Energy loss due to viscous friction between the fluid layers in the pressure-driven flows (Flow in microchannels) and shear driven flows (Couette flows) is understood to know the respective flow behaviors mechanisms. This energy loss is assumed to arise due to the linear and rotational motion of the particles within the fluid. Based on the assumptions in understanding the Energy loss mechanism, higher energy loss indicates stability and less slip of the particles, and the rotation of the particles is less too. For hydrophilic surfaces, the calculated energy loss is higher

than the hydrophobic surfaces, indicating that the slip of the particles is more on hydrophobic surfaces. The less slip behavior and the increase in drag force on hydrophilic surfaces over time results in the reduction of water flow rate. In the case of rheology, higher energy loss is always observed at the far-away end only indicating more stability far away from the rotor end. The shear rate is decreased continuously due to an increase in energy losses along with the Couette flow.

The shear flow behavior mechanism of the Newtonian and Non-Newtonian fluids is different in the different physical phenomenon and depends on various factors. But the basic behavior of the fluids is understood based on the energy loss mechanism due to friction between the particle layers. The flow rate of water in the narrow channels is modified due to the decrease of the air-water interface in the path of the flow. In the Couette flow, fluids exhibit a continuous decrease in the shear rate along the radius. The mechanism of the water flow reduction due to the interface and the shear rate reduction mechanism along the radius in Couette flow is understood by the energy loss mechanism due to friction. Thus, two different phenomena are understood based on the new hypothesis of fluid-particle behavior considering the rotation and cohesive forces of particles.

## List of Figures

Fig. 1.1:(a) Water flow tests in concrete crack surfaces (b) Results of water flow tests [20] .....	5
Fig. 1.2: Velocity profile of the mustard seeds considering slip and rotation behavior [30].....	6
Fig. 2.1: Slip velocities and water flow rates for different types of surfaces. (a) Shear rate vs Slip velocity (b) Pressure drop vs Flow rate. [6].....	12
Fig. 2.2: (a) Slip lengths for different initial densities at the wall surface at the same applied shear rate. (b) Slip lengths for hydrophobicity and shear rate at different times.[9].....	12
Fig. 2.3: (a) Experimental conditions used for sliding of air bubble (b) Plot of adhesive force and volume of the bubble. [10].....	13
Fig. 2.4: Bubble behavior due to shear flow on (a) Hydrophilic surface (b) Hydrophobic surface [15].....	14
Fig. 2.5: Effect of shear flow on (a) Bubble volume (b) nucleation rate [16] .....	15
Fig. 2.6: Dependence of bubble nucleation temperature with (a) Contact angle (b) Bubble radius [18].....	16
Fig. 2.7: Behavior of bubble on (a) Hydrophilic surface (b) Hydrophobic surface.....	16
Fig. 2.8: Couette flow (a) Top view of the inner and outer rotor (b) Side view of Couette flow along with the assumed velocity, actual velocity profiles. ....	17
Fig. 2.9: Energy loss along the channel width for concentric rotating cylinders (inner cylinder is rotating while the outer cylinder is at rest) [20].....	19
Fig. 3.1: (a) Wide Microchannel showing the dimensions of crevice (b) Narrow Microchannel エラー! ブックマークが定義されていません。	
Fig. 3.2: (a) Micro Instrument (MC-1) (b) Spindle needle with jet flowエラー! ブックマークが定義されていません。	
Fig. 3.3: Narrow Microchannels with a change in the number of crevices (a) No crevice (b) 27 Crevices (c) 54 crevices .....エラー! ブックマークが定義されていません。	27
Fig. 3.4: (a) Microchannel with water head (b) Experimental set up for the water flow tests.エラー! ブックマークが定義されていません。	
Fig. 3.5: Showing the Newtonian (closer to the rotor) and.....	34
Fig. 3.6: (a) Consideration of velocity curve for Newtonian analysis, (b) Showing the decreasing and increasing Residual variance pattern.....	35
Fig. 3.7:(a) Showing the decreasing residual variance, (b) Showing the increasing residual variance pattern .....	36
Fig. 3.8:Fitting of velocity profile by (a) quadratic equation (b) Cubic Equation.....	37
Fig. 4.1: Water flow tests of the hydrophilic channel with fewer crevices (27).....	41
Fig. 4.2: Water flow tests of hydrophilic channel with more crevices (54).....	42
Fig. 4.3: Water flow tests comparison of hydrophilic channels with different numbered crevices. ....	42
Fig. 4.4: Comparison of water flow tests with different saturated levels .....	43
Fig. 4.5: Water flow tests on the hydrophobic channel with the presence of crevices (54) .....	43

Fig. 4.6: Observation of luminescence in the hydrophobic microchannels at crevices .....	44
Fig. 4.7: Water flow tests of wide hydrophilic microchannels .....	46
Fig. 4.8: Sequence of images for hydrophilic wide microchannel .....	47
Fig. 4.9: Water flow tests of wide hydrophobic microchannels .....	47
Fig. 4.10: Sequence of images for hydrophobic wide microchannel.....	48
Fig. 4.11: Cornstarch1 10RPM (a) Residual Variance (b)Analytical fit of the Non-Newtonian region of velocity profile. ....	49
Fig. 4.12: Cornstarch1 20RPM (a) Residual Variance (b)Analytical fit of the Non-Newtonian region of velocity profile. ....	50
Fig. 4.13: Cornstarch1 40RPM (a) Residual Variance (b)Analytical fit of the Non-Newtonian region of velocity profile. ....	50
Fig. 4.14: Velocity Profiles of Cornstarch1 (a) From the rotor end (b) From the flow stop end .	51
Fig. 4.15: Oil Emulsion 1RPM (a) Residual variance (b) Analytical fit of Non-Newtonian Region .....	51
Fig. 4.16: Oil Emulsion 5RPM (a) Residual variance (b) Analytical fit of Non-Newtonian Region .....	52
Fig. 4.17: Oil Emulsion 0.3RPM (a) Residual variance (b) Analytical fit of Non-Newtonian Region .....	52
Fig. 4.18: Velocity Profiles of Silicon Oil Emulsion (a) From the rotor end .....	53
Fig. 4.19: Cacl2 10RPM (a) Residual variance (b) Analytical fit of Non-Newtonian Region.....	54
Fig. 4.20: Cacl2 20RPM (a) Residual variance (b) Analytical fit of Non-Newtonian Region.....	54
Fig. 4.21: Alpha value variation of Cacl2.....	54
Fig. 4.22: Cacl2 50RPM (a) Residual variance (b) Analytical fit of Non-Newtonian Region.....	55
Fig. 4.23: Velocity Profiles of Cacl2 (a) From the rotor end (b) From the flow stop end.....	55
Fig. 4.24: PMMA 48RPM (a) Residual Variance (b)Analytical fit of the Non-Newtonian region of velocity profile.....	56
Fig. 4.25: Velocity Profiles of PMMA (a) From the rotor end (b) From the flow stop end.....	56
Fig. 4.26: Drilling Mud 10RPM (a) Residual variance (b) Analytical fit of Non-Newtonian Region .....	57
Fig. 4.27: Drilling Mud 20RPM (a) Residual variance (b) Analytical fit of Non-Newtonian Region .....	57
Fig. 4.28: Drilling Mud 40RPM (a) Residual variance (b) Analytical fit of Non-Newtonian Region .....	58
Fig. 4.29: Drilling Mud 60RPM (a) Residual variance (b) Analytical fit of Non-Newtonian Region .....	58
Fig. 4.30: Velocity Profiles of Drilling mud (a) From the rotor end (b) From the flow stop end	59
Fig. 4.31: Alpha value variation of Drilling mud .....	59
Fig. 4.32: Surfactant 40RPM (a) Residual variance (b) Analytical fit of Non-Newtonian Region .....	60
Fig. 4.33: Surfactant 50RPM (a) Residual variance (b) Analytical fit of Non-Newtonian Region .....	60
Fig. 4.34: Surfactant100RPM (a) Residual variance (b) Analytical fit of Non-Newtonian Region .....	61



Fig. 4.35: Velocity Profiles of Surfactant (a) From the rotor end (b) From the flow stop end.....	61
Fig. 4.36: Alpha value variation of Surfactant.....	62
Fig. 4.37: Shaving Foam 20RPM (a) Residual Variance (b)Analytical fit of the Non-Newtonian region of velocity profile. ....	62
Fig. 4.38: Shaving Foam 40RPM (a) Residual Variance (b)Analytical fit of the Non-Newtonian region of velocity profile. ....	63
Fig. 4.39: Shaving Foam 60RPM (a) Residual Variance (b)Analytical fit of the Non-Newtonian region of velocity profile. ....	63
Fig. 4.40: Shaving Foam 80RPM (a) Residual Variance (b)Analytical fit of the Non-Newtonian region of velocity profile. ....	64
Fig. 4.41: Velocity Profiles of Shaving Foam (a) From the rotor end.....	64
Fig. 4.42: Mayonnaise 5RPM (a) Residual variance (b) Analytical fit of Non-Newtonian Region .....	65
Fig. 4.43: Mayonnaise20RPM (a) Residual variance (b) Analytical fit of Non-Newtonian Region .....	65
Fig. 4.44: Mayonnaise 80RPM (a) Residual variance (b) Analytical fit of Non-Newtonian Region .....	66
Fig. 4.45: Velocity Profiles (a) From the rotor end (b) From the flow stop end .....	66
Fig. 4.46: Alpha value variation of Mayonnaise.....	66
Fig. 4.47: Bentonite 10RPM (a) Residual variance (b) Analytical fit of Non-Newtonian Region .....	67
Fig. 4.48: Bentonite 20RPM (a) Residual variance (b) Analytical fit of Non-Newtonian Region .....	67
Fig. 4.49: Bentonite 30RPM (a) Residual variance (b) Analytical fit of Non-Newtonian Region	68
Fig. 4.50: Bentonite 40RPM (a) Residual variance (b) Analytical fit of Non-Newtonian Region	68
Fig. 4.51: Bentonite 60RPM (a) Residual variance (b) Analytical fit of Non-Newtonian Region	69
Fig. 4.52: Velocity Profiles Bentonite (a) From the rotor end (b) From the flow stop end.....	69
Fig. 4.53: Alpha value variation of Bentonite.....	69
Fig. 4.54: Cornstarch2 0.6RPM (a) Residual variance (b) Analytical fit of Non-Newtonian Region .....	70
Fig. 4.55: Cornstarch2 0.8RPM (a) Residual variance (b) Analytical fit of Non-Newtonian Region .....	70
Fig. 4.56: Cornstarch2 2RPM (a) Residual variance (b) Analytical fit of Non-Newtonian Region .....	71
Fig. 4.57: Cornstarch2 4RPM (a) Residual Variance (b) Division of Newtonian and Non-Newtonian region.....	71
Fig. 4.58: Velocity Profiles Cornstarch2(a) From the rotor end (b) From the flow stop end.....	72
Fig. 4.59: Alpha value variation Cornstarch2.....	72
Fig. 4.60: Cement Paste (CCR2008) 30.9RPM (a) Residual variance (b) Analytical fit of Non-Newtonian Region .....	73
Fig. 4.61: Cement Paste (CCR2008) 41.2RPM (a) Residual variance (b) Analytical fit of Non-Newtonian Region .....	73

Fig. 4.62: Cement Paste (CCR2008) 51.5RPM (a) Residual variance (b) Analytical fit of Non-Newtonian Region .....	74
Fig. 4.63: Cement Paste (CCR2008) 61.8RPM (a) Residual variance (b) Analytical fit of Non-Newtonian Region .....	74
Fig. 4.64: Cement Paste (CCR2008) 72.1RPM (a) Residual variance (b) Analytical fit of Non-Newtonian Region .....	75
Fig. 4.65: Cement Paste (CCR2008) 82.4RPM (a) Residual variance (b) Analytical fit of Non-Newtonian Region .....	75
Fig. 4.66: Velocity Profiles Cement paste (CCR2008) (a) From the rotor end.....	76
Fig. 4.67: Alpha value variation Cement paste (CCR 2008).....	76
Fig. 4.68: Cement Paste (CCR2005) 41.2RPM (a) Residual variance (b) Analytical fit of Non-Newtonian Region .....	76
Fig. 4.69: Cement Paste (CCR2005) 51.5RPM (a) Residual variance (b) Analytical fit of Non-Newtonian Region .....	77
Fig. 4.70: Cement Paste (CCR2005) 72.1RPM (a) Residual variance (b) Analytical fit of Non-Newtonian Region .....	77
Fig. 4.71: Cement Paste (CCR2005) 82.4RPM (a) Residual variance (b) Analytical fit of Non-Newtonian Region .....	78
Fig. 4.72: Velocity Profiles Cement Paste (2005) (a) From the rotor end (b) From the flow stop end.....	78
Fig. 4.73: Alpha Value variation Cement Paste (CCR 2005).....	79
Fig. 5.1 : Velocity profile of the mustard seeds considering slip and rotation behavior [13].....	83
Fig. 5.2: Presence of both Newtonian and Non-Newtonian materials within the same material of laminar flow over a wide range of shear stress. [23] .....	84
Fig. 5.3: Forces developed within the fluid particles when (a) there is a presence of applied shear rate (b) applied shear rate is 0. ....	85
Fig. 5.4: Actual consideration of forces between the particles when the shear rate is applied....	86
Fig. 5.5: Couette flow showing the presence of different regions and importance of cohesive force .....	87
Fig. 5.6: Behavior of Non-Newtonian fluids at (a) High shear rate (b) Low shear rate .....	89
Fig. 5.7: Behavior of Newtonian fluids at (a) High/Low shear rate (b) Very Low shear rate.....	89
Fig. 6.1: Showing the interaction of particles at (a) Hydrophilic Surface (b) Hydrophobic Surface .....	96
Fig. 6.2: Showing the presence of isotropic and non-isotropic nature in (a) Hydrophilic Surface (b) Hydrophobic Surface. ....	97
Fig. 6.3: Comparison of the shift in velocity profile and alpha value variation (a) PMMA upward shift of velocity profiles (b) PMMA increase of alpha value variation (c) Shaving Foam downward shift of velocity profile (d) Shaving Foam decrease of alpha value variation .....	100

## List of Tables

Table 3.1: Micro Instrument (MC-1) Model Description.....	26
Table 3.2: Data acquired for the analytical analysis.....	32
Table 4.1: Summary of water flow tests in microchannels.....	45
Table 4.2: % of volume decrease in the bubble on hydrophilic surface.....	46
Table 4.3: % of volume increase in the bubble on hydrophobic surface.....	48
Table 5.1: Forces present between the fluid particles based on the applied shear rate for different fluids.....	エラー! ブックマークが定義されていません。
Table 6.1: Summary of the analysis of velocity profiles.....	エラー! ブックマークが定義されていません。

## Table of Contents

Abstract.....	i
List of Figures.....	v
List of Tables.....	ix
<b>CHAPTER 1. INTRODUCTION.....</b>	<b>1</b>
1.1 GENERAL OVERVIEW .....	2
1.2 BACKGROUND.....	3
1.3 OBJECTIVE OF RESEARCH .....	6
1.4 CONTRIBUTIONS OF RESEARCH.....	7
1.5 OUTLINE OF THE THESIS.....	7
1.6 REFERENCES .....	7
<b>CHAPTER 2. LITERATURE REVIEW .....</b>	<b>10</b>
2.1 FLOW IN MICROCHANNELS .....	11
2.2 RHEOLOGY.....	17
2.3 CHAPTER SUMMARY .....	20
2.4 REFERENCES .....	20
<b>CHAPTER 3. METHODOLOGY FOR EXPERIMENTATION AND ANALYTICAL ANALYSIS    23</b>	
3.1 METHODOLOGY FOR WATER FLOW TESTS.....エラー!ブックマークが定義されていません。	
3.1.1 Preparation of Microchannel: .....	エラー!ブックマークが定義されていません。
3.1.2 MC-1 Machine Description (PMT Machine):	エラー!ブックマークが定義されていません。
3.1.3 Sandwiching procedure for Microchannels	エラー!ブックマークが定義されていません。
3.1.4 Types of Microchannels:.....	エラー!ブックマークが定義されていません。
3.1.5 Wide Microchannel (WMC).....	エラー!ブックマークが定義されていません。
3.1.6 Narrow Microchannel (NMC) .....	エラー!ブックマークが定義されていません。
3.1.7 Preparation of Experimental Set-up.	エラー!ブックマークが定義されていません。
3.1.8 Procedure for Water Flow Tests .....	エラー!ブックマークが定義されていません。
3.1.9 Imaging of the water flow tests:.....	エラー!ブックマークが定義されていません。

3.2	METHODOLOGY FOR ANALYSIS OF VELOCITY PROFILES .. エラー! ブックマークが定義 されていません。	
3.2.1	Data Collection .....	エラー! ブックマークが定義されていません。
3.2.2	Assumptions in Analysis .....	33
3.2.3	Identification of Newtonian and Non-Newtonian Regions .....	33
3.2.4	Procedure to Fit the Non-Newtonian regions .....	36
3.2.5	Procedure for Categorization of Materials.....	37
3.3	CHAPTER SUMMARY .....	38
<b>CHAPTER 4.</b>	<b>EXPERIMENTAL AND ANALYTICAL RESULTS .....</b>	<b>40</b>
4.1	RESULTS OF WATER FLOW TESTS.....	41
4.1.1	Narrow Microchannels.....	41
4.1.2	Wide Microchannels .....	46
4.2	RESULTS OF VELOCITY PROFILE ANALYSIS .....	49
<b>CHAPTER 5.</b>	<b>NEW THEORY FOR UNDERSTANDING THE FLUID FLOW BEHAVIOR 80</b>	
5.1	PURPOSE OF NEW HYPOTHESIS.....	81
5.2	FLUID SIMULATIONS USING PARTICLES.....	81
5.3	BACKGROUND OF HYPOTHESIS .....	82
5.3.1	Umeya Rheology .....	83
5.4	GENERAL THEORY OF FLUID PARTICLES .....	85
5.4.1	Importance of cohesion.....	86
5.5	NEWTONIAN AND NON-NEWTONIAN BEHAVIOR.....	88
5.6	CHAPTER SUMMARY .....	90
5.7	REFERENCES .....	90
<b>CHAPTER 6.</b>	<b>ANALYSIS AND DISCUSSION .....</b>	<b>94</b>
6.1	ANALYSIS OF WATER FLOW TESTS.....	95
6.1.1	Discussion of Hydrophobic and Hydrophilic Surface Behavior.....	98
6.2	ANALYSIS OF ANALYTICAL RESULTS.....	99
6.2.1	Discussion of Macroscopic Material Behavior.....	102
6.3	KEY FINDINGS OF NEW HYPOTHESIS.....	103
6.3.1	Improvements and Highlights of the Hypothesis.....	103
6.3.2	Major Contributions of the Hypothesis.....	103
6.4	CHAPTER SUMMARY .....	103
6.5	REFERENCES .....	104
<b>CHAPTER 7.</b>	<b>CONCLUSIONS AND FUTURE RECOMMENDATIONS .....</b>	<b>105</b>
7.1	CONCLUSIONS OF WATER FLOW TESTS .....	106
7.2	CONCLUSIONS OF ANALYTICAL ANALYSIS OF VELOCITY PROFILES .....	106
7.3	FUTURE RECOMMENDATIONS .....	107



# **Chapter 1. INTRODUCTION**

## 1.1 General Overview

Fluid flows are classified into different types based on the change of their respective properties like velocity, density, and viscosity with respect to time and space. Some of the fluid flows include Compressible and Incompressible flows, Steady and Unsteady flows, Uniform and Non-uniform flows, Laminar and Turbulent Flows. Most of the liquids exhibit compressible behavior to an extent, the density changes as the temperature and pressure are applied. The assumption of incompressible behavior depends on fluid properties and flow conditions. If there is no change in the fluid properties of the flow at a position that does not change with time, then it is considered as steady flow. All turbulent flows are unsteady. In laminar flow, the fluid particles move in a well-defined path called streamlines and all of them are straight lines and parallel to each other.

Some fluid flows are based on the applied shear or the type of phases present. Couette flow, open-channel flows, pipe flows, and Two-phase flows are some of them. Couette flow is characterized by the shear applied by the rotor on the fluid, but in a pipe, flows are characterized by pressure and tension due to which fluid flows. In two-phase flows, air-liquid, liquid-liquid flows, density, and pressure determine the flow behavior along with the pressure difference. The fluid flows are well described by the Navier-stokes equation irrespective of the type of flow. The basic assumptions of this equation include the conservation of mass, momentum, and energy. The fluid is considered as a continuous media instead of fluid particles.

In all the above-mentioned flows, fluids tend to resist shear in motion. This resistance of the fluid to the applied shear or motion is considered as viscosity. Extensive research has been done to understand the flow behavior and characteristics of all these flows. Several investigations are conducted to understand the flows, to compare the heat transfer characteristics in microchannels. The conventional theory offers reliable predictions for the flow characteristics in microchannels up to a Reynolds number of approximately 2000 based on flow visualizations and analysis. However, the scale of the microchannel size may have a significant impact on the onset of turbulence [1]. The investigations were conducted on smooth as well as rough microchannels [2]. The presence of roughness elements, in rectangular microchannels of a hydraulic diameter of  $153\mu\text{m}$  to  $191\mu\text{m}$ , leads to the early transition in microchannels.

Two-phase flows in microchannels attracted many researchers because of its wide range of applications in chemical processing, medical, bioengineering, oil and gas industries, etc. Initial investigations on two-phase flow are conducted by Hewitt et.al (1982) [3]. The different flow patterns based on the flow of the fluid and liquid have also been identified. The two-phase flow can be classified according to the geometry of interfaces into three main categories namely separated flow, translational or mixed flow, and dispersed flow [4]. Depending on the type of interface separated flows can be divided as film and stratified flow, annular flow, and jet-flow regimes. These kinds of different flow patterns are even observed in the small microchannels as investigated by [5] ranging from  $20\mu\text{m}$  to  $100\mu\text{m}$ . The presence of dissolved gas content in the liquid also causes two-phase flow. Cavitation is one phenomenon, where bubbles are easily formed based on the dissolved gases and the surface properties. The effect of shear flow rate on the bubble nucleation, diffusion, and its transportation is studied by most of the researchers' [6]–[10]. There is much research conducted to understand the slip flow of the fluids in microchannels based on the



bubbles formations on the smooth solid surfaces [11], [12]. The effect of the stabilized air bubble on the shear flow is one unique aspect that has not been probed by researchers. So, in this research phenomenon, water flow rate reduction due to the stabilized air bubbles is understood.

Fluid types are identified based on the direct application of shear to the fluids. Cone-plate flow, Couette flow, parallel-disks flow helps in determining flow curve (shear stress vs shear rate) as well as the properties, types of fluid. Much research has been conducted on various materials like cement paste, surfactants, suspensions, colloidal solutions to understand the local rheological material behavior, and to understand the flow behavior of these materials. Apart from knowing the flow behavior based on the flow curve, the velocity profile of the material plays a prominent role in determining the constitutive laws. A flow curve (shear stress vs shear strain graph) generally represents the rheological behavior of the fluid. The presence of plateau or decrease in the shear stress in flow curve at low shear rates in materials like pastes, suggests that flow instabilities might occur and cause deviations from the ideal behavior. The stress value at which the plateau stress is achieved is considered as critical stress. Viscosity bifurcation is also observed around critical stress: for smaller stresses, the viscosity increases in time, and the material eventually stops flowing, whereas for slightly larger stresses the viscosity decreases continuously with time and the flow accelerates. The presence of plateau is associated with the phase transition. The phase transition starts at the first critical value and gradually occupies the whole gap in Couette flow. These kinds of observations led many researchers to focus on the velocity profiles of different materials in Couette flow[13], [14], [15].

Velocity profiles are measured by using Magnetic Resonance Imaging (MRI), Nuclear magnetic resonance (NMR), using viscometer, etc. In rheology, apart from knowing the shear stress and viscosity to understand the flow behavior, velocity profile also plays a prominent role in deriving the constitutive laws as suggested by S.Jarny et al. (2005) [14], G.Ovarlez et al. (2008) [16]. Most of the materials like emulsions, foams, cornstarch, and cement paste exhibit different behavior at low and high shear rates in Couette flow as suggested in the literature. At low shear rates, the materials get localized near the rotor but for high shear rates, we can observe sheared and un-sheared zones visualizing the two different regions in the velocity profile observed by Cussot et al. (2002) [17]. The profile closer to the moving cylinder has a constant slope and far away the profile has zero slopes. The Power-law model can be fitted easily for low shear rate velocity profiles and are validated with the shear flow curves. The velocity profiles in these flows are assumed to be Newtonian but the actual velocity profiles are non-linear. Currently, we tried to fit the velocity profiles for both the high and low shear rates assuming them to have linear and non-linear profiles (excluding zero slope region) to understand the regularity of flow for partially sheared Couette flows. Data from MRI is collected from the literature available and are analyzed for the presence of Newtonian and Non-Newtonian regions.

## **1.2 Background**

Over the past years, there have been several attempts to come up with well-engineered materials to face the current challenges in infrastructure. The deterioration of concrete structures has been the main concern especially the slow deterioration that occurs due to the water ingress causing the

internal damage to the concrete [18]. This makes the concrete deteriorated and reduces the lifetime of the concrete structure. The main inlet for the water ingress is the hairline concrete cracks. Self-healing of concrete is necessary to avoid the water ingress and the entry of other harmful products thereby maintaining the structural lifetime. Self-healing enhances the structure to regain its earlier structural soundness and capacity [19].

In the process of self-healing, many interesting approaches have been proposed so far and one of them is the water permeation into the concrete crack surface. Recent findings [20] show that the formation of air bubbles block the water flow in these crack channels. The following Fig. 1.1, illustrates the typical results of water flow through a straight crack, water flow reduction occurs without any visible healing products, but instead, visible air cavities are present. Moreover, Kayondo et al. (2017) [21] conducted experiments on microchannels by using a wooden surface with the presence of crevices, observed water flow reduction due to no visible air bubbles with the naked eye. It was understood that the bubbles formed at the crevices are cause the braking behavior of the bubbles leading to the water flow reduction. So, motivated by this study and understanding the well-known equations of flow such as Darcy and Weisbach equation, Hagen Poiseuille equations for normal microchannels, their contribution for porous surfaces is studied. However, these equations do not represent the actual flow behavior occurring in the narrow microchannels with the presence of air bubbles. In wastewater treatment plants, the formation of bubbles in the filter beds has a significant effect on the pressure loss, flow rate as mentioned by Scardina et al. (2004) [22]. The effect of the air bubble and its growth on the effect of the water flow rate has been researched in this part of research by varying different parameters.

The air-water interface consists of water molecules, the behavior and the tendencies of these surfaces are largely understood by the thermodynamic perspective of surface tension [23]–[27] in which the molecular behavior of the molecules and its stability is not clear. In this research, the molecules on this surface are hypothesized to behave as a solidified and anchored at the crevice portions in hydrophilic surfaces. This anchorage of the solidified water molecules is responsible for the water flow reduction in the narrow gaps. A considerable number of researchers attempted to clearly explain the discrepancies that exist at the air-water interface [23], [28], [29]. Experiments about the presence of one phase (example air) in the flow path of another phase (example water) have been performed for the first time in our laboratory. Most of the researchers focused on the effect of one phase on the flow behavior another phase in a channel. However, a very limited study is available about the air-water interface study. To understand the hypothesis, an experimental investigation is done by the indirect approach of conducting the water flow tests in narrow gaps.

Water possesses unusual properties, totally different from other substances with similar molecular masses. The strong nature of its hydrogen bonds causes several anomalous properties such as high melting and boiling points, low compressibility, unusual solubility properties, and several other properties. Besides its inherent properties, water displays a lot of uniqueness in combination with other substances, and in different environments and conditions. Though largely studied about the various water phenomenon, water in its three states is still a strange substance. The nature of waters physical interaction with other states of matter is one of the emphasis of this research. The

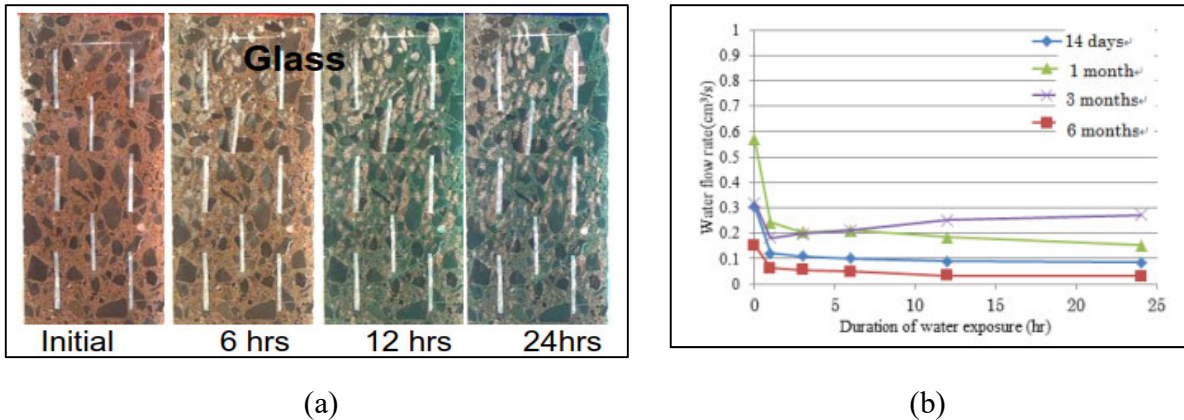


Fig. 1.1:(a) Water flow tests in concrete crack surfaces (b) Results of water flow tests [20]

performance of different microsystems is determined by the flow behavior of the liquid in these systems.

As mentioned earlier, Couette flow is a simple example of shear flow. The new material flow properties and the rheological parameters are determined by using Couette flow. It helps in determining the flow behavior as well as the usage of materials in different fields of fluids. The velocity profiles obtained by MRI and NMR studies for different materials have been tried to understand by using different flow models. The power-law flow model, which is widely accepted, was used by [14] to understand the Velocity curve. But this model was able to explain the behavior at high shear rates only but not the low shear rates. The other flow models like the Bingham model, also could not capture the entire shear rate decrease behavior in the Couette flow. Velocity profiles in these Couette flows are assumed to be linear profiles in the entire region but these profiles are indeed Non-linear. So, these velocity profiles can be theoretically fit by either quadratic equation or the Cubic Equation as mentioned by Yamazaki et al. (2016) and Sato et al. (2017) respectively.

Daniel et al. (2000) [30] conducted NMR tests using mustard seeds. The velocity profiles obtained by using these seeds showed slip behavior at integral multiples of  $r/d$  up to a certain distance and is eventually lost after a certain value. However, there is an increase in the rotation of the particles from the point of loss of slip behavior. It suggested that “Slip without rotation” is the motion in high shear and “Rotation without slip” is the motion in low shear even in solid motion. The same concept can be applied to understand our target “liquid motion” that is “flow”. The rotation of particle must be stagnated once the slip happens. That is why no attenuation of motion takes place where momentum conservation law is satisfied and thus the law of Newtonian can be applied where the energy is maintained. It is also important that the rotation of the particle gets started once the slip is stagnated near the flow end. Based on this understanding, in our lab, Nakayama et al. (2019) made an important contribution of the presence of the Newtonian region (present close to the rotor) and Non-Newtonian region (present away from the rotor).

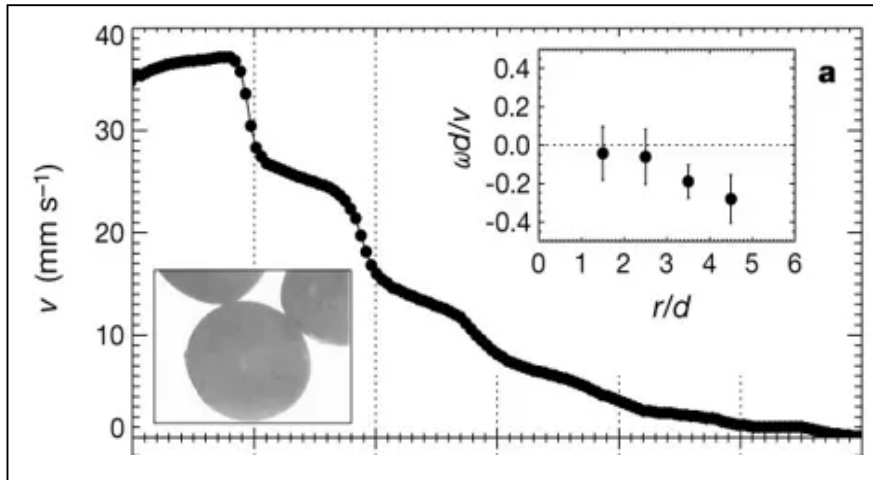


Fig. 1.2: Velocity profile of the mustard seeds considering slip and rotation behavior [30]

In the current study, based on previous research conducted in the lab, the grouping of the velocity profiles of various fluids is established, in which shear rate attenuation is studied and is correlated to the well-known macroscopic characteristics.

### 1.3 Objective of Research

The main purpose of this research is to understand the attenuation behavior present in different phenomena and understand them by a common mechanism. In this study, based on the fluid shear flow of water in narrow channels the phenomenon of water flow reduction is studied experimentally. The following are the objectives relating to the

1. Understand the water flow reduction mechanism in microchannels of range  $\leq 0.5\text{mm}$ .
2. To identify and validate the presence of braking mechanism, responsible for water flow reduction
3. Effect of different external parameters on the water flow rate in microchannels.
4. Hypothesis for understanding the effect of air-water interface on the water flow rate.

Additionally, another phenomenon occurring in the Couette flow is the attenuation of the shear rate during the viscous flow of fluids. The different objectives of this kind of study are

1. To find the regularity of flow of fluids in partially sheared Couette flows
2. To understand the shear rate decrease behavior by analytically understanding the various velocity profiles.
3. Classification of different Non-Newtonian material types based on analytical understanding.

## **1.4 Contributions of Research**

The phenomenon of water flow reduction in narrow microchannels is understood due to the presence of the braking effect of air bubbles present in the flow path. Different nature of the surface of the interface is also given importance in understanding the water flow reduction in microchannels. The water flow reduction mechanism on the different types of surface are explained.

To explain the mechanism of water braking due to the interface, it is hypothesized that the solidified behavior of the molecules is present at the gas-liquid interface. The solidified molecules present at the air-water interface are anchored at the hydrophilic crevices causing the reduction in water flow rate. However, in hydrophobic channels, the solidified molecules form a continuous sheet of water molecules including the surface and the interface. The water flow reduction in these is due channels is due to the presence of only air bubbles in the flow path of the water flow.

In Couette flow, the mechanism of shear rate decrease in the material is identified by analytical analysis of velocity profiles. Based on the analysis, the classification of macroscopic characteristics of the materials is distinguished. Finally, a new hypothesis is introduced to understand the behavior of the material based on the energy loss mechanism due to friction.

## **1.5 Outline of the Thesis**

“Chapter 1” introduces the topic and the general background of this research and helps in understanding the further chapters.

“Chapter 2” describes the previous research conducted in this field of study.

“Chapter 3” provides the methodology used for understanding the objective of the research and helps in understanding the experimental work and analytical analysis.

“Chapter 4” provides the detailed results of the conducted water flow experiments and the analytical results of the velocity curve fitting.

“Chapter 5” describes the new theory for understanding the phenomena of shear flow attenuation and water flow reduction.

“Chapter 6” provides the discussion of the results and the mechanisms involved in understanding them.

“Chapter 7” includes the Conclusions and the future recommendations of this research.

## **1.6 References**

- [1] D. Liu and S. V Garimella, “Investigation of Liquid Flow in Microchannels,” *J. Thermophys. HEAT Transf.*, vol. 18, no. 1, doi: 10.2514/1.9124.
- [2] “Experimental investigation of water flow in smooth and rough silicon microchannels Related content,” 2006, doi: 10.1088/0960-1317/16/7/037.

- [3] C. J. Martin, “Annular two phase flow.,” 1983, doi: 10.1016/0017-9310(72)90222-0.
- [4] T. Ishii, Mamoru; Hibiki, *Thermofluid dynamics of two-phase flow*. 2011.
- [5] Akimi Serizawa, Z. Feng, and Zensaku Kawara, “Two-Phase Flow in Microchannels,” in *Experimental Thermal and Fluid Science*, vol. 26, no. 6–7, CRC Press, 2002, pp. 703–714.
- [6] T. F. Groß, G. Ludwig, and P. F. Pelz, “Experimental and theoretical investigation of nucleation from wall-bounded nuclei in a laminar flow,” in *Open Archives of the 16th International Symposium on Transport Phenomena and Dynamics of Rotating Machinery, ISROMAC 2016*, 2016.
- [7] T. F. Groß, G. Ludwig, and P. F. Pelz, “Experimental evidence of nucleation from wall-bounded nuclei in a laminar flow,” *J. Phys. Conf. Ser.*, vol. 656, no. 1, p. 012034, 2015, doi: 10.1088/1742-6596/656/1/012034.
- [8] C. N. Fluids, *Cavitation in Non-Newtonian Fluids*. .
- [9] N. Ashraÿ, D. M. Binding, and K. Walters, “Cavitation effects in eccentric-cylinder flows of Newtonian and non-Newtonian fluids,” vol. 56, pp. 5565–5574, 2001.
- [10] J. Li and P. Cheng, “Bubble cavitation in a microchannel,” *Int. J. Heat Mass Transf.*, vol. 47, no. 12–13, pp. 2689–2698, 2004, doi: 10.1016/j.ijheatmasstransfer.2003.11.020.
- [11] D. Tretheway, X. Liu, and C. Meinhart, “Analysis of slip flow in microchannels,” *Proc. 11th Int. Symp. Appl. Laser Tech. to Fluid Mech.*, no. 1, pp. 8–11, 2002.
- [12] Y. Kurotani and H. Tanaka, “A novel physical mechanism of liquid flow slippage on a solid surface,” 2020.
- [13] P. Coussot, *Rheometry of Pastes , Suspensions , and*. 2005.
- [14] S. Jarny, N. Roussel, S. Rodts, F. Bertrand, R. Le Roy, and P. Coussot, “Rheological behavior of cement pastes from MRI velocimetry,” *Cem. Concr. Res.*, vol. 35, no. 10, pp. 1873–1881, 2005, doi: 10.1016/j.cemconres.2005.03.009.
- [15] S. Jarny, N. Roussel, R. Le Roy, and P. Coussot, “Modelling thixotropic behavior of fresh cement pastes from MRI measurements,” *Cem. Concr. Res.*, vol. 38, no. 5, pp. 616–623, 2008, doi: 10.1016/j.cemconres.2008.01.001.
- [16] G. Ovarlez, S. Rodts, A. Ragouilliaux, P. Coussot, J. Goyon, and A. Colin, “Wide-gap Couette flows of dense emulsions: Local concentration measurements, and comparison between macroscopic and local constitutive law measurements through magnetic resonance imaging,” *Phys. Rev. E - Stat. Nonlinear, Soft Matter Phys.*, vol. 78, no. 3, pp. 1–32, 2008, doi: 10.1103/PhysRevE.78.036307.
- [17] P. Coussot *et al.*, “Coexistence of liquid and solid phases in flowing soft-glassy materials,” *Phys. Rev. Lett.*, vol. 88, no. 21, pp. 2183011–2183014, 2002, doi: 10.1103/PhysRevLett.88.218301.
- [18] J. G. Cabrera, “Deterioration of concrete due to reinforcement steel corrosion,” *Cem. Concr. Compos.*, vol. 18, no. 1, pp. 47–59, Jan. 1996, doi: 10.1016/0958-9465(95)00043-7.

- [19] H. M. Jonkers, “Self Healing Concrete: A Biological Approach,” in *Springer Series in Materials Science*, vol. 100, Springer Verlag, 2007, pp. 195–204.
- [20] H. Ikomaa, T. Kishib, Y. Sakaib, and M. Kayondo, “Elucidation of rapid reduction of water flow through concrete crack regarded as self-healing phenomenon,” *J. Ceram. Process. Res.*, vol. 16, pp. 22–27, 2015.
- [21] M. K. Muzafalu, “Experimental study on the effect of the air - water interface created at wall surface on water flow in narrow gaps,” 2017.
- [22] P. Scardina and M. Edwards, “Air Binding of Granular Media Filters,” *J. Environ. Eng.*, vol. 130, no. 10, pp. 1126–1138, Oct. 2004, doi: 10.1061/(ASCE)0733-9372(2004)130:10(1126).
- [23] X. Zhuang, P. B. Miranda, D. Kim, and Y. R. Shen, “Mapping molecular orientation and conformation at interfaces by surface nonlinear optics,” *Phys. Rev. B - Condens. Matter Mater. Phys.*, vol. 59, no. 19, pp. 12632–12640, 1999, doi: 10.1103/PhysRevB.59.12632.
- [24] R. Khatib, E. H. G. Backus, M. Bonn, M. J. Perez-Haro, M. P. Gaigeot, and M. Sulpizi, “Water orientation and hydrogen-bond structure at the fluorite/water interface,” *Sci. Rep.*, vol. 6, no. April 2016, pp. 1–28, 2016, doi: 10.1038/srep24287.
- [25] S. Nihonyanagi *et al.*, “Unified molecular view of the air/water interface based on experimental and theoretical  $\chi(2)$  spectra of an isotopically diluted water surface,” *J. Am. Chem. Soc.*, vol. 133, no. 42, pp. 16875–16880, 2011, doi: 10.1021/ja2053754.
- [26] M. V. Berry, “The molecular mechanism of surface tension,” *Phys. Educ.*, vol. 6, no. 2, pp. 79–84, 1971, doi: 10.1088/0031-9120/6/2/001.
- [27] A. Marchand, J. H. Weijs, J. H. Snoeijer, and B. Andreotti, “Why is surface tension a force parallel to the interface?,” *Am. J. Phys.*, vol. 79, no. 10, pp. 999–1008, 2011, doi: 10.1119/1.3619866.
- [28] P. Salucci *et al.*, “Ultrafast Hydrogen-Bond Dynamics in the Infrared,” *Science (80-. )*, vol. 301, no. September, pp. 1698–1702, 2003.
- [29] W. Gan, D. Wu, Z. Zhang, Y. Guo, and H. Wang, “Orientation and Motion of Water Molecules at Air/Water Interface,” *Chinese J. Chem. Phys.*, vol. 19, no. 1, pp. 20–24, 2006, doi: 10.1360/cjcp2006.19(1).20.5.
- [30] D. M. Mueth, G. F. Debregeas, P. J. Eng, S. R. Nagel, and H. M. Jaeger, “Signatures of granular microstructure in dense shear flows,” *Nature*, vol. 3, pp. 385–389, 2000.

## **Chapter 2. LITERATURE REVIEW**



The shear flow of the fluid observed in pipe flows called as Poiseuille flow and in concentric cylinders (shear applied by the rotor) is called the Couette flow. The understanding of these flows is different and used for different types of applications. Extensive research has been conducted in the field of Poiseuille flow (including the flow in microchannels, two-phase flow also) and Couette flow individually. However, little research has been done considering both these flows and understanding the mechanisms involved in them. In the previous research, water flow was reduction was observed in the microchannels with crevices [1]. In Couette flow, based on the flow curves shear rate attenuation mechanism is studied by [2]–[4] but the theory couldn't be applied to the other different materials. The mechanisms involved in these flows are little different yet related.

## 2.1 Flow in Microchannels

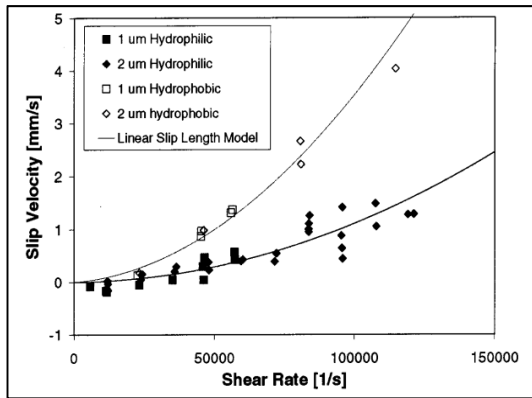
Much research has been done in understanding the flow behavior and characteristics in microchannels. The dependency of the flow rate in the microchannels due to the slip behavior on the surfaces of the microchannels was first observed by [5] and later equations are developed by other researchers [6]–[8]. Equations for the flow rate considering the slip behavior of the flow along with Poiseuille flow is given by .....Equation 2-3. In the Fig. 2.1 (a) the slip velocity for the hydrophobic surface is much higher compared to the hydrophilic channel. In the Fig. 2.1 (b), water flow rate is increased in the hydrophobic channels compared to the hydrophilic channels at the same applied pressure drop. As there is an increase of slip velocity behavior in hydrophobic channels, water flow rate increases in these channels. The presence of viscous forces, compressibility of the fluid, surface roughness and dissolved gas is not considered in this study. Dissolved gas is important to consider (even at microscale) and understand the slip behavior even more clearly.

$$Q_{poiseuille} = \frac{2wh^3 \Delta p}{3\mu L} \dots\dots\dots \text{Equation 2-1}$$

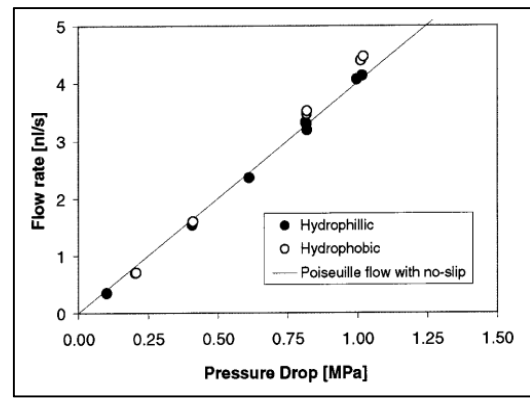
$$Q_{slip} = 2hw \cdot u_{slip} \dots\dots\dots \text{Equation 2-2}$$

$$Q = Q_{poiseuille} + Q_{slip} \dots\dots\dots \text{Equation 2-3}$$

A similar kind of research conducted by Tanaka Hajime et al. (2020) [9] to understand the mechanism of slip behavior, also shows a higher slip behavior for the hydrophobic surfaces as shown in Fig. 2.2. In this research, the focus was on the slippage of the simple viscous fluid, in which flow-induced instability arises from the density dependence of viscosity. The mechanism for the slip behavior is given importance and concluded that the presence, the time of formation, and the stability of the bubble on the surface are equally responsible for the slip behavior. At lower shear rates and higher contact angles the bubbles formed are stable due to which higher slip lengths are recorded. However, at higher shear rates and higher contact angles the bubbles formed are highly unstable and the slip behavior also. The presence of dissolved gases (which is not studied

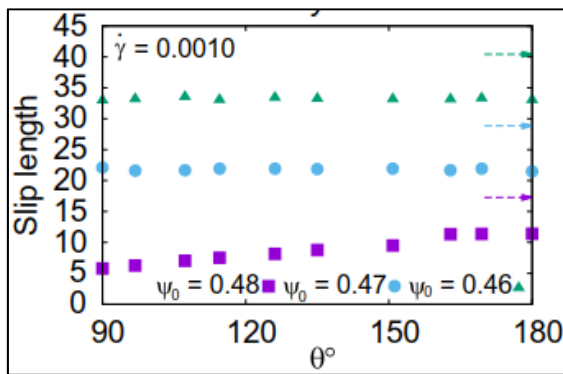


(a)

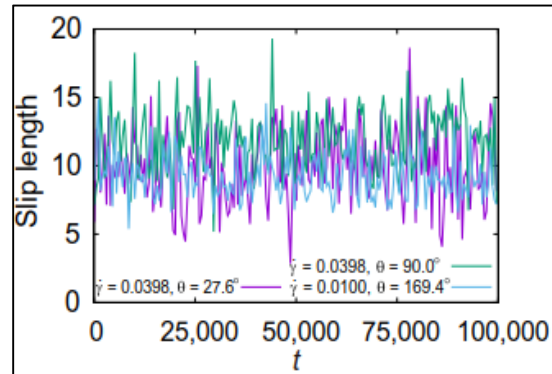


(b)

Fig. 2.1: Slip velocities and water flow rates for different types of surfaces. (a) Shear rate vs Slip velocity (b) Pressure drop vs Flow rate. [6]



(a)



(b)

Fig. 2.2: (a) Slip lengths for different initial densities at the wall surface at the same applied shear rate. (b) Slip lengths for hydrophobicity and shear rate at different times.[9]

in this research) should also be taken into consideration to have a realistic understanding of the phenomenon of slip behavior.

Apart from the slip behavior of the fluids over the hydrophobic and hydrophilic surfaces, it is also necessary to understand the retention of the bubbles or the work of adhesion on these surfaces from the point of view of the effect on flow rate. The work of adhesion between the droplet and solid surface is investigated by [10], [11]. The equations used for the adhesion of liquid drop on the surfaces are also used for the air bubble by researchers [12]–[14]. The air bubble is attached to the plate surface and immersed in the water to experimentally observe the bubble movement on

$$F_{adh} = kw\gamma(\cos \theta_{min} - \cos \theta_{max}) \dots \dots \dots \text{Equation 2-4}$$

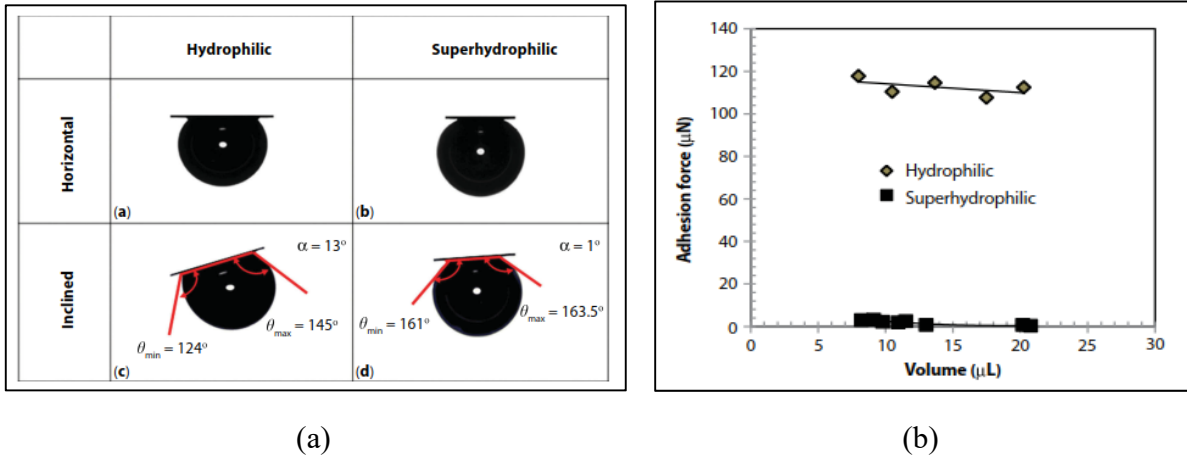


Fig. 2.3: (a) Experimental conditions used for sliding of air bubble (b) Plot of adhesive force and volume of the bubble. [10]

the inclined hydrophilic and super-hydrophilic surfaces as in Fig. 2.3. The force of retention or the force of cohesion is calculated by using .....Equation 2-4. It was concluded that the hydrophilic surface has more adhesion in holding the air bubble and slides from the surface at higher inclinations for the same bubble volume compared to the super-hydrophilic surfaces. The width of the contact of the air bubble and the receding, advancing contact angles at the position of the sliding of the air bubble are liable for cohesive force. The presence of super-hydrophilicity on the surface makes the air bubble to a greater contact angle and reduces the contact width of the air bubble. The bubble movement on inclined hydrophobic surface was also investigated by [14]. In this research, the upward and downward facing bubbles on an inclined surface, immersed in water, are studied to understand the bubble movement. The adhesive force is much higher for the downward facing bubble along with the contact width of the bubble. In this case, a compressive hydrostatic pressure is applied at the apex of the bubble increasing the contact area and the thereby the adhesion force. Surface orientation and bubble volume significantly affect the adhesion force and the stability of bubbles on the hydrophobic surfaces.

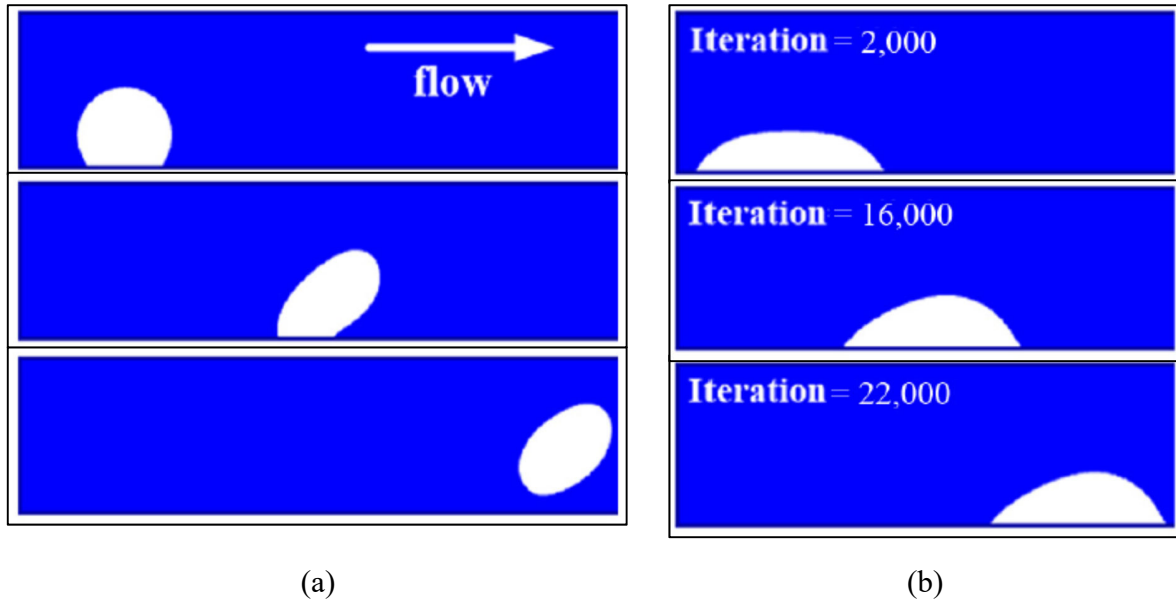


Fig. 2.4: Bubble behavior due to shear flow on (a) Hydrophilic surface (b) Hydrophobic surface [15]

A similar kind of study is conducted to understand the bubble characterizations on the hydrophobic surface in microchannels using the lattice Boltzmann simulation method [15]. In his study, it was mentioned that the nature of the formation of the air bubble on the hydrophilic or hydrophobic surface is opposite to the formation of a droplet. Resembling the drops, air bubbles also represent the wettability of the surfaces. The static and dynamic properties of the bubble are simulated using a single component multiphase lattice Boltzmann method. In the dynamic state, high flow speed makes the bubbles unstable, while low solid-liquid interaction weakened the mobility and deformation of bubbles as shown in Fig. 2.4. To maintain the gas-liquid interface steadily on the wall, a small contact angle and a symmetric shape of the bubble should be realized.

Bubble formation occurs due to cavitation or when there is a heat transfer between the surfaces (called incipient boiling). Recent experiments conducted by [16], [17] show that the formation of bubbles due to cavitation during the shear flow is a self-excited process in the gaps of up to 0.5mm. The presence of dissolved gas is considered analytically (which helps in the nucleation of bubbles from the cavities present on the surface) for understanding the bubble formation. The effect of flow shear rate on bubble volume and nucleation rate for different gap sizes and crevice sizes is studied. The effect of these bubble formation on the flow rate in microchannels is not considered.

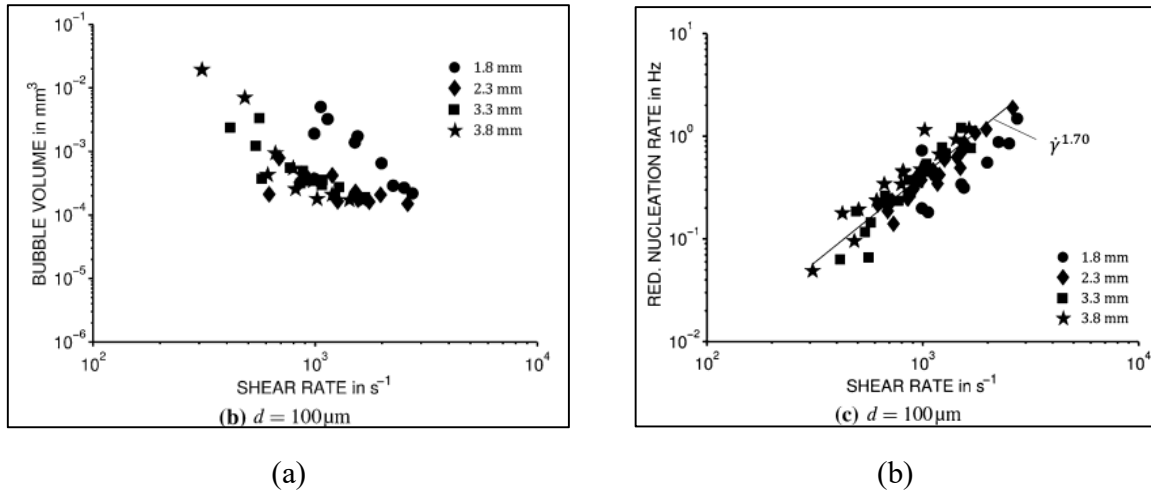
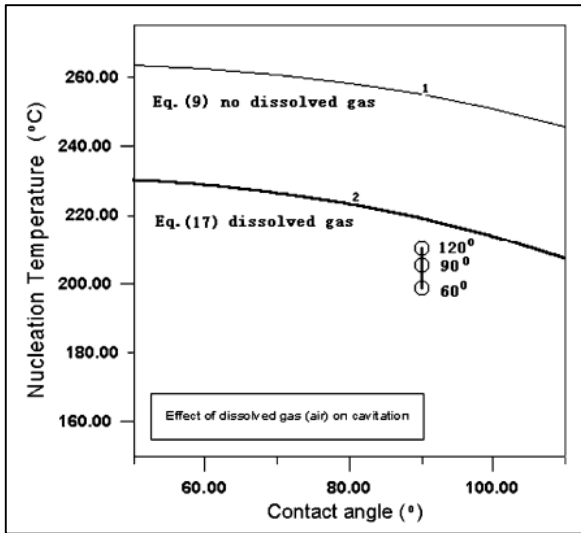


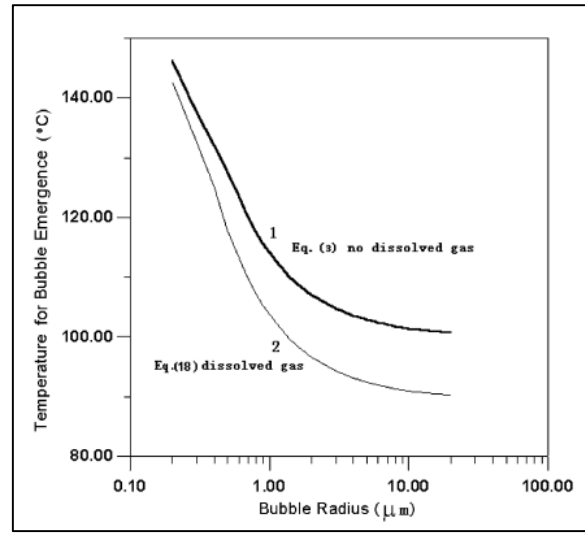
Fig. 2.5: Effect of shear flow on (a) Bubble volume (b) nucleation rate [16]

In the research conducted by [18], the effect of microchannel size, mass flow rate, and heat flux on boiling incipience or bubble cavitation in liquid are discussed. It was concluded that to effectively reduce the nucleation temperature can be lowered by using a large contact angle between the fluid and the substrate, and the existence of dissolved gas, randomly residual vapor (gas)-trapped, and corners. The larger flow rate reduces the formation of air bubbles. The numerical model presented in the study does not consider the heat conduction effects on the surface of the substrate. This heat conduction in the substrate may play an important role in the heat transfer process. These results clarify the nucleation of the bubble or the formation of the vapor surface due to incipient boiling.

When two immiscible liquids 1 and 2 are in contact, the free energy change in expanding their “interfacial” area by unit area is known as interfacial energy or interfacial tension [19]. The process is explained by the creation of two separate unit areas of liquid 1 and liquid 2 and then they are brought into contact. This energy is always positive. When two media 1 and media 2 are required to separate in a media 3, the energy required is given as  $W_{132}$  and is given by  $W_{132} = \gamma_{13} + \gamma_{23} - \gamma_{12}$  ..... Equation 2-5. Surface energy equations for hydrophilic and hydrophobic surface are given in  $\gamma_{23}(1 - \cos \theta) = \gamma_{13} + \gamma_{23} - \gamma_{12}$  ..... Equation 2-6 and  $\gamma_{23}(1 + \cos \theta) = \gamma_{13} + \gamma_{23} - \gamma_{12}$  ..... Equation 2-7 respectively. If  $W_{132}$  is negative media 2 spreads entirely on or totally wets media 1. That means the interfacial energy of media 12 is much greater than the sum of individual energies of media 12 and media 13. If  $W_{132}$  is positive media 2 spreads on media 1 with a contact angle ranging from  $0^\circ$  to  $180^\circ$ . The sum of interfacial energies of media 13 and media 23 is greater than media 12.

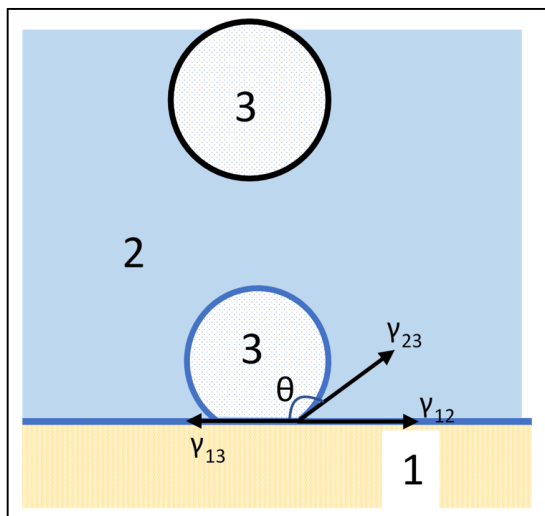


(a)

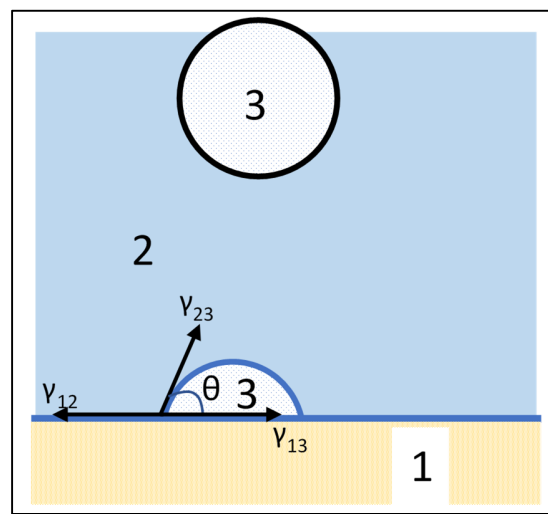


(b)

Fig. 2.6: Dependence of bubble nucleation temperature with (a) Contact angle (b) Bubble radius [18]



(a)



(b)

Fig. 2.7: Behavior of bubble on (a) Hydrophilic surface (b) Hydrophobic surface

1 – Solid Surface 2 – Liquid Media 3 – Gas Media

$$W_{132} = \gamma_{13} + \gamma_{23} - \gamma_{12} \dots \dots \dots \text{Equation 2-5}$$

$$\gamma_{23}(1 - \cos \theta) = \gamma_{13} + \gamma_{23} - \gamma_{12} \dots \dots \dots \text{Equation 2-6}$$

$$\gamma_{23}(1 + \cos \theta) = \gamma_{13} + \gamma_{23} - \gamma_{12} \dots \dots \dots \text{Equation 2-7}$$

## 2.2 Rheology

Rheology is the study of the flow of matter. Viscosity, shear behavior of the fluid material is determined based on the rheology. Couette flow, Cone-plate viscometer are used to understand the rheological properties of different materials. In the current study, circular Couette partially sheared flows are considered for the analytical analysis. The mechanism of shear flow rate induced in these flows is assumed to be Newtonian and the Navier-stokes equation is applied to understand the velocity distribution as well as shear rate behavior. The velocity equation based on the rotation of the inner cylinder and outer cylinder at rest is given by

$$v = \frac{\omega}{\frac{1}{r_i^2} - \frac{1}{r_o^2}} \cdot \left( \frac{1}{r} - \frac{r}{r_o^2} \right) \dots \dots \dots \text{Equation 2-8}$$

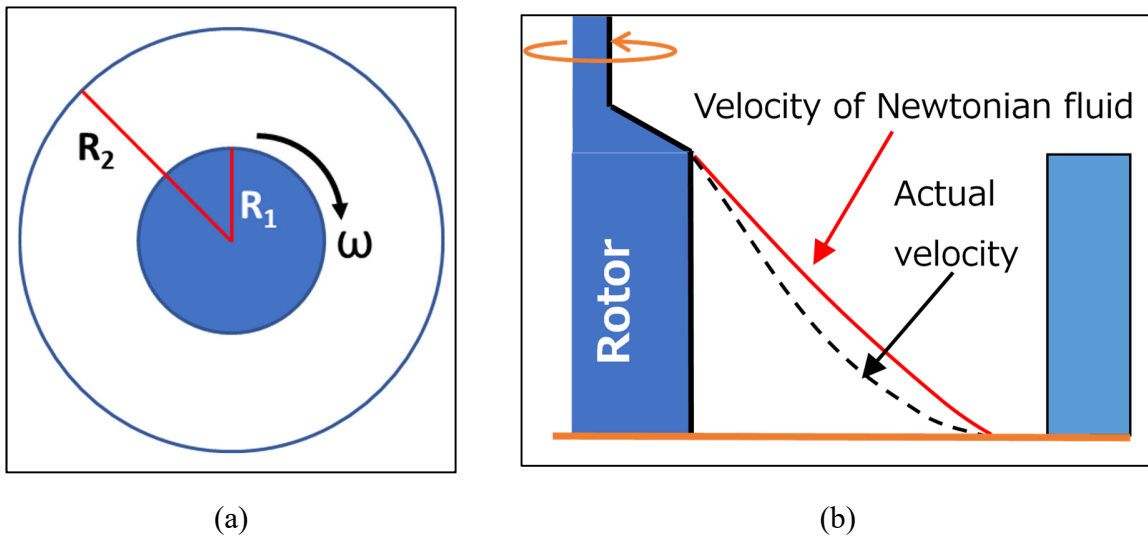


Fig. 2.8: Couette flow (a) Top view of the inner and outer rotor (b) Side view of Couette flow along with the assumed velocity, actual velocity profiles.

$$v = r\omega(r) \dots \dots \dots \text{Equation 2-9}$$

$$M = 2\pi hr^2\tau \dots \dots \dots \text{Equation 2-10}$$

$$\tau = k\dot{\gamma}^n \dots \dots \dots \text{Equation 2-11}$$

$$v(r) = \frac{n}{2} \left( \frac{M}{2\pi hk} \right)^{\frac{1}{n}} r \left( r^{-\frac{2}{n}} - r_2^{-\frac{2}{n}} \right) \dots \dots \dots \text{Equation 2-12}$$

$$v(r) = \left( \frac{M}{2\pi hk} \right)^{\frac{1}{n}} r \left( \int_r^{r_c} \frac{1}{x} \left( \frac{1}{x^2} - \frac{1}{r_c^2} \right)^{\frac{1}{n}} dx \right) \dots \dots \dots \text{Equation 2-13}$$

The flow curve obtained by using the viscometer or MRI is used to understand the flow behavior and the rheological parameters. Various flow curve models like the power-law, Herschel-Buckley model are used to define the material behavior. The velocity equations obtained by using the flow curve equations and the torque characteristics cannot explain the velocity curve characteristics [2].

Equations of velocity are given by  $v(r) = \frac{n}{2} \left( \frac{M}{2\pi hk} \right)^{\frac{1}{n}} r \left( r^{-\frac{2}{n}} - r_2^{-\frac{2}{n}} \right) \dots \dots \dots \text{Equation 2-12}$  and  $v(r) = \left( \frac{M}{2\pi hk} \right)^{\frac{1}{n}} r \left( \int_r^{r_c} \frac{1}{x} \left( \frac{1}{x^2} - \frac{1}{r_c^2} \right)^{\frac{1}{n}} dx \right) \dots \dots \dots \text{Equation 2-13}$ .

The inability to understand the velocity profiles in Couette flows is due to the assumption of Newtonian behavior and the same shear rate at each point of the radius value. So, it is necessary to overcome these assumptions to understand the velocity profile behavior of materials. No-slip conditions at the walls are used to obtain the velocity profiles from the MRI, NMR, or viscometer experiments. The energy loss mechanism due to the friction between the particles in Couette flow is calculated using the equation. The larger energy losses induce the stability of the flow as mentioned in the research [20]. Higher energy losses are observed at the outer rotor radius indicating higher stability while the fluid at the rotating rotor end has more disturbances and less stability.

$$\frac{dH}{dS} = 4\mu \frac{\omega_1 R_1}{h^2} \frac{R_1^4}{r^4} \frac{(1-\eta)^2}{\eta^2} \frac{1}{(1-\eta^2)^2} \left[ \frac{\eta^2}{\eta^2-1} \frac{r}{R_1} + \frac{R_1}{r} \frac{1-\lambda}{1-\eta^2} \right]^{-1} \dots \dots \dots \text{Equation 2-14}$$



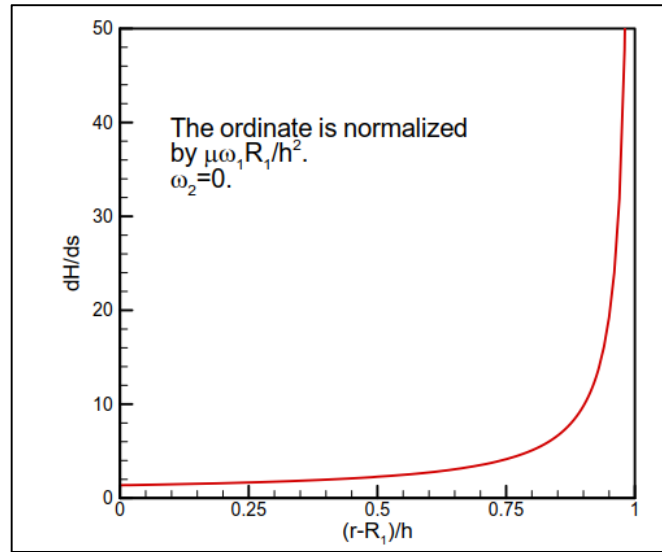


Fig. 2.9: Energy loss along the channel width for concentric rotating cylinders (inner cylinder is rotating while the outer cylinder is at rest) [20].

Some of the researchers A.Fall et al. (2015) [21] studied the local phenomenon of discontinuous shear thickening (in cornstarch) by velocity-controlled rheometers. Shear flow behavior in soft glassy state of nearly hard suspensions exhibits slip, making velocimetry valuable. For steady-state rheological behavior of concentrated suspension, a hard-sphere shape like 370nm diameter PMMA is observed using NMR velocimetry by H.Wassenius et al. (2005) [22]. A study on emulsion stability and “texture” was carried out aiming to evaluate potential problems for commercial applications. Rheo-NMR analysis is performed to evaluate wall slip and structure stability problems along with the validation of data from traditional data obtained from the rheometer by Domenico Gabriele et al. (2009) [23].

In the case of drilling mud, viscosity bifurcation is observed in the Couette flow when a shear force is applied. The fluids progressively stop flowing till they reach a certain critical shear rate. Above this critical stress value, they go on flowing at a larger value. Slope break is observed at the solid-liquid interface as observed by Ragouilliaux et al. (2006). [24].

When surfactant solutions are subjected to certain shearing, they correspond to shear banding, i.e., a region of high shear rate coexisting with a region of low shear rate. Julie Drappier et al. (2005) [25] determined velocity profiles under shear using MRI to observe the coexistence of high and low shear rate region, called shear banding. The studies from both NMR and conventional rheometer by S. Rodts et al. (2005) [26] show that foam cannot flow steadily below a critical, apparent shear rate or critical shear stress. At low velocities, the shear localizes in a layer of thickness decreasing with the apparent shear rate.

Research on Couette flows of different materials helped in understanding the materials, observations of new kinds of behavior like viscosity bifurcation, shear localization, etc. By

understanding the trends in the behavior of the materials they are used in different industrial applications. Continuous research is being conducted in the direction to engineer the materials and use them for different types of applications. However, the basic physical mechanism responsible for the flow of these fluids in Couette flow is lacking.

The presence of dissolved gas in water is considered by most of the researchers for the formation and movement of the air bubble. The air bubble is externally attached to the surface or injected in the liquid flow for understanding the bubble behavior. The water flow reduction mechanism in microchannels and concrete crack surfaces observed by the previous research using equilibrated water (containing dissolved gas) is studied using glass microchannels.

Many equations and much literature are present in understanding the velocity profiles of different materials in Couette flow. No-slip behavior is considered at the wall to exclude the boundary effects on material behavior. But the mechanism of decrease in the shear rate in the Couette flow is not yet understood. Theoretical analysis of velocity profiles is achieved to understand the mechanism of shear rate decrease in the Couette flow.

### **2.3 Chapter Summary**

In this chapter, previous literature has been explained regarding the flow in microchannels along with two-phase flow. Different flow patterns identified by the previous research for the two-phase flow based on the behavior of the fluids is described. Moreover, the flow behavior of fluids on the hydrophilic and hydrophobic surfaces (also called wettability) is included. The focus is then shifted to the behavior of the single air bubble on these different surfaces and the related equations based on the forces between the bubble and surface. The characteristic behavior of different types of surfaces is understood based on the previous literature.

However, for rheological aspects of the fluids, they are clearly understood based on the Couette flows and flow curves. Different microscopic behavior of the materials like jamming, viscosity bifurcation, shear banding lead to the study of velocity profiles. The macroscopic understanding of the material behavior is clearly established based on the flow curve. Various researchers provided different equations measuring the velocity profile but could not be established exactly. The energy loss mechanisms occurring inside the Couette flow are also considered to for mechanistic understanding of the materials.

### **2.4 References**

- [1] M. K. Muzafalu, "Experimental study on the effect of the air - water interface created at wall surface on water flow in narrow gaps," 2017.
- [2] S. Jarny, N. Roussel, S. Rodts, F. Bertrand, R. Le Roy, and P. Coussot, "Rheological behavior of cement pastes from MRI velocimetry," *Cem. Concr. Res.*, vol. 35, no. 10, pp. 1873–1881, 2005, doi: 10.1016/j.cemconres.2005.03.009.
- [3] S. Jarny, N. Roussel, R. Le Roy, and P. Coussot, "Modelling thixotropic behavior of fresh cement pastes from MRI measurements," *Cem. Concr. Res.*, vol. 38, no. 5, pp. 616–623, 2008, doi: 10.1016/j.cemconres.2008.01.001.

- [4] N. Roussel, R. Le Roy, and P. Coussot, “Thixotropy modelling at local and macroscopic scales,” *J. Nonnewton. Fluid Mech.*, vol. 117, no. 2–3, pp. 85–95, 2004, doi: 10.1016/j.jnnfm.2004.01.001.
- [5] E. Schnell, “Slippage of Water over Nonwetable Surfaces,” *J. Appl. Phys.*, vol. 27, no. 10, pp. 1149–1152, 1956, doi: 10.1063/1.1722220.
- [6] C.-H. Choi, K. J. A. Westin, and K. S. Breuer, “Apparent slip flows in hydrophilic and hydrophobic microchannels,” *Phys. Fluids*, vol. 15(10), no. April 2003, pp. 2897–2902, 2003, doi: 10.1063/1.1605425.
- [7] D. C. Tretheway, X. Liu, and C. D. Meinhart, “Analysis of Slip Flow in Microchannels,” *Proceedings of 11th International Symposium on Applications of Laser Techniques to Fluid Mechanics*, no. 1, p. (pp. 8-11).
- [8] C.-H. Choi, K. J. A. Westin, and K. S. Breuer, “To slip or not to slip-Water flows in hydrophilic and hydrophobic microchannels,” *Proc. IMECE2002 ASME Int. Mech. Eng. Congr. Expo.*, pp. 557–564, 2002.
- [9] Y. Kurotani and H. Tanaka, “A novel physical mechanism of liquid flow slippage on a solid surface,” 2020.
- [10] C. W. Extrand and Y. Kumagai, “Liquid drops on an inclined plane: The relation between contact angles, drop shape and retentive force.pdf,” *J. Colloid Interface Sci.*, vol. 170, no. 2, pp. 515–521, 1995.
- [11] R. A. Brown, F. M. ORR, JR, and L. E. Scriven, “Static Drop on an Inclined Plate Analysis by the Finite Element Method.pdf,” *J. Colloid Interface Sci.*, vol. 73, no. 1, pp. 76–87, 1980.
- [12] C. Antonini, F. J. Carmona, E. Pierce, M. Marengo, A. Amirfazli, and I. Industriale, “General Methodology for Evaluating the Adhesion Force of Drops and Bubbles on Solid Surfaces,” *Am. Chem. Soc.*, vol. 25, no. 11, pp. 6143–6154, 2009, doi: 10.1021/la804099z.
- [13] K. . Mittal, “Advances in Contact Angle , Wettability and Adhesion.” scrivener, p. 500, 2015.
- [14] A. Kibar, R. Ozbay, M. A. Sarshar, Y. T. Kang, and C. Choi, “Bubble Movement on Inclined Hydrophobic Surfaces,” *Am. Chem. Soc.*, vol. 33, no. 43, pp. 12016–12027, 2017, doi: 10.1021/acs.langmuir.7b02831.
- [15] P. Du, H. Hu, F. Ren, and D. Song, “Bubble characterizations on hydrophobic surface using lattice Boltzmann simulation with large density ratios,” *Int. J. Numer. Methods Heat Fluid Flow*, vol. 27, no. 6, pp. 1311–1322, 2016, doi: 10.1108/HFF-02-2016-0062.
- [16] T. F. Groß, G. Ludwig, and P. F. Pelz, “Experimental and theoretical investigation of nucleation from wall-bounded nuclei in a laminar flow,” in *Open Archives of the 16th International Symposium on Transport Phenomena and Dynamics of Rotating Machinery, ISROMAC 2016*, 2016.
- [17] T. F. Groß, G. Ludwig, and P. F. Pelz, “Experimental evidence of nucleation from wall-bounded nuclei in a laminar flow,” *J. Phys. Conf. Ser.*, vol. 656, no. 1, p. 012034, 2015, doi: 10.1088/1742-6596/656/1/012034.

- [18] J. Li and P. Cheng, “Bubble cavitation in a microchannel,” *Int. J. Heat Mass Transf.*, vol. 47, no. 12–13, pp. 2689–2698, 2004, doi: 10.1016/j.ijheatmasstransfer.2003.11.020.
- [19] J. Israelachvili, *Intermolecular and Surface Forces*. 2011.
- [20] H. S. Dou, B. C. Khoo, and K. S. Yeo, “Energy loss distribution in the plane Couette flow and the Taylor-Couette flow between concentric rotating cylinders,” *Int. J. Therm. Sci.*, vol. 46, no. 3, pp. 262–275, 2007, doi: 10.1016/j.ijthermalsci.2006.05.003.
- [21] A. Fall *et al.*, “Macroscopic discontinuous shear thickening versus local shear jamming in cornstarch,” *Phys. Rev. Lett.*, vol. 114, no. 9, pp. 1–5, 2015, doi: 10.1103/PhysRevLett.114.098301.
- [22] H. Wassenius and P. T. Callaghan, “NMR velocimetry studies of the steady-shear rheology of a concentrated hard-sphere colloidal system,” *Eur. Phys. J. E*, vol. 18, no. 1, pp. 69–84, 2005, doi: 10.1140/epje/i2004-10155-4.
- [23] D. Gabriele, M. Migliori, R. Di Sanzo, C. O. Rossi, S. A. Ruffolo, and B. de Cindio, “Characterisation of dairy emulsions by NMR and rheological techniques,” *Food Hydrocoll.*, vol. 23, no. 3, pp. 619–628, 2009, doi: 10.1016/j.foodhyd.2008.05.002.
- [24] A. Ragouilliaux, B. Herzhaft, F. Bertrand, and P. Coussot, “Flow instability and shear localization in a drilling mud,” *Rheol. Acta*, vol. 46, no. 2, pp. 261–271, 2006, doi: 10.1007/s00397-006-0114-2.
- [25] J. Drappier, D. Bonn, J. Meunier, S. Lerouge, J. P. Decruppe, and F. Bertrand, “Correlation between birefringent bands and shear bands in surfactant solutions,” *J. Stat. Mech. Theory Exp.*, no. 4, 2006, doi: 10.1088/1742-5468/2006/04/P04003.
- [26] S. Rodts, J. C. Baudez, and P. Coussot, “From ‘discrete’ to ‘continuum’ flow in foams,” *Europhys. Lett.*, vol. 69, no. 4, pp. 636–642, 2005, doi: 10.1209/epl/i2004-10374-3.

**Chapter 3.      METHODOLOGY FOR  
EXPERIMENTATION AND  
ANALYTICAL ANALYSIS**

### **3.1 Methodology for Water Flow Tests**

Water flow in microchannels (< 1mm) differs from normal channels due to the differences in the scale of study. The flow in these channels sometimes follows the normal conventional theory and the flow properties would agree with the theory. But, in some cases, there will be a disparity in the theoretical understanding and experimental observations. Based on such behaviour, a different phenomenon was observed in the concrete cracks when water was used for self-healing of concrete. Large water flow reduction was observed during the early stages of the water flow rate. Concrete cracks can be deemed as a porous microchannel and experimentation can be carried. Experiments have been conducted on different surfaces like wood, aluminium, and plastic emulating the concrete crack surface. It was concluded that the bubble formation at the crevices is responsible for the water flow reduction. To understand this water flow rate reduction and the mechanisms involved in it, a different set of experiments have been conducted. The experiments include conducting the water flow tests with different geometries of microchannels and different porous nature. The water flow rate was measured for each different kind of microchannel and different conditions. In this chapter, the materials used for the preparation of microchannel, the process of preparation of microchannel, and the procedure for performing water flow tests are described.

#### **3.1.1 Preparation of Microchannel:**

Two different kinds of microchannels are prepared based on the width of the microchannel for different study purposes. One is wide microchannel (WMC) of width 0.3mm and depth 0.5mm and the other is narrow microchannel (NMC) with a width of 9.33mm and depth 0.2mm as shown in Fig. 3.1 (a) and (b) respectively. The microchannels are prepared by sandwiching the two glass plates together. One of the glass plates is engraved with the necessary pattern of the microchannel and is attached to the other normal glass plate. In previous literature, the water flow tests were conducted using different kinds of materials like the wood plate, aluminium plate, and plastic plates. The microchannel was prepared by sandwiching the glass plate and wood plate. The microchannel gap was provided by using the Teflon sheets of 0.3mm thick kept in between the wooden plate and glass plate. The crevices are prepared with the help of nails at random positions. In the present case, the microchannel gap is engraved with the needle of diameter 1mm and the crevices are provided precisely with a spindle needle on the glass plate with the help of Micro Instrument (Micro MC-1 described in Table 1).

The preparation of the Microchannel and the experimental set-up involves many steps. Initially, clean, and clear glass plates of dimensions 75mm x 26mm x 1.3mm are chosen for the preparation of the microchannel. The microchannel pattern to be engraved on the glass plate is created with the help of the software package attached to the Micro Instrument. Different diameter needles are used for making the groove of microchannel and crevices. The microchannel is prepared by sandwiching the grooved and non-grooved glass plates. Water head is provided for the microchannel, to maintain constant pressure above microchannel, to conduct the water flow tests. Water head is manually prepared by acrylic plates and water is poured continuously to the water head. The following sections explain the detailed preparation of microchannel, experimental

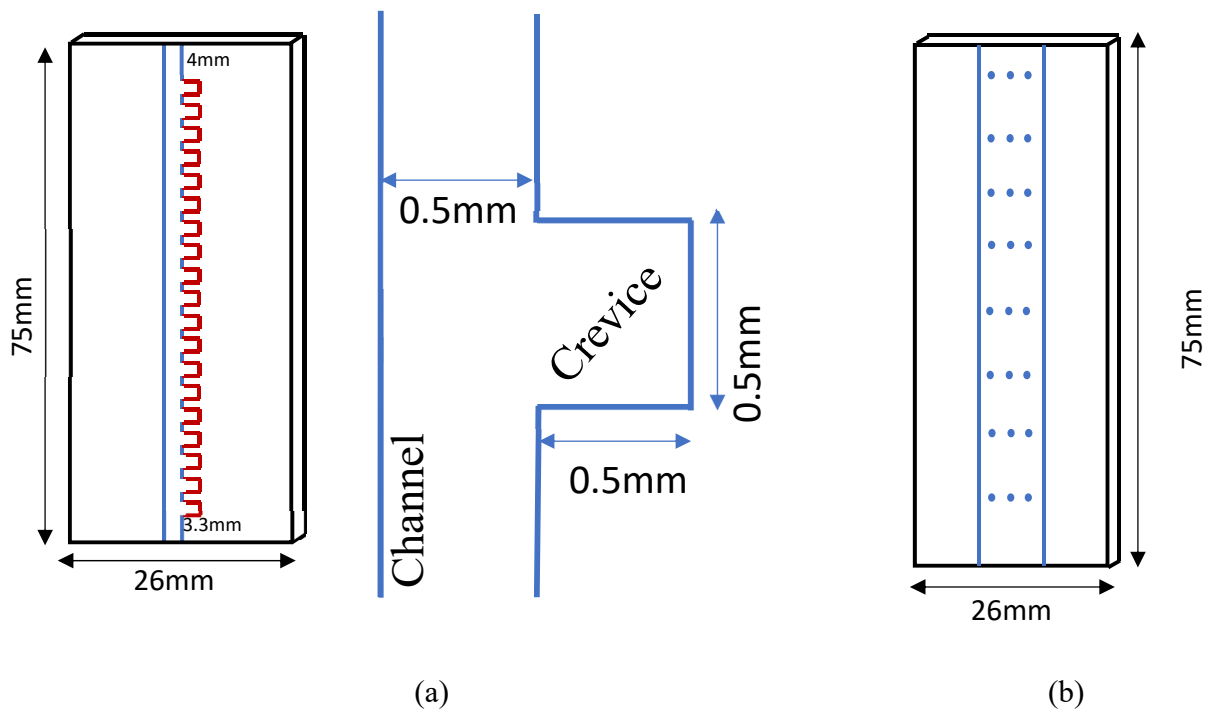


Fig. 3.1: (a) Wide Microchannel showing the dimensions of crevice (b) Narrow Microchannel

set-up, and the procedure for water flow tests. Care is taken at each step to ensure the required mechanism in the microchannels.

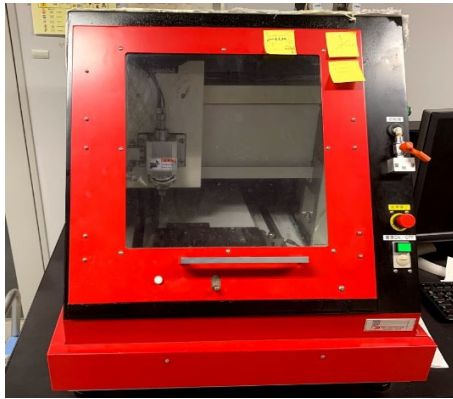
### 3.1.2 MC-1 Machine Description (PMT Machine):

A micro instrument (MC-1) is used for the preparation of the microchannel. The instructions to the machine are given using a computer PC with the help of a software. The configuration of the machine is as shown in table 1.

The schematic diagram of the instrument and the needle used for preparing the microchannel is shown in Fig. 3.2 (a) and (b) respectively. Mark II software is used to prepare the required pattern of the microchannel. After that, a code is generated for giving instructions to the micro instrument for preparing the channel. The minimum diameter of the spindle needle present is 0.3mm. The spindle needle is rotated at a speed of 5000rpm. There spindle speed motion for the horizontal and vertical motion, should as minimum as possible. Otherwise, the needle may break, and it gets engraved into the microchannel making the microchannel unfit for the water flow tests. The wet process is used for the preparation for a smooth transition of the needle and for removing the small glass particles formed.

Table 3.1: Micro Instrument (MC-1) Model Description

1	Model name	Micro MC-1
2	Processing method	Wet/dry
3	Body dimensions	W600 x D795 x H720 mm
4	Bodyweight	100kg (including control unit)
5	Main components	Aluminum material
6	Spindle speed	5,000 to 10,000 rpm
7	Table size	X210 x Y297 (A4 size)
8	Effective stroke	X268 x Y328 x Z100
9	Repeated positioning accuracy	$\pm 10 \mu\text{m}$
10	Control resolution	$1 \mu\text{m}$
11	Cooler pump	100V AC
12	Air pressure	0.5Mpa 30NL / min
13	Power supply	100V (3A)



(a)



(b)

Fig. 3.2: (a) Micro Instrument (MC-1) (b) Spindle needle with jet flow

### 3.1.3 Sandwiching procedure for Microchannels

Two glass plates of dimensions 75mm x 26mm x 1.3mm are used to prepare the microchannel. One of the glass plates engraved with the spindle needle to represent the microchannel with a certain pattern. The patterned glass plate and the normal glass (Clean and clear without any undulations) plate are cleaned properly with Distilled water for three to four times so that there are



no impurities present on the glass plates. The two glass plates are then transferred into a 1:3 ratio solution of Hydrogen Peroxide ( $H_2O_2$ ) and Sulphuric acid ( $H_2SO_4$ ). This mixture solution is called a piranha solution. Piranha solution is very dangerous, being both strongly acidic and a strong oxidizer. It is used to clean organic residues from the substrate and removes most organic matter. Additionally, it will hydroxylate the most surfaces, making them highly hydrophilic. The two glass plates put in the piranha solution should be undisturbed for 10 ~ 15mins. The two glass plates are then removed from the mixture solution and cleaned properly again using distilled water. An air blower is used to remove the distilled water from the glass plates. Each glass plate is blown with air and made sure that they are very much without any residual water present on the surfaces. The plates are then sandwiched together manually, by applying force, to form a microchannel. Proper care should be taken so that the two glass plates will not slide each other while pressing against each other. The prepared microchannel is kept in a drying oven at  $645^\circ C$  for 5hrs. The microchannel is removed from the oven after the cooling of the chamber.

### **3.1.4 Types of Microchannels:**

Different types of microchannels of different heights are prepared to understand the water flow reduction mechanism. The microchannels are classified and identified based on the perpendicular distance between the crevice surface and non-crevice surface.

### **3.1.5 Wide Microchannel (WMC)**

The term wide microchannel is used as the channel depth is more compared to the other microchannel. The pattern of the wide microchannel used in this study is as shown in Fig. 3.1(a). The microchannel consists of channel length 75mm, width 0.5mm, and depth 0.3mm. Square shape crevices are attached at one of the boundary surfaces of the microchannel at regular spacings. The total number of crevices engraved on the microchannels are 29. The minimum possible width of the microchannel obtained with the help of the instrument was 0.3mm. Width of 0.3mm microchannel was tried to prepare but the spindle needle was broken each time the preparation was made. Even though the speed of the needle was reduced, the 0.3mm width microchannel was not prepared. So, the microchannel width of 0.5mm was considered along the length of the glass plate of 75mm. As the minimum width of the channel was 0.5mm, crevices of square shape with length 0.5mm are provided. If the crevice dimensions are greater than 0.5mm, the bubble formed may block the entire microchannel and if it is less than 0.5mm, a bubble formed may get easily washed away. We need the bubbles to stabilize at a specific position along the path of the water flow, so, these kinds of dimensions were chosen for the microchannel. However, the depth of microchannel can be easily controlled and 0.3mm depth was provided for the microchannel based on the crevice dimensions.

Two different types of microchannels are used in the current study by changing the surface characteristics of the glass plate. One microchannel is normal with a hydrophilic surface (the surface on which water easily stays) and another microchannel is a hydrophobic surface (water readily slips from the surface). The hydrophilic channel is prepared after manufacturing the

microchannel itself, as the piranha solution is effective in preparing it. The hydrophobic surface is difficult to prepare as the piranha solution makes the surface highly hydrophilic. However, Hydrophobic surface is prepared by pouring the hydrophobic liquid (used for cleaning the glass panes of the car) is poured into the channel and left as it is for around 1hr. With this process, the surface of the microchannel along with the crevices then behaves as a hydrophobic surface. Two different surfaces are chosen here to understand the bubble formation mechanism on these two different surfaces. The water used for the water flow tests is Equilibrated water having the Dissolved Oxygen (DO) values greater than 95%.

### 3.1.6 Narrow Microchannel (NMC)

As the name itself suggests, the microchannels depth is narrow. Three different patterns are considered to understand the effect of each parameter on the water flow rate. These patterns differ in the number of crevices present in each microchannel. The channel dimensions of each pattern are 75mm x 9.33mm x 0.2mm. Width of 0.2mm was chosen to emulate the concrete crack surfaces. The patterns of the narrow microchannel are as shown in Fig. 3.3. Pattern 1 (Fig. 3.3(a)) has no crevices, pattern 2 (Fig. 3.3(b)) has 27 crevices and pattern 3 (Fig. 3.3(c)) has 54

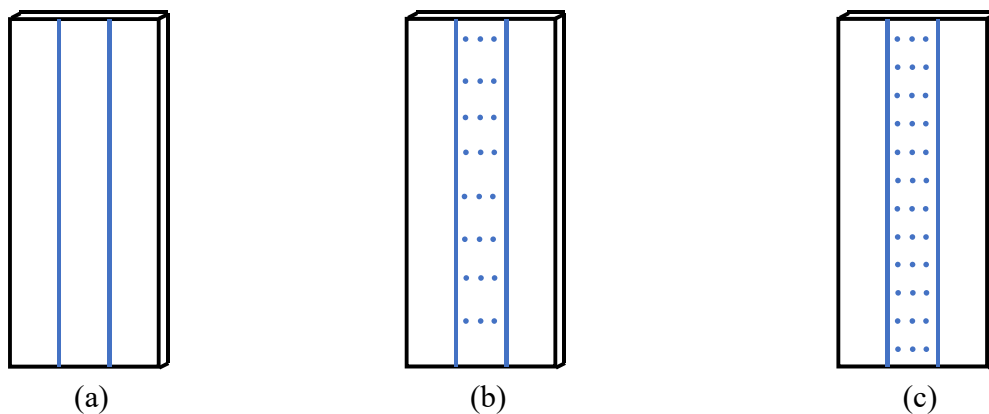


Fig. 3.3: Narrow Microchannels with a change in the number of crevices (a) No crevice (b) 27 Crevices (c) 54 crevices

crevices. This is the minimum diameter possible for the crevice using the spindle needle of the micro instrument is 300 $\mu$ m. So, the crevice diameter is chosen as 300 $\mu$ m and the depth is considered as 180 $\mu$ m. These three different patterned microchannels are prepared by the procedure mentioned above.

In these microchannels also, the effect of the change in the surface characteristics of the microchannel is studied. The microchannel with the only maximum number of crevices is chosen to be hydrophobic to understand the effects on the water flow in a striking manner. The hydrophobic surface is prepared by pouring the hydrophobic liquid (used for cleaning the glass panes of the car) is poured into the channel and left as it is for around 1hr. Different types of water with different Dissolved oxygen levels (Degassed water (DO < 40%), Equilibrated water (DO >

95%)) are used to check the possibility of the formation of air bubbles at the Crevice surface of the microchannels and the condition required for the water flow reduction. The luminescent powder is used for the water flow to identify the formation of air bubbles on the crevice part in microchannels. The luminescence is identified only in the presence of UV light.

### 3.1.7 Preparation of Experimental Set-up

After preparing the microchannels with the help of a micro instrument (MC-1) and sandwiching the of glass plates, the water pressure head is provided to the microchannel to allow the water flow. The experimental setup consisting of microchannel and water pressure head is as shown in Fig. 3.4 (a). Acrylic plates are used for making the water pressure head above the microchannel glass plate. The acrylic plates of 100mm x 100mm are cut to required dimensions to prepare the water head and fit it above the microchannel. The water pressure head is sealed by silica gel to prevent any leakages due to the water flow. Proper care must be taken to ensure that there are no leakages by pouring the water, before conducting the water flow tests, in the pressure head and observed for 2mins. If there are no leakages present, the microchannel is then ready for conducting the experiments. The overall preparation, making the microchannel, and making the pressure head requires at least 3days.

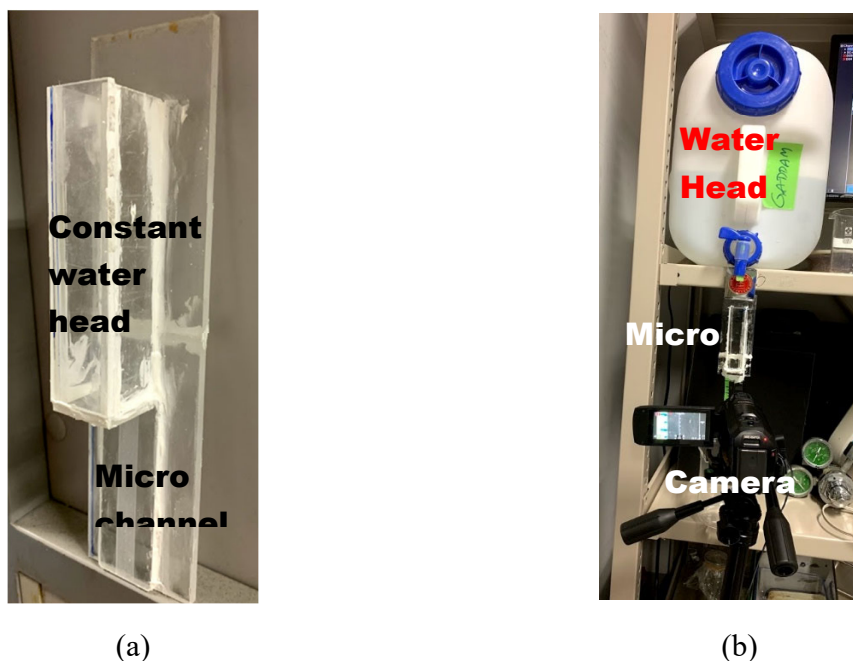


Fig. 3.4: (a) Microchannel with water head (b) Experimental set up for the water flow tests.

The prepared microchannel is held vertically against support to conduct water flow tests as shown in Fig. 3.4 (b). A constant pressure head is maintained all the time during the water flow tests. Water is flown continuously from the tank and is constantly monitored so that the water level does not fall below a certain level. The imaging of the microchannel is done with the help of

the camera mounted on a tripod. Enough light is provided for the microchannel so that the bubble formation and behaviour are captured clearly. Same procedure is followed for both narrow microchannels and wide microchannels. For the case of luminescent powder usage (for detecting air bubbles) in microchannels, UV light is used for the microchannel to capture the presence of the luminescence in the microchannels.

### **3.1.8 Procedure for Water Flow Tests**

The following procedure for water flow tests is followed for both Narrow microchannels and Wide microchannels. After the preparation of the microchannel, along with the water pressure head, the microchannel is ready for conducting the water flow tests. Prior to the water flow tests, it is essential to remove any residual air gaps present in the microchannel as they affect the final water flow rate results. The air gaps in the microchannel are removed by degassing the air from the microchannel using the vacuum chamber. The microchannel is kept for degassing in vacuum chamber for about 2hrs to completely remove the air gaps from the microchannel. The microchannel is then used for conducting the water flow tests. There may be a case of air gaps formed at the beginning of the water flow tests, then the water flow test is stopped and the microchannel is again put in a vacuum chamber to remove any residual air gaps. After, ensuring the complete vacuuming of the microchannel, water flow tests are conducted.

The vacuumed microchannel is held vertically against support to perform the water flow tests. A certain water head is maintained all the time during the water flow tests. Two types of water are used for water flow tests. One type is equilibrated water of dissolved oxygen (DO) level greater than 95%, and the other type is degassed water with dissolved oxygen (DO) level less than 40%. Equilibrated water is obtained from the laboratory and is stored for 1 week to increase the levels of dissolved oxygen (DO). The dissolved oxygen level of equilibrated remains almost constant when stored for more than 1 week. However, degassed water increases its dissolved oxygen levels (DO) rapidly within hours. So, it is tricky to use degassed for the water flow tests and is necessary to prepare only during the time of the experiment. The prepared degassed water should be used as early as possible to reduce the effect of an increase in DO levels of water. In the current experiment, the degassed water is prepared just when the experiment starts and is used for 2hrs. The remaining water is continuously degassed and used after 2hrs. This cycle is repeated until the end of the experiment and a certain constant pressure head is maintained overall the experiment. The water pressure head can be easily maintained and monitored when the equilibrated water is used. A separate water head is provided to continuously pour the water to the prepared pressure head above microchannel.

After making the microchannel free from the air gaps and maintaining the water pressure head, the water is flown in the microchannel under the influence of gravity. The water flow rate is calculated at periodical intervals by collecting the water in the beaker for every 10mins. The water weight is measured and noted for every 10mins during the initial two hours and for every 30mins for the remaining experiment for wide microchannels. The narrow microchannels have a very less flow rate, so the water is collected every 30mins from the start to the end of the experiment. The

collected data for each pattern and type of microchannel is analysed and compared to understand the flow behaviour in different conditions.

### **3.1.9 Imaging of the water flow tests:**

The microchannels are visualized with the help of a camera mounted on a tripod for bubble formation and its effect on the water flow as shown in Fig. 3.4 (b). The visualization technique is used for both narrow microchannels and wide microchannels. In the case of narrow microchannels, the bubble formation at the crevice part in the flow path is studied. Video recording is done for the whole experiment focusing only on a certain portion of the microchannel including around 5-6 crevices and water flow path of 18mm. This small portion was necessary to understand the bubble formation in the microchannel with crevices. A sequence of images is obtained along with the time for the microchannel, based on video recording, showing the different stages of bubble formation in the microchannel. The obtained images are analysed using Image J software to know the bubble portions, area of bubble, and the width of the water flow at the bubble formed area. Based on these results analytical area of the water flow and in turn, the water flow rate is calculated.

For wide microchannels, the imaging technique was useful for visualizing the air bubbles formed at the crevice parts. Luminescent powder was used in these microchannels and the microchannel was illuminated with the UV light to visualize the luminescence using the camera. The experimental room should be dark and only UV light is shed on the microchannel as luminescence is easily observed under these conditions. Akin to the narrow microchannels, sequential images are obtained for the presence of luminescence in wide microchannels also. The presence of luminescence indicates the formation of micro air bubbles at the crevice portion of the microchannel. While capturing the video for the visualization of the microchannel the light intensity on the microchannel should not change. If there is any slight change in the intensity of the light, the comparison of the images does not serve a meaningful purpose. The position of the camera and the microchannel are undisturbed during the whole experiment.

## **3.2 Methodology for Analysis of Velocity Profiles**

Velocity profiles of the materials in Couette flow are studied with the help of different constitutive equations. But none of the models could explain and understand the flow regularity and behavior of the material. This chapter includes the methodological and rational procedure followed in the analytical analysis of velocity profiles to understand the regularity of the flow of fluids under shear in the Couette flow. It also helps in understanding the shear rate transfer mechanism occurring during the fluid flow. Velocity profile (obtained from the Couette flow) fitting is necessary to understand the regularity of flow and the shear rate transfer mechanism during the flow. So, much data is acquired to understand these mechanisms for different Non-Newtonian fluids. Experimental velocity data is obtained from the various literature for different materials and are analyzed with certain assumptions. In this chapter, velocity data collection and the methodology used for the analysis of velocity profiles are described.

### 3.2.1 Data Collection

Velocity profiles of the materials subjected to shear force in Couette flow are considered in the current analysis. Researchers have focused on the velocity profiles of Couette flow in the early

Table 3.2: Data acquired for the analytical analysis

S. No.	Material	RPM range (rpm)
1	Cornstarch 1 [1]	10, 20, 40, 60
2	Silicon Oil Emulsion [2]	0.3, 1, 5, 10
3	Cacl2 [3]	2, 5, 10, 20
4	PMMA [4]	0.192, 0.48, 1.8, 9.6, 48
5	Drilling Mud [5]	2, 6, 10, 20, 40
6	Surfactant [6]	10, 20, 40, 50, 100
7	Shaving Foam [7]	10, 20, 40, 60, 80
8	Bentonite [8]	10, 20, 30, 40, 60
9	SGM Mayonnaise [9]	5, 20, 80
10	Cornstarch 2 [10]	0.6, 0.8, 1, 2, 3, 4
11	Cement Paste (CCR 2008) [11]	30.9, 41.2, 51.5, 61.8, 72.1, 82.4
12	Cement Paste (CCR 2005) [12]	20.6, 41.2, 51.5, 72.1, 82.4

2000s. Most of the data gathered ranges from 2000-2010. The data considered is not old and can be used for the analytical analysis. The velocity profiles are obtained for the different wide variety of materials like Cornstarch, Silicon Oil emulsion, Cement paste, Bentonite, Shaving Foam, Surfactant, Mayonnaise, etc. The velocity data is obtained from the well-published journal papers. The velocity profiles in all these papers are experimentally obtained by applying techniques like NMR, MRI, etc. for different RPM values. Usually, the velocity profiles are plotted with the original values obtained from the experiment, but some velocity profiles are normalized and are plotted. For these cases, the maximum velocity value is calculated based on the applied RPM value and the radius of the value. The actual values are then obtained by multiplying the normalized values with the maximum velocity profile of each value. All the velocity profiles in the literature are obtained only when the steady flow is reached at an applied RPM. No-slip boundary condition is considered during the flow at the rotating rotor.

The data is obtained by digitizing the plots with the help of a web plot digitizer. The experimental values of the velocity profile for a specific RPM value are digitized and saved in an excel worksheet format. This procedure is repeated for every material velocity profile and RPM value. The arranged data consists of the radius value (m), position value (m), and velocity value (m/s).

Radius value is the distance from the center of the rotor, position value is the distance from the flow stop end. The radius at which the flow stops is called a critical radius ( $r_c$ ). The position value is the difference between the critical radius and the radius value at which the velocity is to be measured. More than 50 velocity profile data are obtained, based on digitization, to analytically analyze and understand the regularity of flow, material behavior. The velocity data obtained for the various materials and RPM values are given in Table 1. All the data is stored in Excel worksheets. Different sheets are used for different materials and each RPM data of the same material is separated in the same sheet. The velocity profiles are plotted again and checked with original figures to ensure the data acquired is correct. After obtaining all the three values of radius, position, and velocity, and checking the data further analysis is done.

### **3.2.2 Assumptions in Analysis**

The velocity profiles are assumed to have a Newtonian and Non-Newtonian region in each profile. Even though the materials are Non-Newtonian, an intuitive Newtonian region is assumed to be present in each velocity profile. Fig. 3.5 shows the presence of Newtonian and Non-Newtonian regions in a single velocity profile. The red line is fitted linearly by the Newtonian equation and is considered as the Newtonian region line, while the violet line is fitted non-linearly and is considered as the Non-Newtonian. The presence of the Newtonian region varies for each applied RPM value. The region closer to the rotor side is considered as a Newtonian region while the region immediately after the Newtonian region, till the flow stop end, is treated as a Non-Newtonian region. The velocity profiles in Non-Newtonian regions can be understood either by the quadratic or cubic equations as the velocity profiles in these regions are considered as the Non-linear. As an initial assumption, a simple quadratic equation is assumed to fit the Non-Newtonian velocity profile of the Couette flow. If the assumption does not explain the regularity of the flow, then a cubic equation is used. The analysis is restricted to the quadratic and cubic equation only as the higher degree of non-linearity is highly unrealistic and rare.

In the present analysis, partially sheared Couette flows are only considered to understand the behavior of material based on the velocity profile. In fully sheared flows, the material behavior is influenced by the outer wall. So, actual behavior is not obtained for these flows and is not considered in the present analysis. The material behavior categorization is considered based on the distinctive behaviors observed in analyzing the velocity profiles. This kind of analytical analysis is novel, and the current analysis is performed with reasoning for each step considered and are given below.

### **3.2.3 Identification of Newtonian and Non-Newtonian Regions**

The analysis of velocity profiles starts by distinguishing the Newtonian and Non-Newtonian regions. The Newtonian velocity equation obtained by solving the Navier-stokes is used for understanding the Newtonian behavior. Since the region close to the rotor is considered as Newtonian Region, Newtonian velocity equation is used to fit the portion of the curve near to

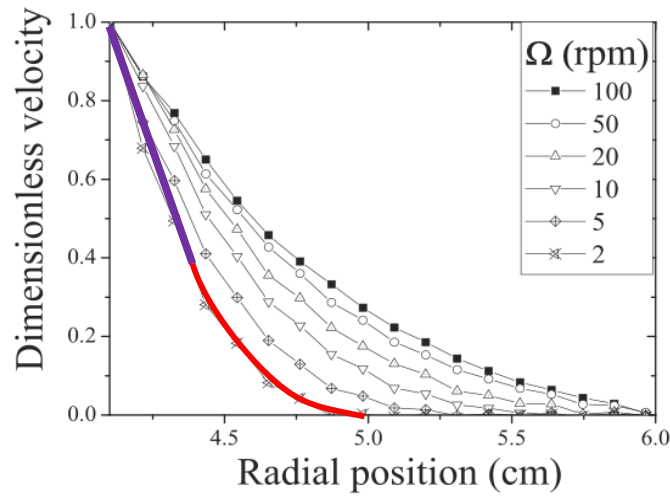


Fig. 3.5: Showing the Newtonian (closer to the rotor) and Non-Newtonian Regions (away from the rotor) [3].

$$v_n = \frac{\omega}{\left(\frac{1}{r_i^2} - \frac{1}{r_o^2}\right)} \left(\frac{1}{r} - \frac{r}{r_o^2}\right) \dots\dots\dots \text{Equation 3-1}$$

$$\text{Residual Variance} = \frac{\sum \text{sum of squares of residuals}}{n - p - 1} \dots\dots\dots \text{Equation 3-2}$$

the rotor. To identify the Newtonian region, the data analysis is started by analyzing the velocity profiles with the Newtonian velocity equation 1. The analysis is performed by assuming only some region of the curve, which always starts from the rotor end and ends at the specified radius value (starting from near the rotor and always less than the outer radius value) as shown in Fig. 3.6 (a). The velocity profile of this region is fit by equation 1 based on the least-squares criteria and the outer radius value is obtained for that region. The obtained outer radius value should be greater than the assumed specified radius value and less than the actual critical radius value. Excel solver add-in is used for estimating the least-squares values and obtaining the outer radius value of the region. The residual variance of this region is calculated by equation 2. As an example, consider  $R_1$  and  $R_2$  are the inner and outer radii of the Couette flow and the critical radius value as  $r_c$  ( $R_1 < r_c < R_2$ ) for a certain applied RPM value for the material. Now, a specified radius value of  $r_1$  is considered ( $R_1 < r_1 < r_c < R_2$ ). The portion of the velocity profile between  $R_1$  and  $r_1$  is tried to fit with the Newtonian equation. A certain outer radius ( $r_{12}$ ) value is present for this region (lying



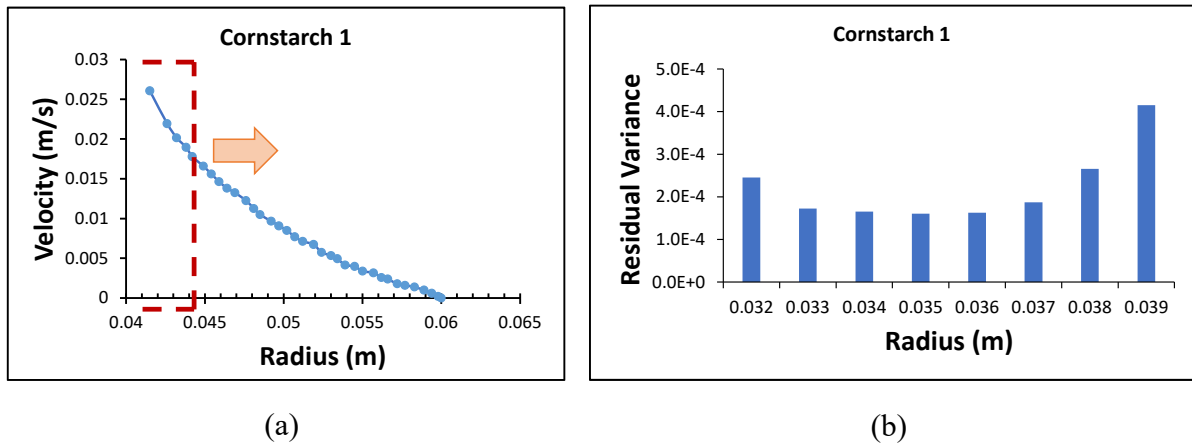


Fig. 3.6: (a) Consideration of velocity curve for Newtonian analysis, (b) Showing the decreasing and increasing Residual variance pattern

between  $R_1$  to  $r_1$ ) of the velocity curve and is found based on the least-squares criteria. The value of  $r_{12}$  should lie between  $r_1$  and  $r_c$ . This is because the shear flow of the material in the Couette flow occurs only between Inner radius ( $R_1$ ) and critical radius ( $r_c$ ). After obtaining the sum of least squares of all the data based on the  $r_{12}$  value, the residual variance of the region is calculated by using

equation 2. This residual variance value is specific to the radius ( $r_1$ ) obtained in the region starting from  $R_1$  and ending at  $r_1$ . Different radius values  $r_2, r_3, r_4, \dots$  and so on are considered until the critical radius value ( $r_c$ ) and the residual variance for each region are calculated. The plot of the residual variance against the radius values helps in understanding the Newtonian and Non-Newtonian regions.

The residual variance is the variation around the regression line. The variation is estimated based on the values calculated for the best fit of the curve. Each variation or the residual is the difference between the actual values and the calculated values. Residual variation is determined as the sum of the squares of all the residuals calculated over  $n-p-1$ ,  $p$  is the number of variation parameters. The residual variance calculated by the above procedure is plotted against the radius values.

Three types of residual variance pattern are observed (a) Decreasing and Increasing (Fig. 3.7 (a)), (b) Increasing (Fig. 3.7 (b)), (c) Decreasing (Fig. 3.5 (b)). In the case of increasing and decreasing residual variance, the radius at which the residual variance starts increasing is considered as the start of the Non-Newtonian region. The region nearer to the rotor is regarded as the Newtonian region. The region starting from the radius at which residual variance increases till the end of flow is considered as Non-Newtonian Region. However, for the case of the Increasing residual pattern case, the Newtonian region is never found. So, the whole region is considered as the Non-Newtonian region and is fitted either by quadratic or Cubic Equation. The pattern of decreasing residual variance pattern is difficult to interpret. As the residual variance decreases the velocity

profile is considered to approach the Newtonian profile. However, this region is also considered as a Non-Newtonian profile region and is fitted by either cubic equation or quadratic equation based on the variation of material parameter alpha ( $\alpha$ ).

### 3.2.4 Procedure to Fit the Non-Newtonian regions

The Newtonian and Non-Newtonian regions are obtained by the procedure mentioned above. The Newtonian regions are however fitted by the Newtonian equation. In the case of Non-Newtonian regions, they can be either fitted by quadratic or cubic equations. To find the best

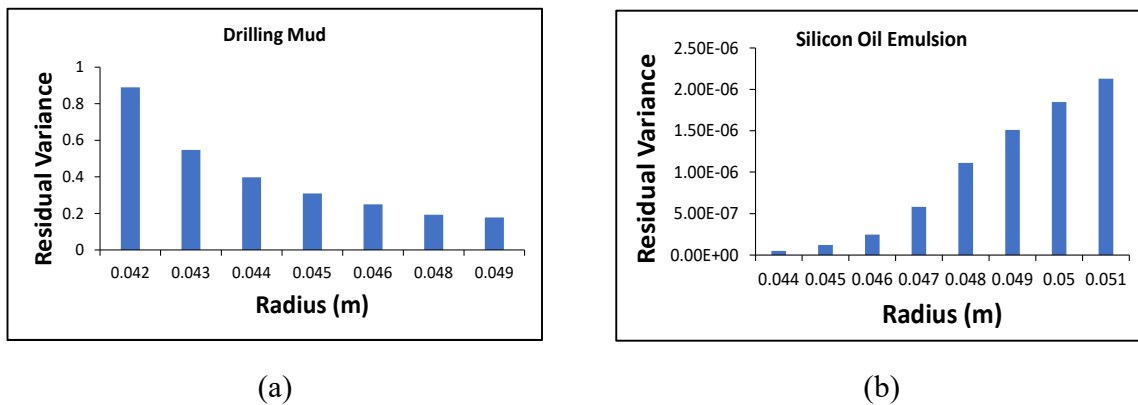


Fig. 3.7:(a) Showing the decreasing residual variance, (b) Showing the increasing residual variance pattern

equation fit, the variation of the parameter alpha ( $\alpha$ ) against the radius is considered to understand the actual fit to the velocity curve. The initial non-linearity assumed for the velocity profile is quadratic. Now the Non-Newtonian region in all the different velocity profiles are attempted to fit according to the equation 3 where  $r_c$  is the critical radius at which velocity is 0;  $r$  is the radius;  $\alpha$ ,  $\beta$  and  $k$  are parameters depending on the material;  $n$  is the extent of non-linearity of the velocity profile.

The primary objective is not to fit the velocity profiles but to understand the behavior of the material based on the analytical analysis. As the velocity profile is free of Newtonian behavior a quadratic term is considered for the analysis. The non-linearity in the velocity profiles is valued based on values of  $n$  as 1,2 or 3.

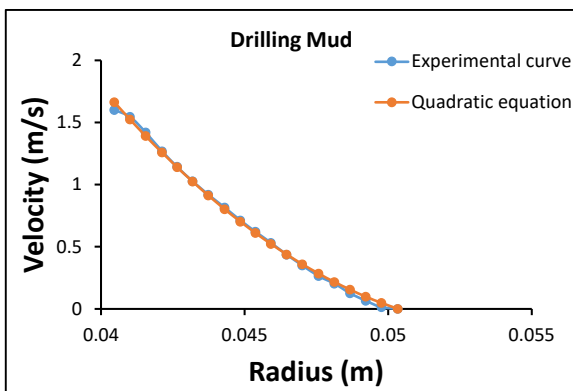
The variation of alpha value is obtained for each radius value and is plotted. The alpha value is calculated using Equation 4 obtained by varying the parameters  $k$ ,  $\beta$ , and  $n$  in the equation to fit the velocity equation based on the least-squares criteria. The Excel solver add-in used for obtaining the least-squares mostly depends on the assumed initial values of  $k$ ,  $\beta$ , and  $n$ . So, different random values are given for each iteration for 3-4 times to arrive at the least square value every time. The alpha value is then calculated by the obtained values of  $k$ ,  $n$  for each radius value ( $r$ ). The alpha value variation decides the extent of non-linearity or the additional non-linearity present in each

velocity profile. Some velocity profiles do not show any variation of alpha with radius indicating that the quadratic equation is the best suited for the velocity profile. While others show either linear or non-linear variation suggesting that the cubic equation (Equation 5) is best suitable for the Non-Newtonian region. The velocity profiles fitted by either quadratic or cubic equation perfectly match the entire velocity profiles and are shown in Fig. 3.8. The fitting of the velocity profiles is obtained by varying the material parameters and minimizing the sum of squares of the residuals. The shear behavior and the shear rate transfer mechanism in these Non-Newtonian regions can be easily understood.

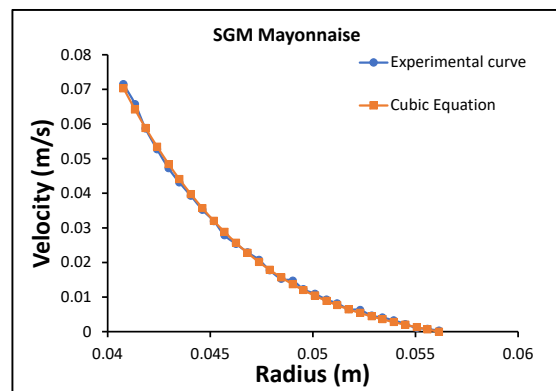
$$V = \alpha(r_c - r)^2 + \beta(r_c - r) \dots\dots\dots \text{Equation 3-3}$$

$$\alpha = k(r_c - r)^n \dots\dots\dots \text{Equation 3-4}$$

$$v = \gamma(r_c - r)^3 + \beta(r_c - r) \dots\dots\dots \text{Equation 3-5}$$



(a)  $\alpha = 9229.05, \beta = 77.46$



(b)  $\gamma = 14279.3, \beta = 1.2$

Fig. 3.8: Fitting of velocity profile by (a) quadratic equation (b) Cubic Equation

### 3.2.5 Procedure for Categorization of Materials

Non-Newtonian fluids are of two different types namely pseudoplastic and dilatant fluids. In the process of understanding the fitting of velocity profiles for the shear rate transfer mechanism, the different types of analysis done are utilized for identifying the different types of materials. The presence of the Newtonian region, the variation of the material parameter alpha, the regularity of velocity profiles with applied RPM values gives the distinctive features for understanding the different material behavior. The general classification of Non-Newtonian materials is either Pseudo plastic (shear thinning) or Dilatant. (Shear thickening). By understanding these behaviors, the current classification of materials is estimated.

### 3.3 Chapter Summary

In this chapter, the methodology of investigations for the water flow tests has been presented. Different patterns of microchannels with crevices and without crevices are prepared using glass microchannels to understand the water flow behavior. Procedure for the water flow tests along with imaging of the air bubbles is developed to understand the water flow rate and visualize the air bubble formation. The quantitative effect of this phenomena has been investigated by varying the number of crevices in the microchannels. Moreover, understanding the formation of air bubble different surfaces like hydrophilic and hydrophobic are considered. Finally, water flow rate in both the types of surface microchannels is understood.

In Couette flows, velocity profiles of different materials are considered for understanding the macroscopic behavior of materials. So, the velocity profiles are analytically analyzed based on the Newtonian fit and theoretical non-linear equations to understand the overall behavior of velocity profiles. Accordingly, suitable fit for the various velocity profiles using the equations is obtained.

### 3.4 References

- [1] A. Fall *et al.*, “Macroscopic discontinuous shear thickening versus local shear jamming in cornstarch,” *Phys. Rev. Lett.*, vol. 114, no. 9, pp. 1–5, 2015, doi: 10.1103/PhysRevLett.114.098301.
- [2] G. Ovarlez, S. Rodts, A. Ragouilliaux, P. Coussot, J. Goyon, and A. Colin, “Wide-gap Couette flows of dense emulsions: Local concentration measurements, and comparison between macroscopic and local constitutive law measurements through magnetic resonance imaging,” *Phys. Rev. E - Stat. Nonlinear, Soft Matter Phys.*, vol. 78, no. 3, pp. 1–32, 2008, doi: 10.1103/PhysRevE.78.036307.
- [3] G. Ovarlez, F. Mahaut, S. Deboeuf, N. Lenoir, S. Hormozi, and X. Chateau, “Flows of suspensions of particles in yield stress fluids,” *J. Rheol. (N. Y. N. Y.)*, vol. 59, no. 6, pp. 1449–1486, 2015, doi: 10.1122/1.4934363.
- [4] H. Wassenius and P. T. Callaghan, “NMR velocimetry studies of the steady-shear rheology of a concentrated hard-sphere colloidal system,” *Eur. Phys. J. E*, vol. 18, no. 1, pp. 69–84, 2005, doi: 10.1140/epje/i2004-10155-4.
- [5] A. Ragouilliaux, B. Herzhaft, F. Bertrand, and P. Coussot, “Flow instability and shear localization in a drilling mud,” *Rheol. Acta*, vol. 46, no. 2, pp. 261–271, 2006, doi: 10.1007/s00397-006-0114-2.
- [6] J. Drappier, D. Bonn, J. Meunier, S. Lerouge, J. P. Decruppe, and F. Bertrand, “Correlation between birefringent bands and shear bands in surfactant solutions,” *J. Stat. Mech. Theory Exp.*, no. 4, 2006, doi: 10.1088/1742-5468/2006/04/P04003.
- [7] S. Rodts, J. C. Bauddez, and P. Coussot, “From ‘discrete’ to ‘continuum’ flow in foams,” *Europhys. Lett.*, vol. 69, no. 4, pp. 636–642, 2005, doi: 10.1209/epl/i2004-10374-3.
- [8] N. Roussel, R. Le Roy, and P. Coussot, “Thixotropy modelling at local and macroscopic scales,” *J. Nonnewton. Fluid Mech.*, vol. 117, no. 2–3, pp. 85–95, 2004, doi: 10.1016/j.jnnfm.2004.01.001.
- [9] P. Coussot *et al.*, “Coexistence of liquid and solid phases in flowing soft-glassy materials,”

- Phys. Rev. Lett.*, vol. 88, no. 21, pp. 2183011–2183014, 2002, doi: 10.1103/PhysRevLett.88.218301.
- [10] A. Fall, N. Huang, F. Bertrand, G. Ovarlez, and D. Bonn, “Shear thickening of cornstarch suspensions as a reentrant jamming transition,” *Phys. Rev. Lett.*, vol. 100, no. 1, 2008, doi: 10.1103/PhysRevLett.100.018301.
- [11] S. Jarny, N. Roussel, R. Le Roy, and P. Coussot, “Modelling thixotropic behavior of fresh cement pastes from MRI measurements,” *Cem. Concr. Res.*, vol. 38, no. 5, pp. 616–623, 2008, doi: 10.1016/j.cemconres.2008.01.001.
- [12] S. Jarny, N. Roussel, S. Rodts, F. Bertrand, R. Le Roy, and P. Coussot, “Rheological behavior of cement pastes from MRI velocimetry,” *Cem. Concr. Res.*, vol. 35, no. 10, pp. 1873–1881, 2005, doi: 10.1016/j.cemconres.2005.03.009.

**Chapter 4.      EXPERIMENTAL AND  
ANALYTICAL RESULTS**

#### 4.1 Results of Water Flow Tests

The obtained experimental and analytical results are summarized below.

##### 4.1.1 Narrow Microchannels

Water flow tests are conducted to understand the flow behavior of water in the microchannel. Water is collected at the end of microchannel using a beaker for every specified interval of time. The water flow rate is calculated at the end of each time until the completion of the experiment. The results of water flow tests conducted twice on hydrophilic microchannel with a smaller number of crevices (27) are as shown below. Both the results have similar kinds of water flow reduction as can be observed from the graph as shown in Fig. 4.1.

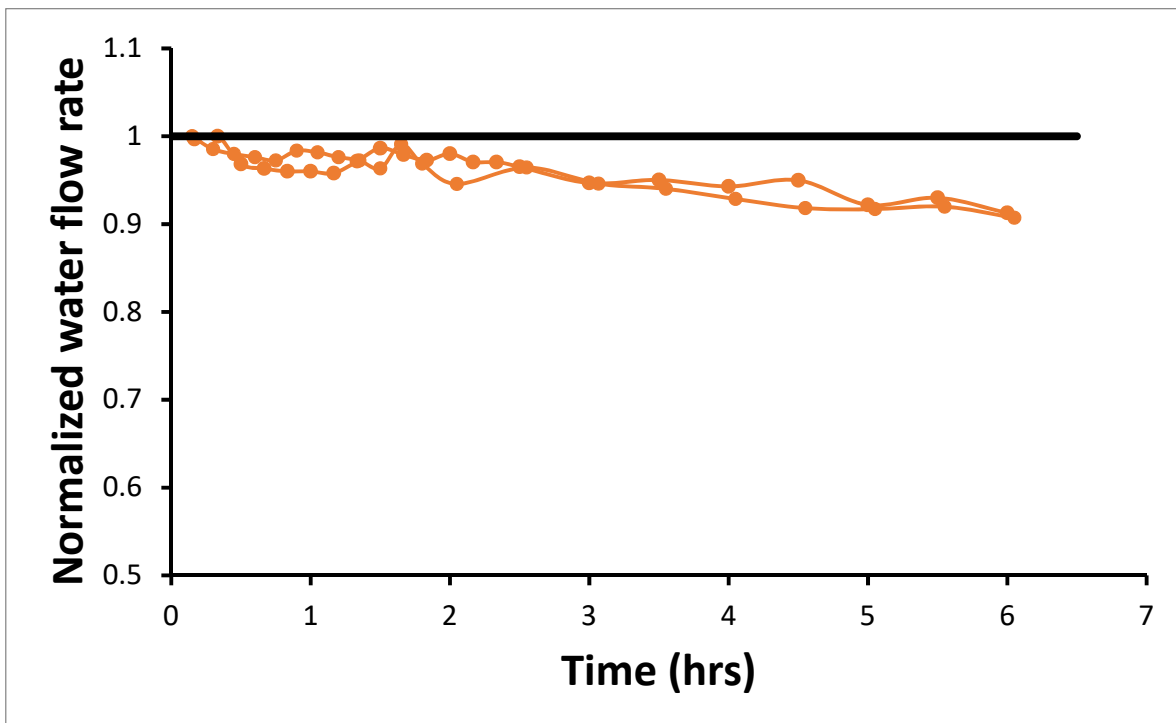


Fig. 4.1: Water flow tests of the hydrophilic channel with fewer crevices (27)

Results of water flow tests conducted on hydrophilic microchannel with a larger number of crevices (54) are as shown in Fig. 4.2. The experiments were conducted twice, and these results are shown. Both the results have little different kinds of water flow reduction as can be observed from the graph as shown. However, the final reduction value of water flow at the end of the experiment is almost the same value of around 0.82. Water flow tests are also conducted on hydrophilic microchannel with no crevices. The comparison of water flow tests in these hydrophilic microchannels for a different number of crevices present is shown in Fig. 4.3.

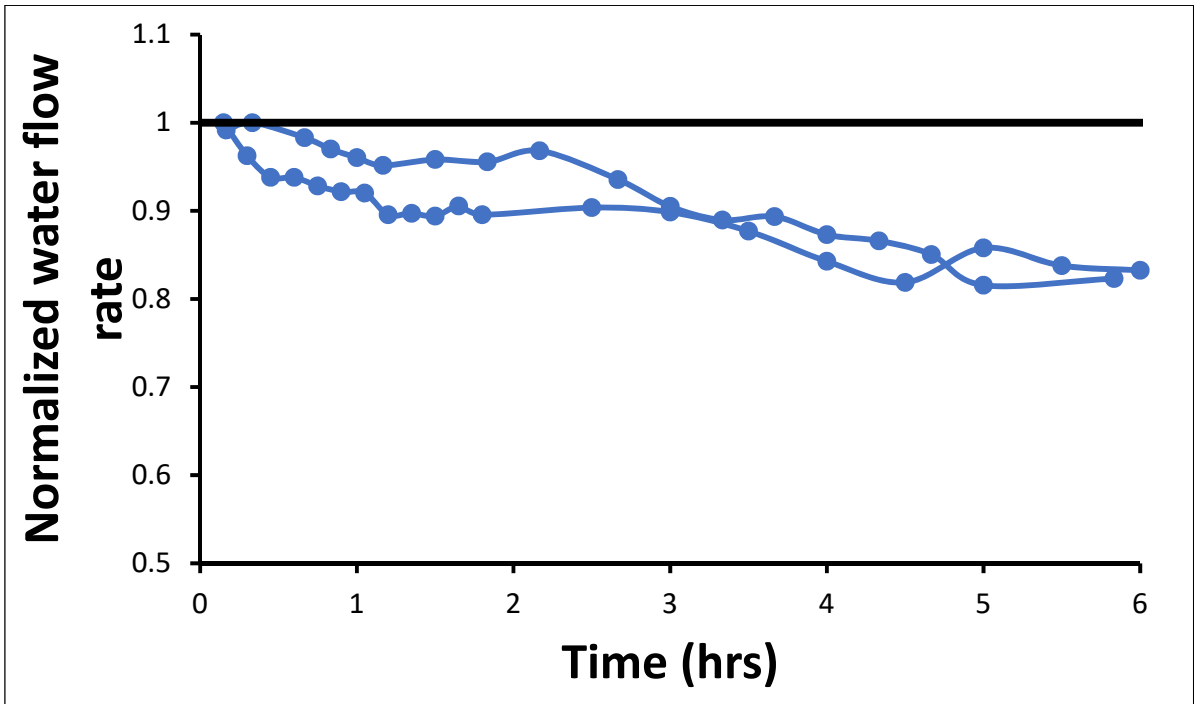


Fig. 4.2: Water flow tests of hydrophilic channel with more crevices (54).

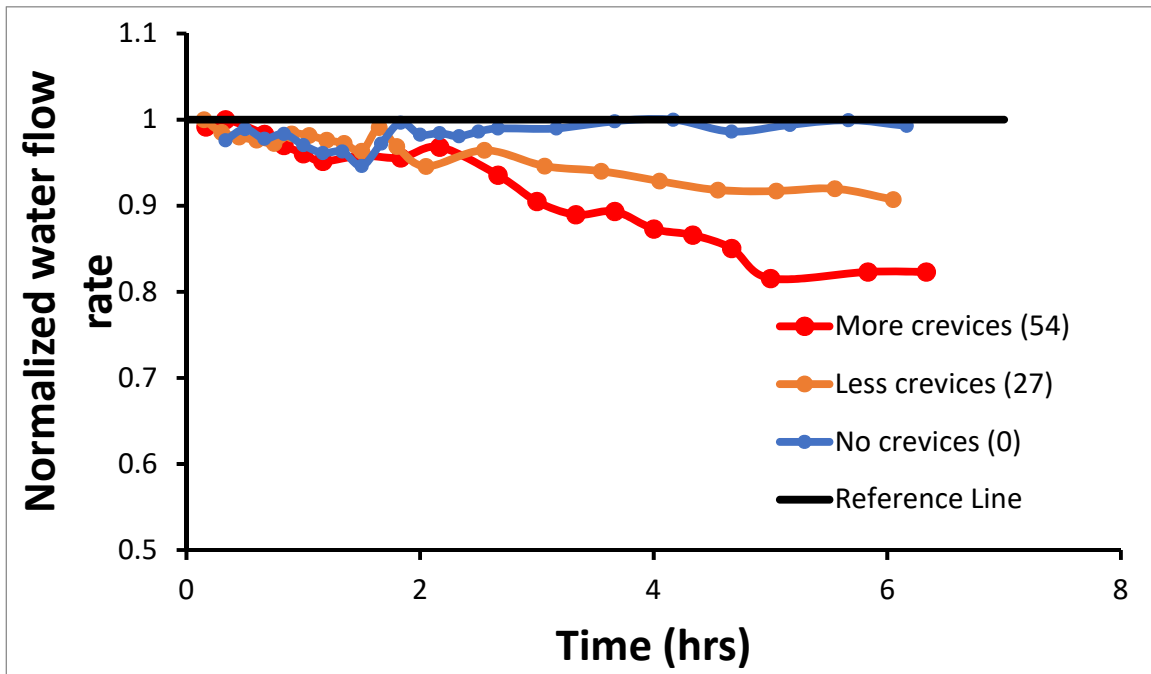


Fig. 4.3: Water flow tests comparison of hydrophilic channels with different numbered crevices.



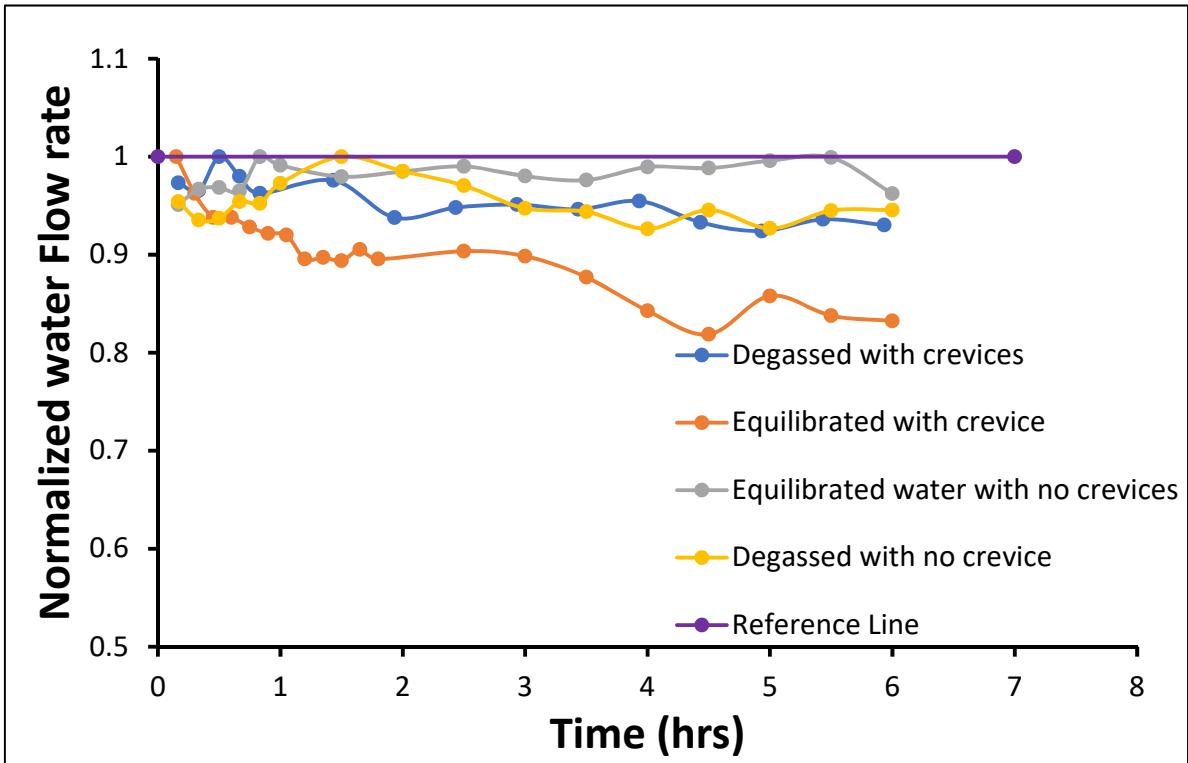


Fig. 4.4: Comparison of water flow tests with different saturated levels of water and with crevices, no crevices.

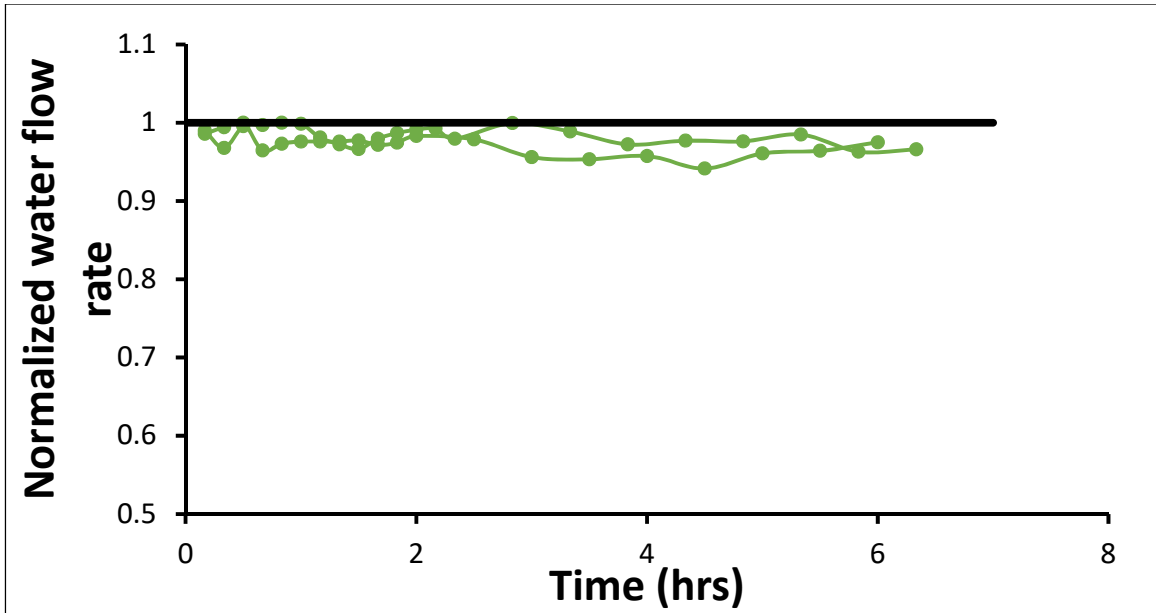


Fig. 4.5: Water flow tests on the hydrophobic channel with the presence of crevices (54)

To understand the effect of crevices and degassed water on the water flow rate in microchannels, a comparison of the results with different combinations are as shown in Fig. 4.4. Further, to probe the effect of the type of surface on the water flow rate, the hydrophobic microchannel is used. In this case, luminescence is used to understand the behavior of water at the crevice locations. The water flow tests are conducted using a hydrophobic channel with a larger number of crevices (54). The experiments were conducted twice, and these results are shown in Fig. 4.5. Both the results have little different kinds of water flow reduction as can be observed from the graph. However, the final reduction value of water flow at the end of the experiment is almost the same around 0.96. Video recording is done for the complete experiment and the images are extracted from the video at each hour. These images for hydrophobic microchannels are shown in Fig. 4.6.

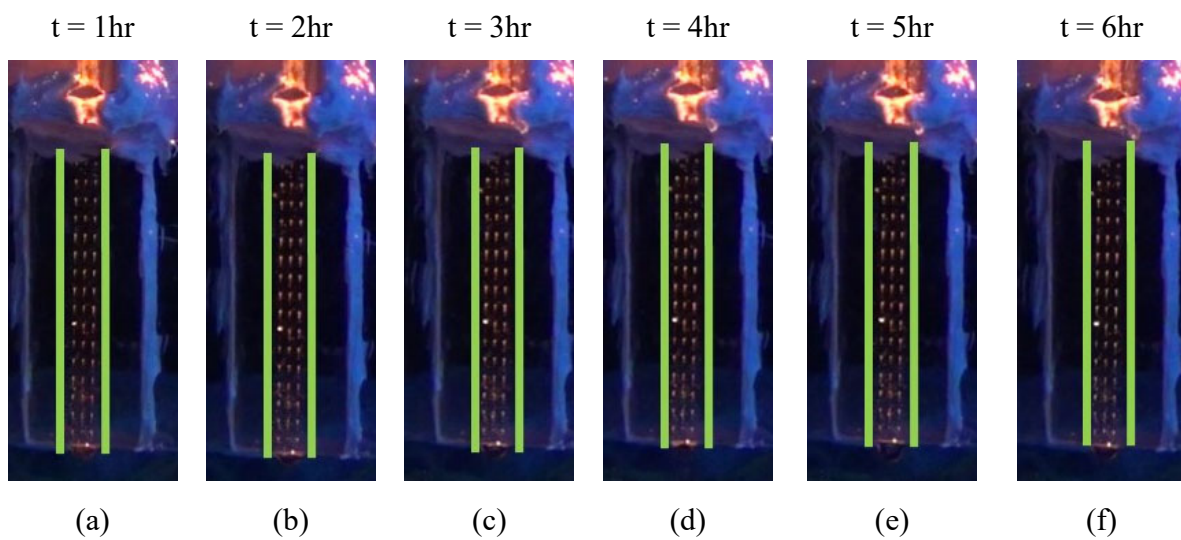


Fig. 4.6: Observation of luminescence in the hydrophobic microchannels at crevices

Finally, the results of the water flow tests obtained by using glass microchannels for different conditions are tabulated in Table 4.1. The parameters considered during the water flow tests are Type of surface, Type of saturated water, Number of crevices, and Size of crevices.

Table 4.1: Summary of water flow tests in microchannels.

Type of Water		Type of Surface		Number of Crevices			Size of Crevices	Result
Equilibrated water	Degassed water	Hydrophilic	Hydrophobic	54	27	0	0.3mm	No decrease
Equilibrated water	Degassed water	Hydrophilic	Hydrophobic	54	27	0	0.3mm	10% decrease
Equilibrated water	Degassed water	Hydrophilic	Hydrophobic	54	27	0	0.3mm	18% decrease
Equilibrated water	Degassed water	Hydrophilic	Hydrophobic	54	27	0	0.3mm	No decrease
Equilibrated water	Degassed water	Hydrophilic	Hydrophobic	54	27	0	0.3mm	No decrease
Equilibrated water	Degassed water	Hydrophilic	Hydrophobic	54	27	0	0.3mm	No decrease

#### 4.1.2 Wide Microchannels

Water flow tests in wide microchannels are also conducted using the same procedure as for narrow microchannels. The result of the water flow test using the wide microchannel for hydrophilic and hydrophobic channels is as shown in Fig. 4.7 and Fig. 4.9 respectively. In this case, bubble formation at the crevices is viewed by direct observation using a video camera, and the pictures extracted for the case of the hydrophilic microchannel is shown in Fig. 4.8 and for hydrophobic channels in Fig. 4.10. The bubble volume changes at the crevice portion and the %change in the volume are tabulated in Table 4.2 and Table 4.3 for hydrophilic and hydrophobic channels respectively.

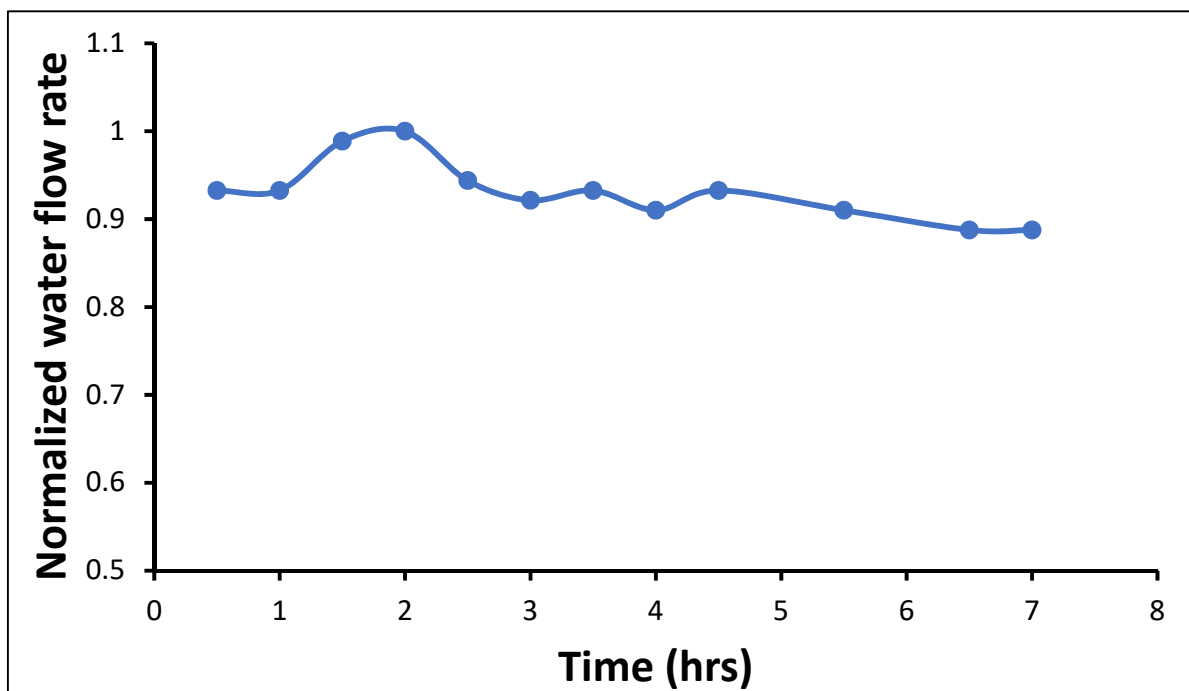


Fig. 4.7: Water flow tests of wide hydrophilic microchannels

Table 4.2: % of volume decrease in the bubble on the hydrophilic surface.

Bubble 1 (from top)	-42.96	-50.70	-61.27	-61.27	-70.42	-71.83
Bubble 2	-28.17	-28.17	-43.66	-50.00	-48.59	-48.59
Bubble 3	-22.71	-32.67	-38.25	-40.24	-42.63	-44.22
Bubble 4	-18.06	-29.68	-36.13	-35.48	-38.71	-39.35

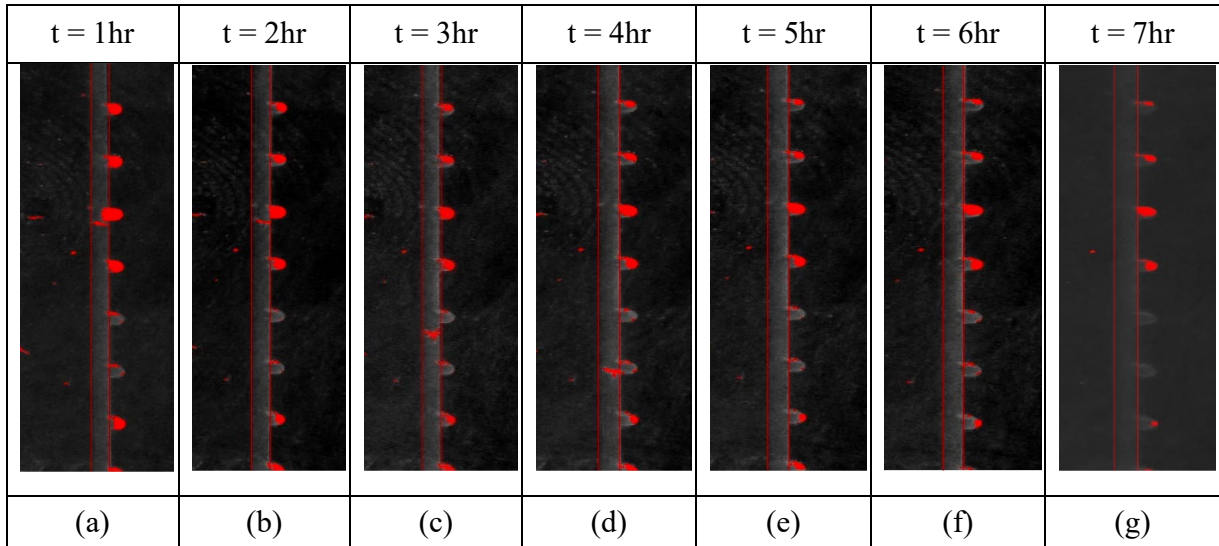


Fig. 4.8: Sequence of images for hydrophilic wide microchannel

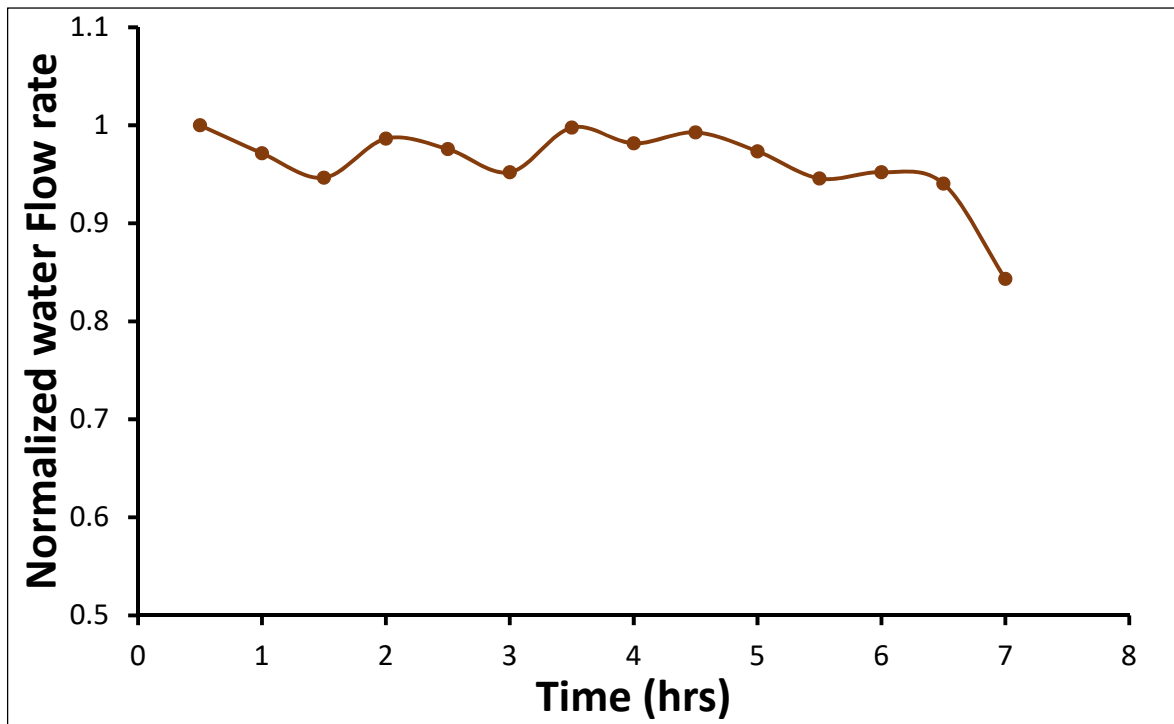


Fig. 4.9: Water flow tests of wide hydrophobic microchannels

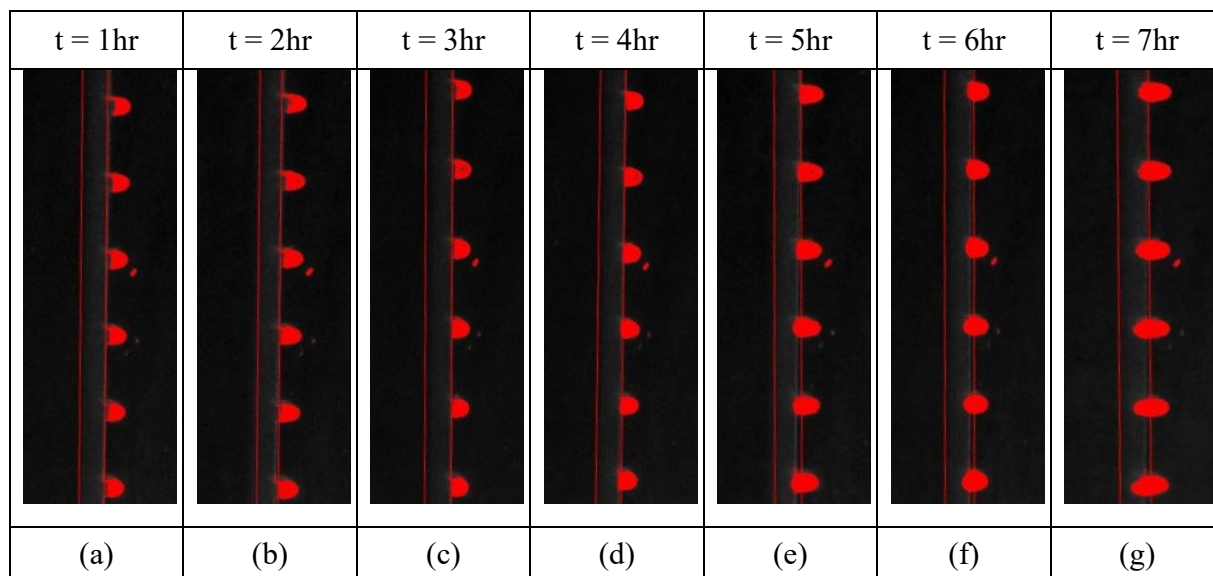


Fig. 4.10: Sequence of images for hydrophobic wide microchannel

Table 4.3: % of volume increase in the bubble on hydrophobic surface.

Bubble 1 (from top)	0.61	6.67	18.79	27.27	39.39	58.79
Bubble 2	4.29	9.82	24.54	31.29	46.01	55.83
Bubble 3	2.37	9.47	23.08	31.36	48.52	63.31
Bubble 4	1.75	7.60	23.39	37.43	53.22	67.84
Bubble 5	1.23	14.72	22.09	34.36	48.47	66.26
Bubble 6	2.40	17.96	31.74	43.11	68.86	84.43

## 4.2 Results of Velocity Profile Analysis

The total number of velocity profiles analyzed for the understanding the attenuation of shear rate and velocity profiles are 50. The velocity profiles considered here are only partially sheared flows as the fully sheared flows have the boundary effects on the actual flow behavior of the material. Normally, the velocity profiles are plotted starting from the inner rotating rotor. However, here we tried to plot the velocity profiles from the flow stop end (radius at which the velocity of the flow is 0). The plotted velocity profiles are as shown below.

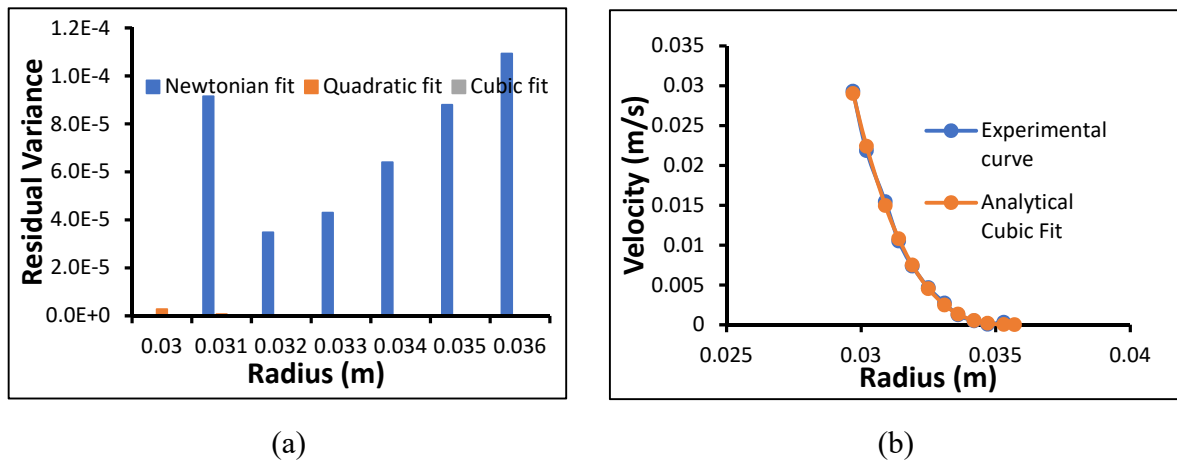
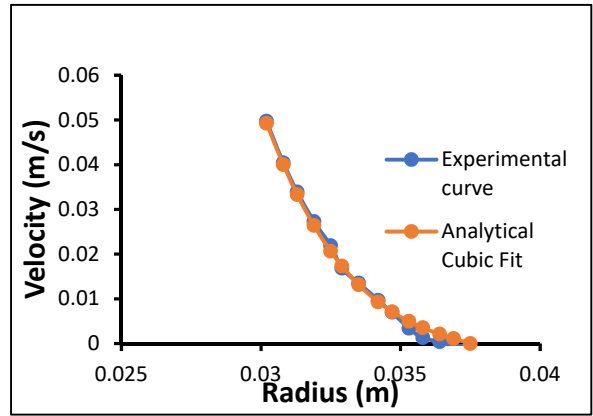
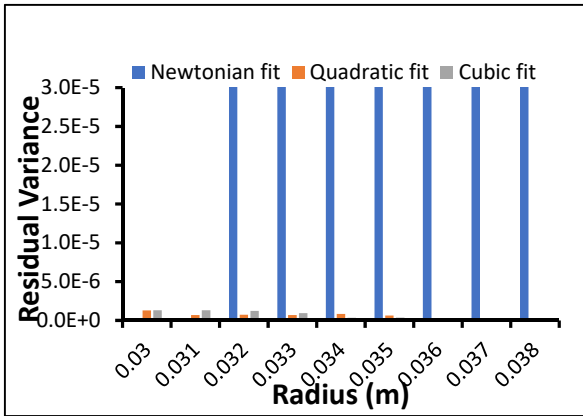


Fig. 4.11: Cornstarch1 10RPM (a) Residual Variance (b) Analytical fit of the Non-Newtonian region of velocity profile.

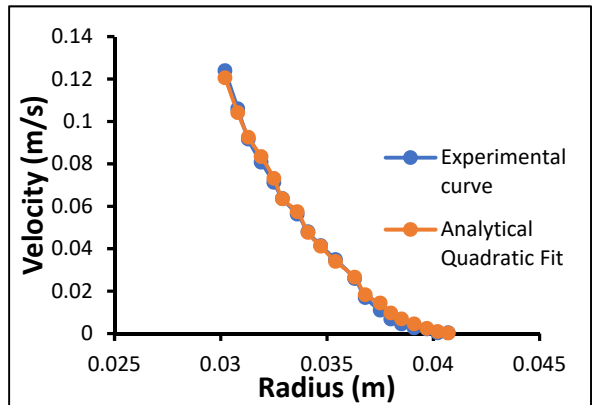
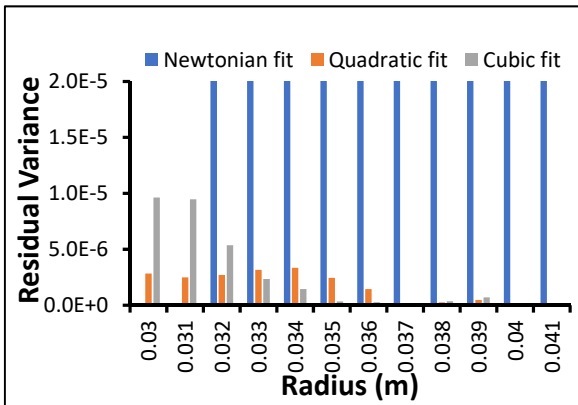
Residual variance of each velocity profile is calculated using Newtonian fit from rotor side and Non-Newtonian fit from the flow stop end, and the velocity profile is fit based on the understanding of residual variance. The velocity profiles with decreasing and increasing residual variance show Newtonian and Non-Newtonian regions. But this is misleading as the Non-Newtonian fit gives much less residual variance. Only decreasing or only increasing residual variance patterns of velocity profiles have only Non-Newtonian region. Alpha value variation of each velocity profile is plotted to know the extent of non-linearity of the material. The alpha value variation and the actual velocity profiles along with the perfect fit are plotted as shown below for each material and RPM value.



(a)

(b)

Fig. 4.12: Cornstarch1 20RPM (a) Residual Variance (b) Analytical fit of the Non-Newtonian region of velocity profile.



(a)

(b)

Fig. 4.13: Cornstarch1 40RPM (a) Residual Variance (b) Analytical fit of the Non-Newtonian region of velocity profile.



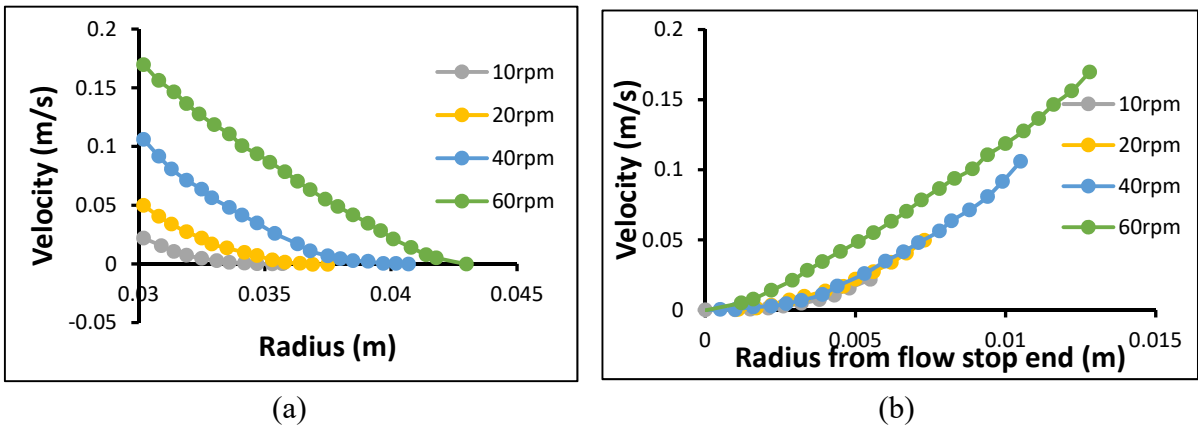


Fig. 4.14: Velocity Profiles of Cornstarch1 (a) From the rotor end (b) From the flow stop end

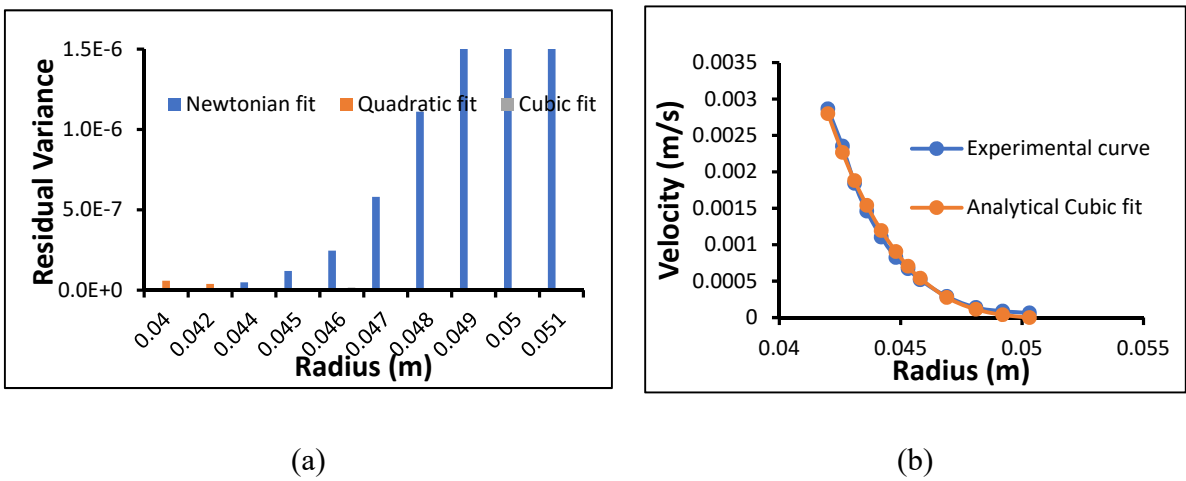
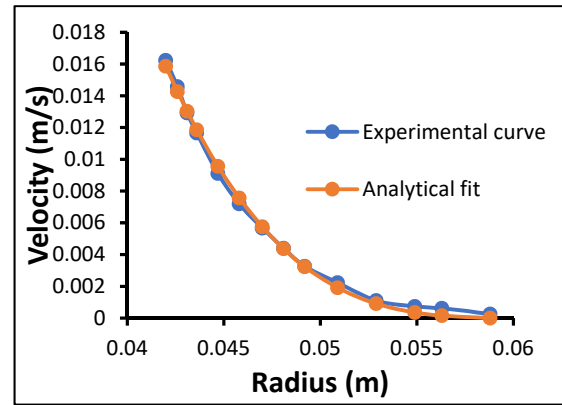
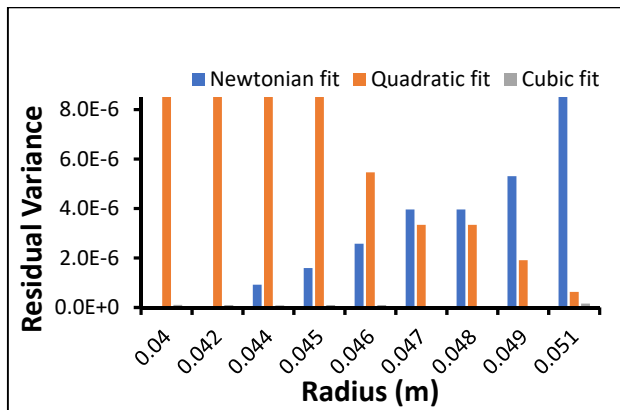


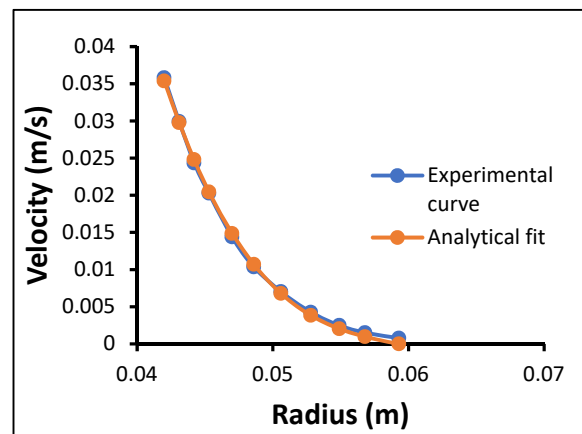
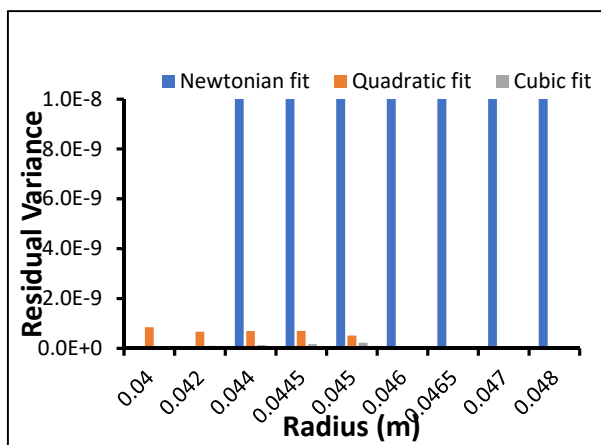
Fig. 4.15: Oil Emulsion 1RPM (a) Residual variance (b) Analytical fit of Non-Newtonian Region



(a)

(b)

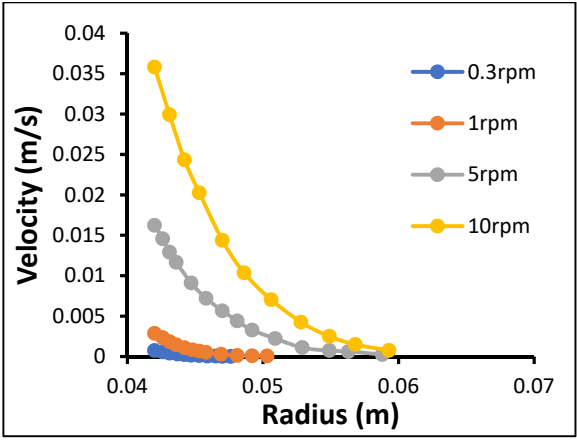
Fig. 4.16: Oil Emulsion 5RPM (a) Residual variance (b) Analytical fit of Non-Newtonian Region



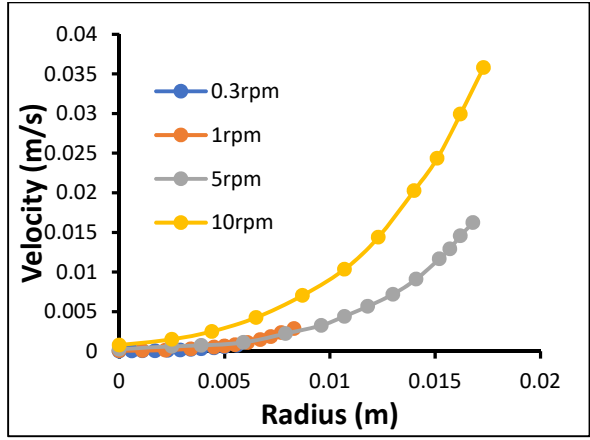
(a)

(b)

Fig. 4.17: Oil Emulsion 0.3RPM (a) Residual variance (b) Analytical fit of Non-Newtonian Region



(a)



(b)

Fig. 4.18: Velocity Profiles of Silicon Oil Emulsion (a) From the rotor end  
(b) From the flow stop end

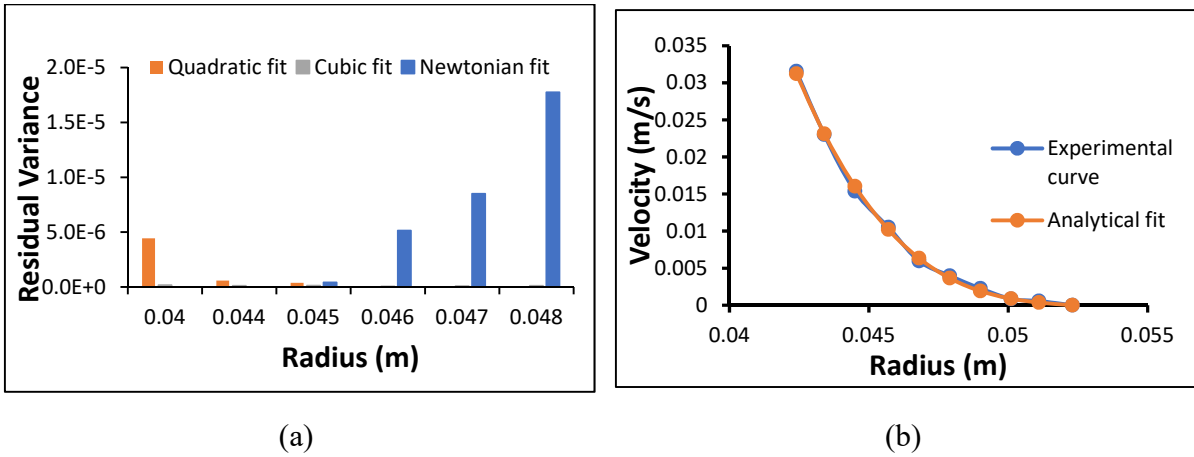


Fig. 4.19: Cacl2 10RPM (a) Residual variance (b) Analytical fit of Non-Newtonian Region

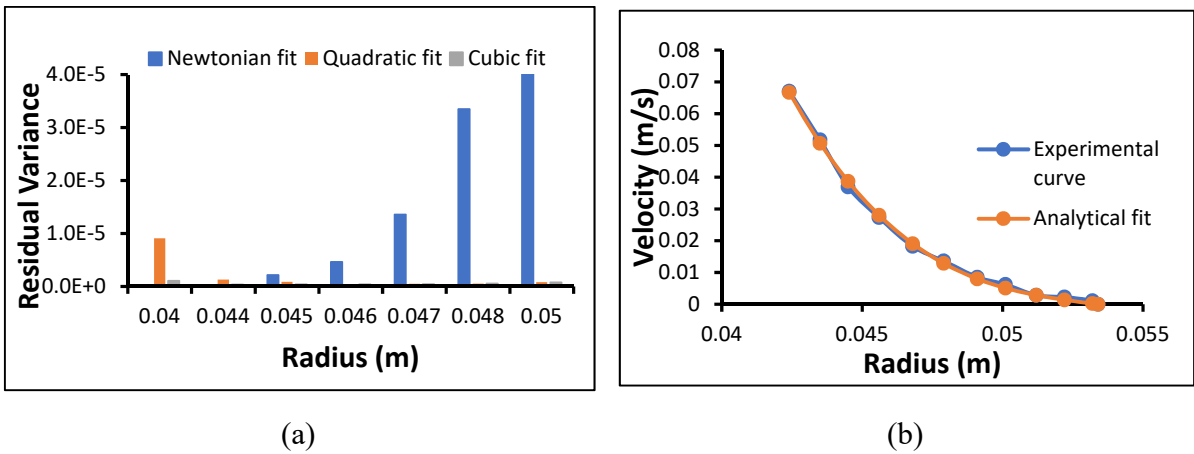


Fig. 4.20: Cacl2 20RPM (a) Residual variance (b) Analytical fit of Non-Newtonian Region

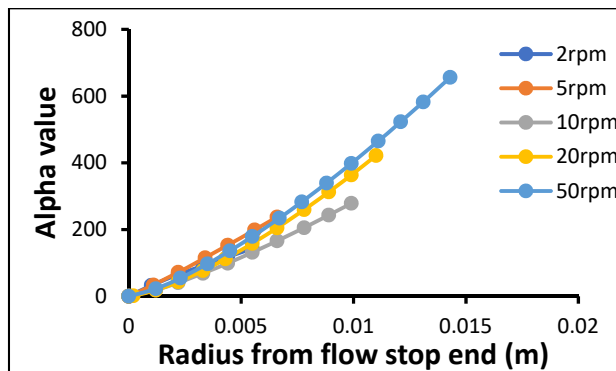
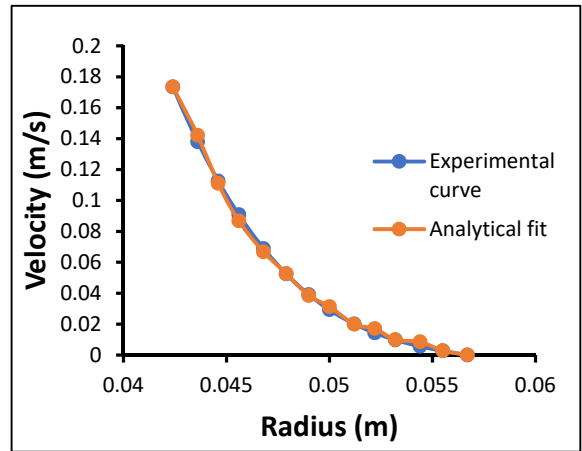
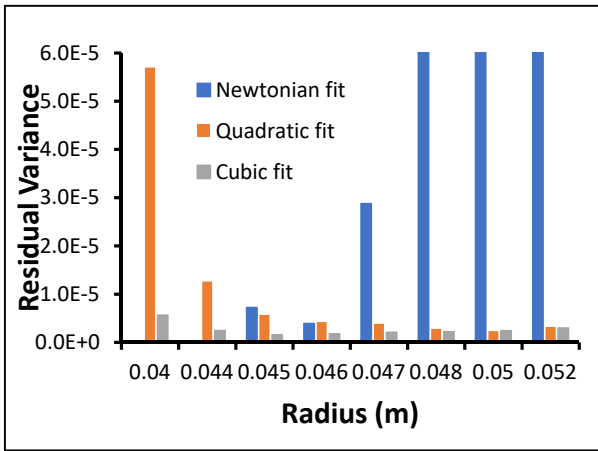


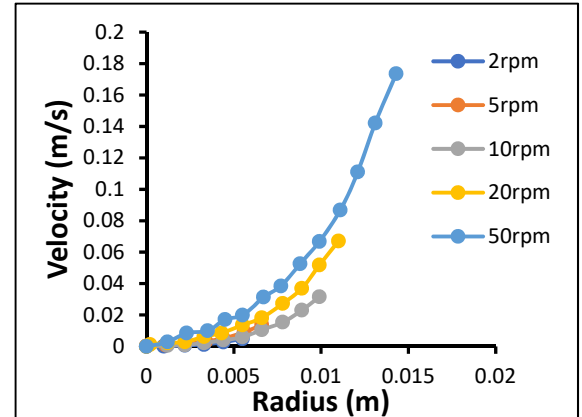
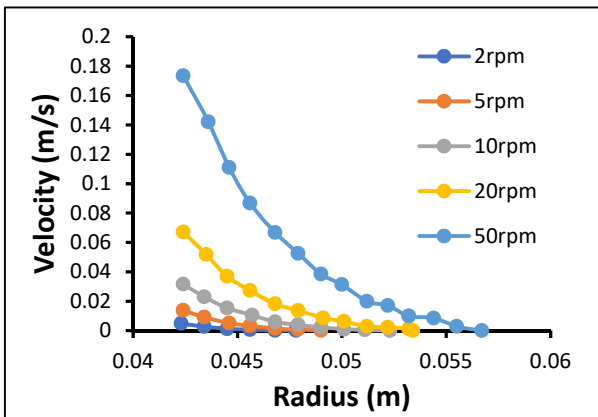
Fig. 4.21: Alpha value variation of Cacl2



(a)

(b)

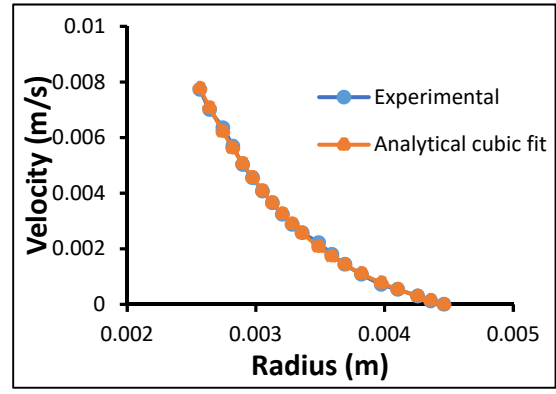
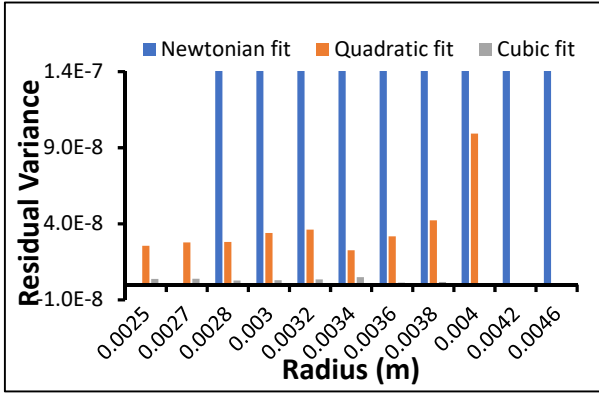
Fig. 4.22: Cacl2 50RPM (a) Residual variance (b) Analytical fit of Non-Newtonian Region



(a)

(b)

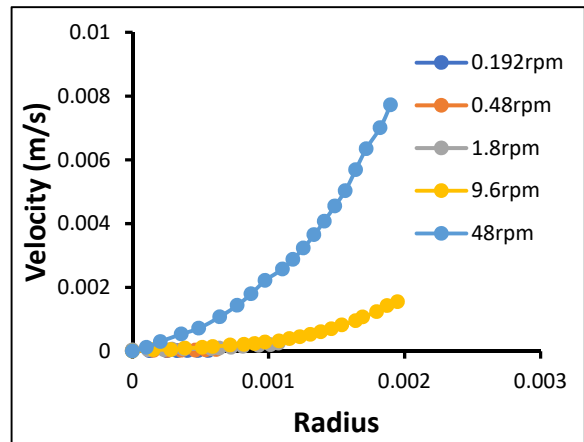
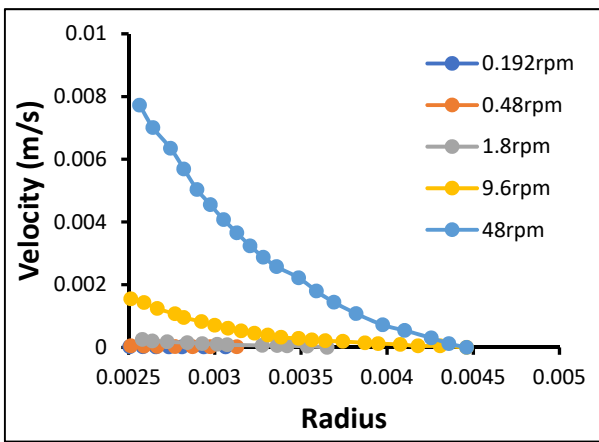
Fig. 4.23: Velocity Profiles of Cacl2 (a) From the rotor end (b) From the flow stop end



(a)

(b)

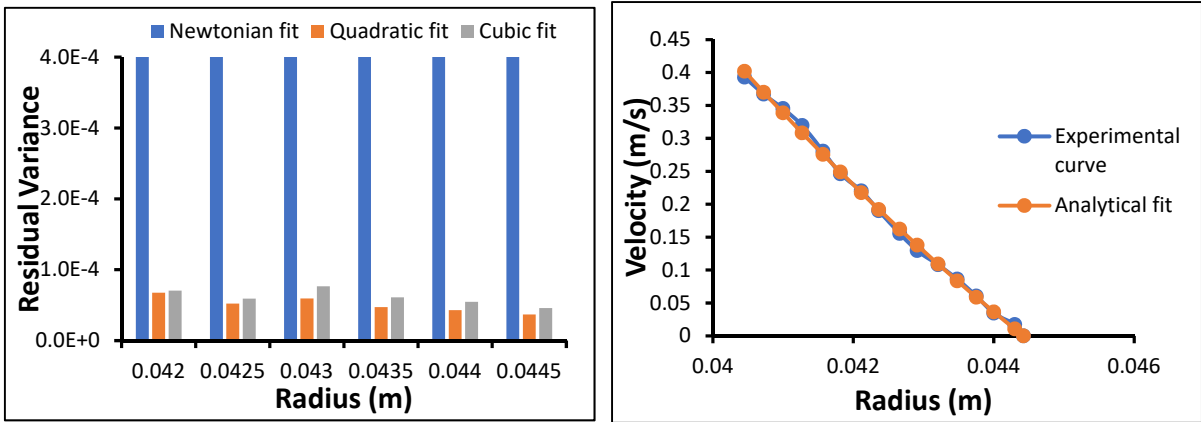
Fig. 4.24: PMMA 48RPM (a) Residual Variance (b) Analytical fit of the Non-Newtonian region of velocity profile.



(a)

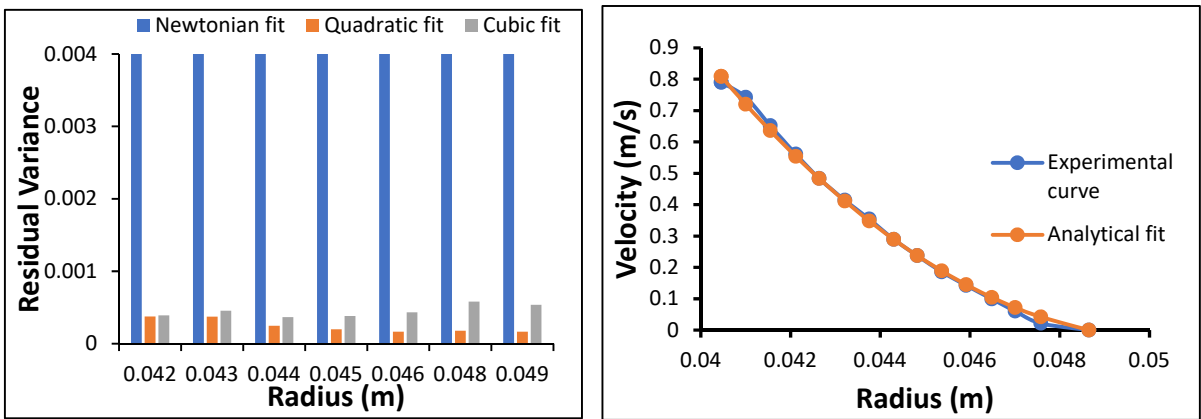
(b)

Fig. 4.25: Velocity Profiles of PMMA (a) From the rotor end (b) From the flow stop end



(a) (b)

Fig. 4.26: Drilling Mud 10RPM (a) Residual variance (b) Analytical fit of Non-Newtonian Region



(a) (b)

Fig. 4.27: Drilling Mud 20RPM (a) Residual variance (b) Analytical fit of Non-Newtonian Region

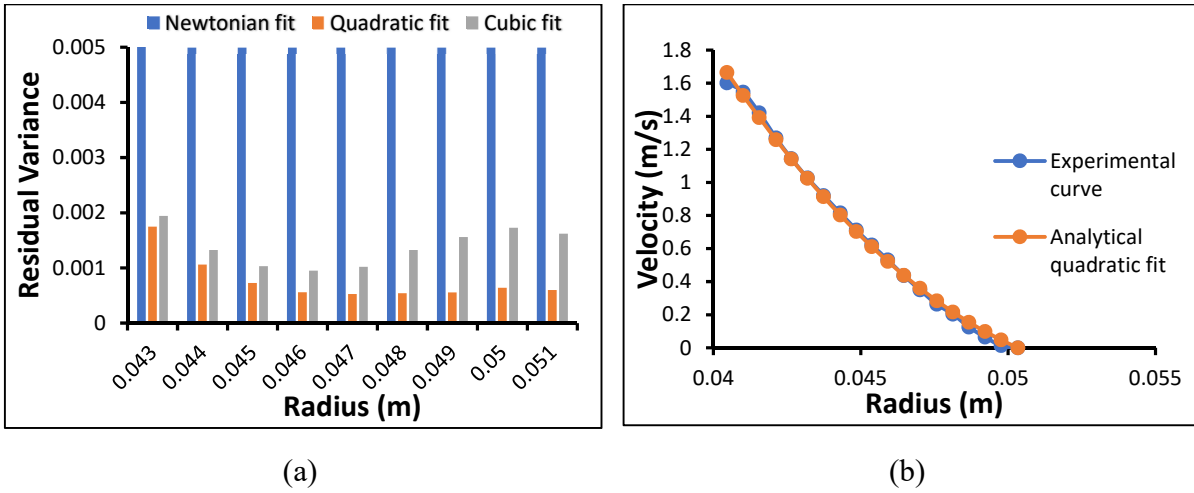


Fig. 4.28: Drilling Mud 40RPM (a) Residual variance (b) Analytical fit of Non-Newtonian Region

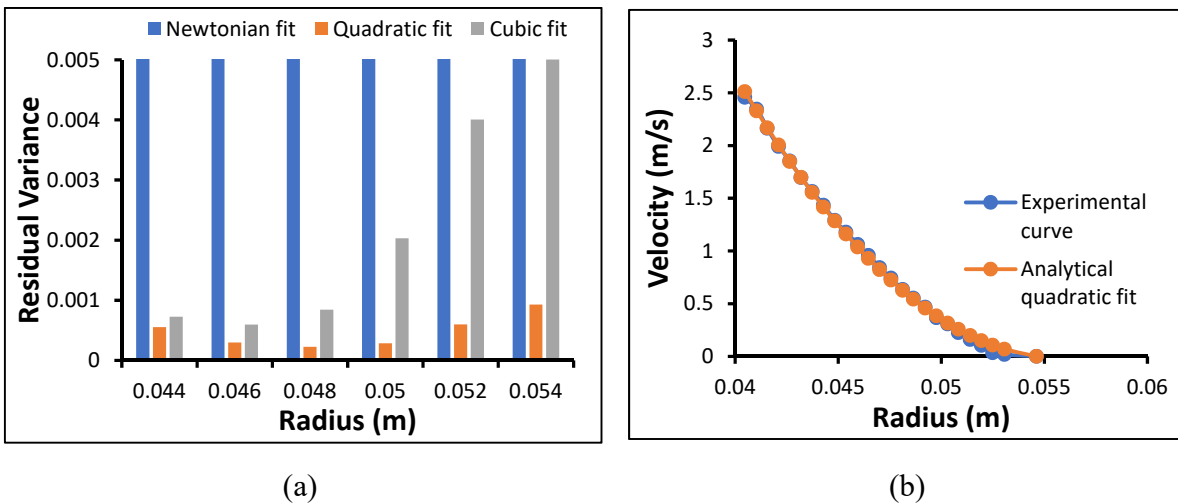
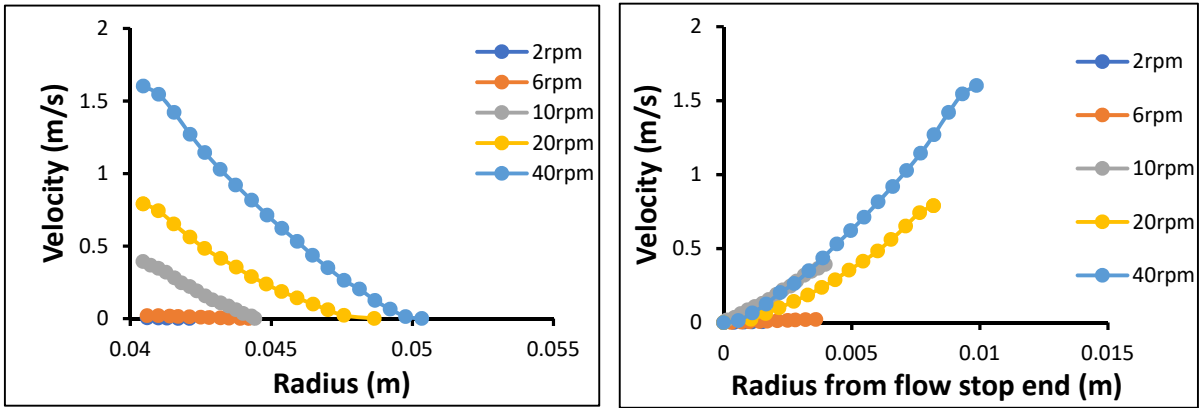


Fig. 4.29: Drilling Mud 60RPM (a) Residual variance (b) Analytical fit of Non-Newtonian Region





(a)

(b)

Fig. 4.30: Velocity Profiles of Drilling mud (a) From the rotor end (b) From the flow stop end

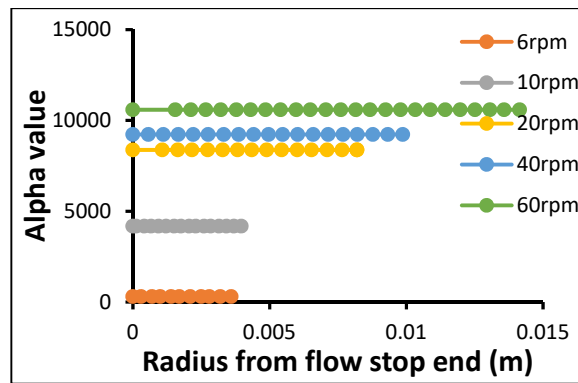
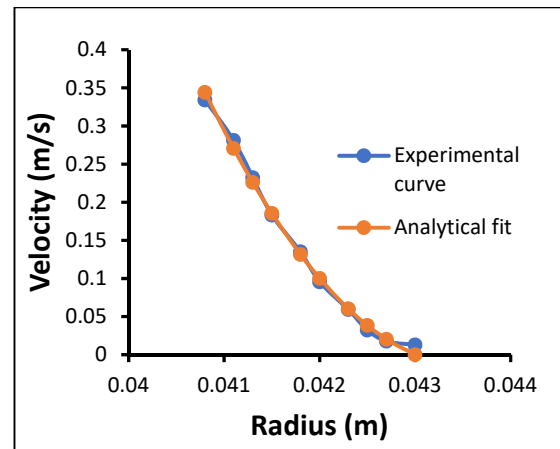
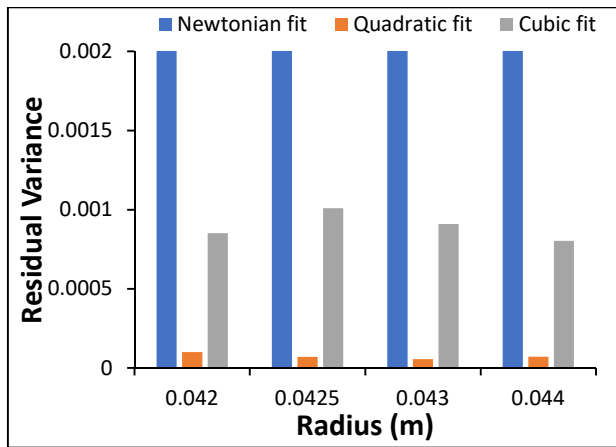


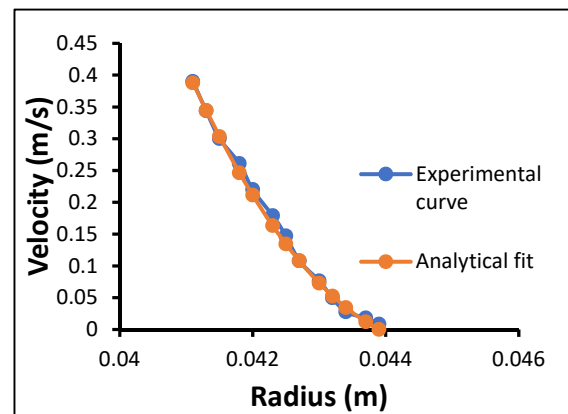
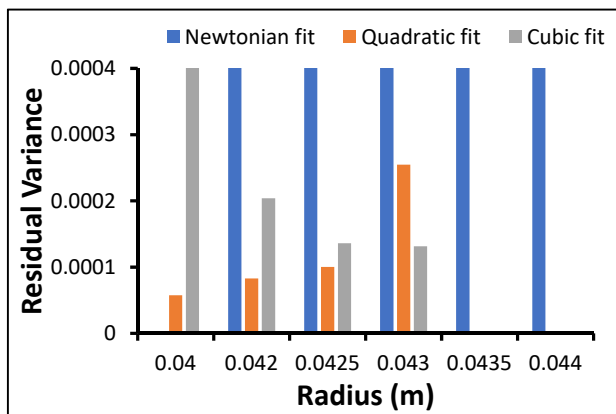
Fig. 4.31: Alpha value variation of Drilling mud



(a)

(b)

Fig. 4.32: Surfactant 40RPM (a) Residual variance (b) Analytical fit of Non-Newtonian Region



(a)

(b)

Fig. 4.33: Surfactant 50RPM (a) Residual variance (b) Analytical fit of Non-Newtonian Region

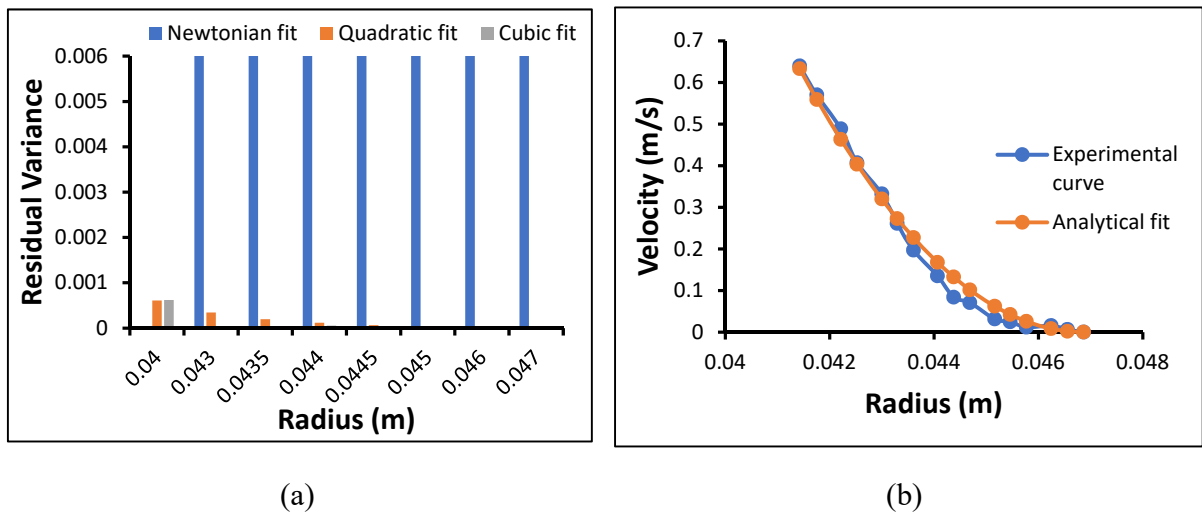


Fig. 4.34: Surfactant100RPM (a) Residual variance (b) Analytical fit of Non-Newtonian Region

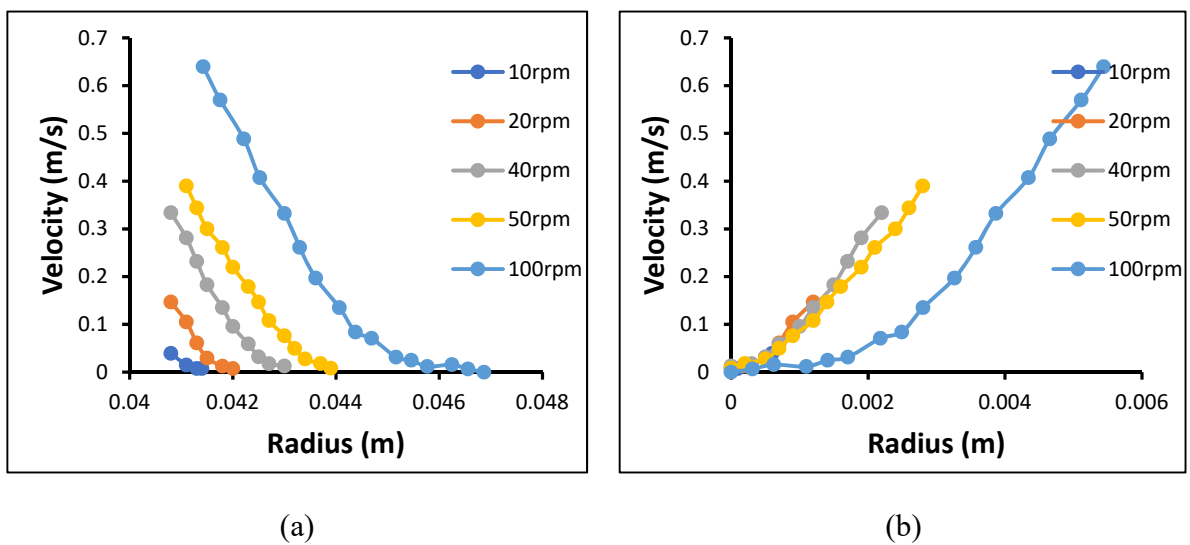


Fig. 4.35: Velocity Profiles of Surfactant (a) From the rotor end (b) From the flow stop end

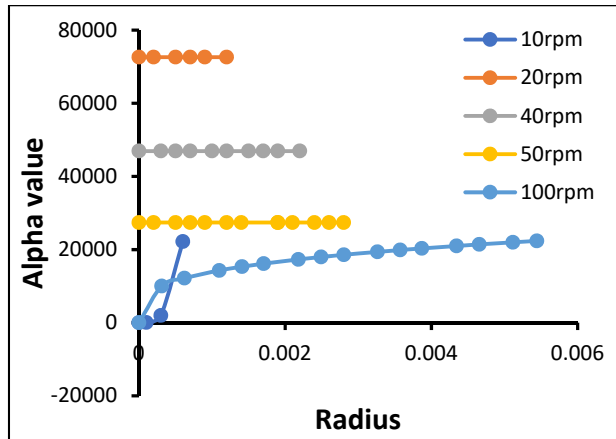


Fig. 4.36: Alpha value variation of Surfactant

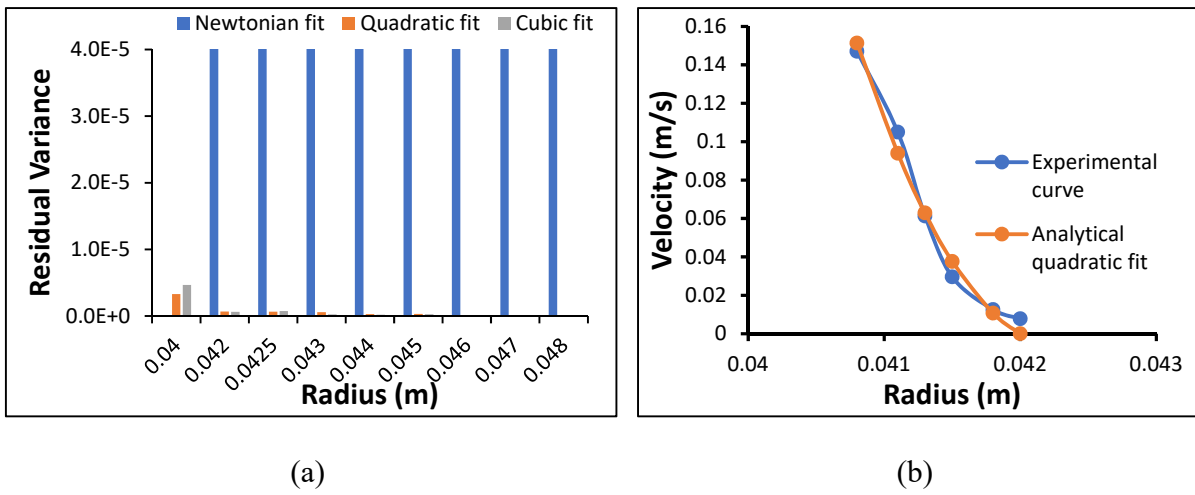
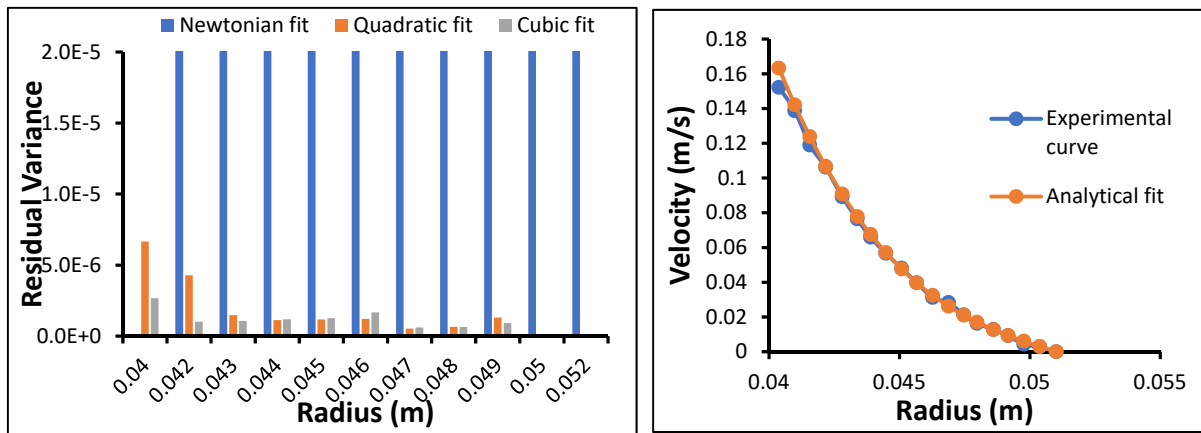


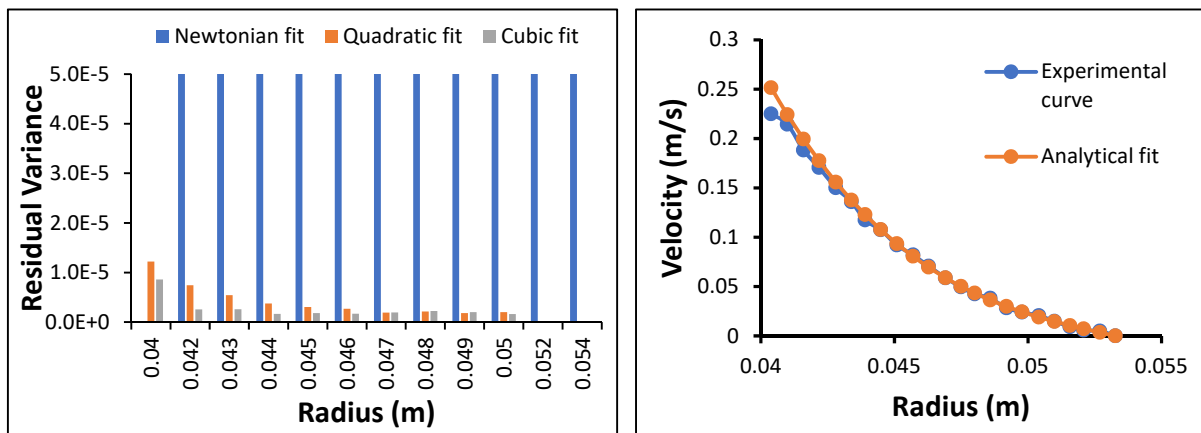
Fig. 4.37: Shaving Foam 20RPM (a) Residual Variance (b)Analytical fit of the Non-Newtonian region of velocity profile.



(a)

(b)

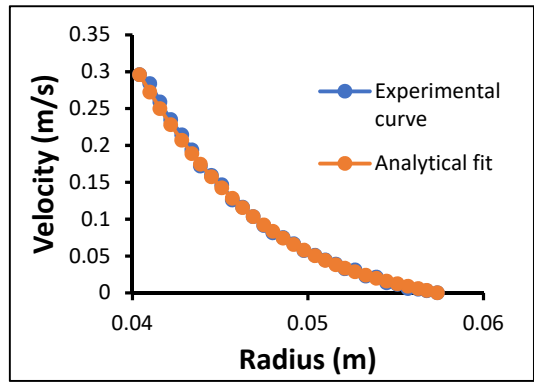
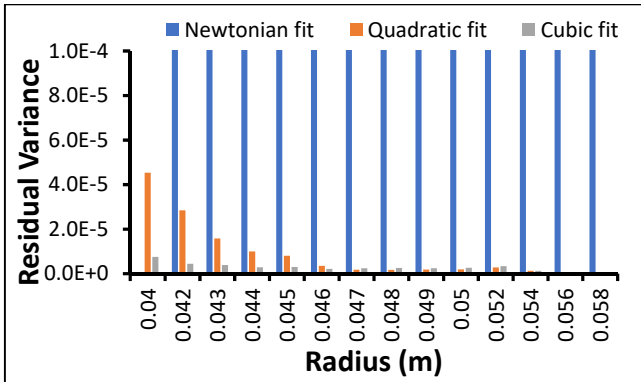
Fig. 4.38: Shaving Foam 40RPM (a) Residual Variance (b)Analytical fit of the Non-Newtonian region of velocity profile.



(a)

(b)

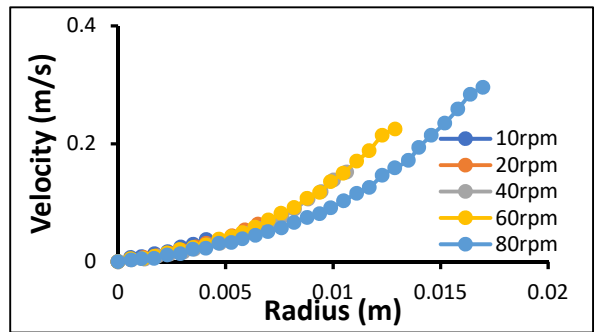
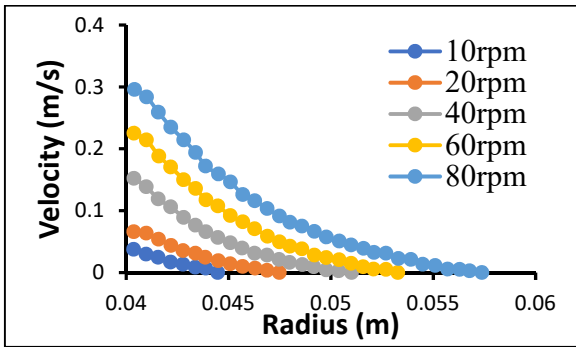
Fig. 4.39: Shaving Foam 60RPM (a) Residual Variance (b)Analytical fit of the Non-Newtonian region of velocity profile.



(a)

(b)

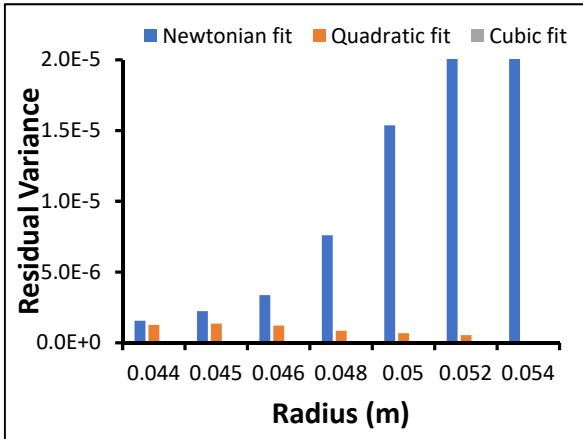
Fig. 4.40: Shaving Foam 80RPM (a) Residual Variance (b)Analytical fit of the Non-Newtonian region of velocity profile.



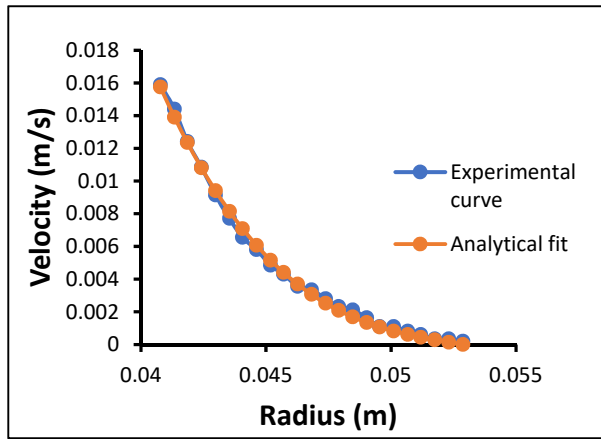
(a)

(b)

Fig. 4.41: Velocity Profiles of Shaving Foam (a) From the rotor end (b) From the flow stop end

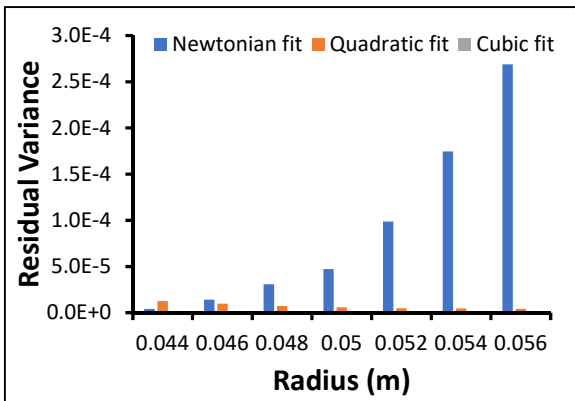


(a)

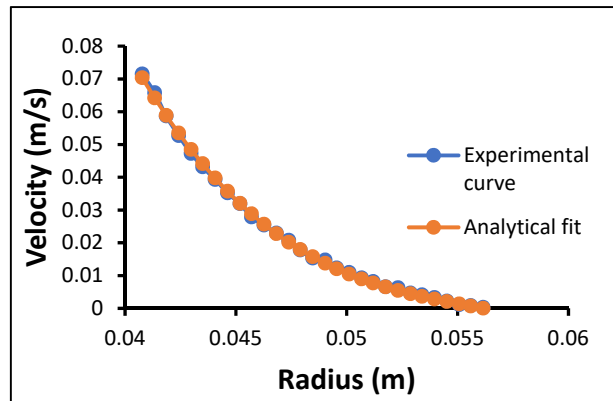


(b)

Fig. 4.42: Mayonnaise 5RPM (a) Residual variance (b) Analytical fit of Non-Newtonian Region



(a)



(b)

Fig. 4.43: Mayonnaise 20RPM (a) Residual variance (b) Analytical fit of Non-Newtonian Region

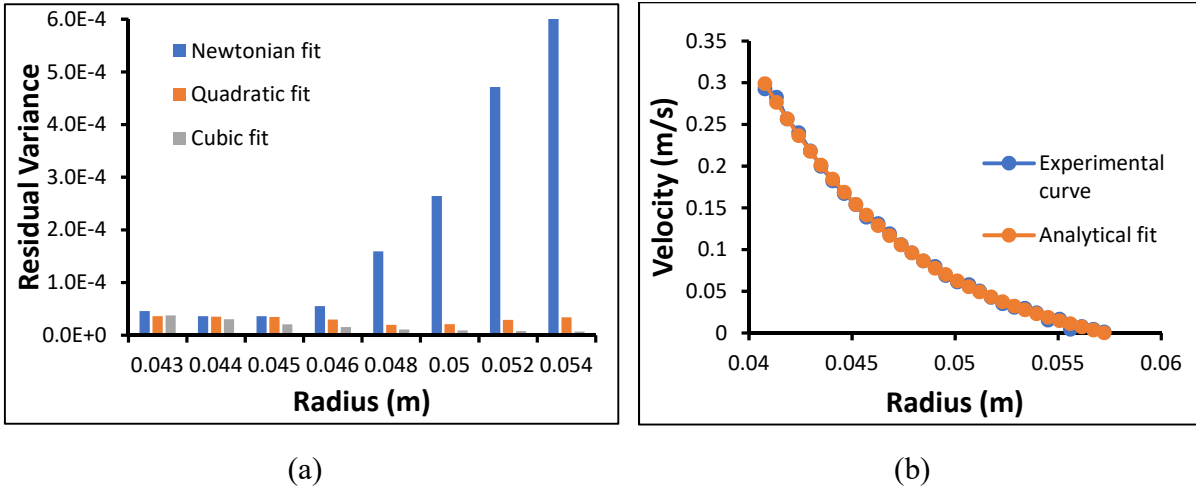


Fig. 4.44: Mayonnaise 80RPM (a) Residual variance (b) Analytical fit of Non-Newtonian Region

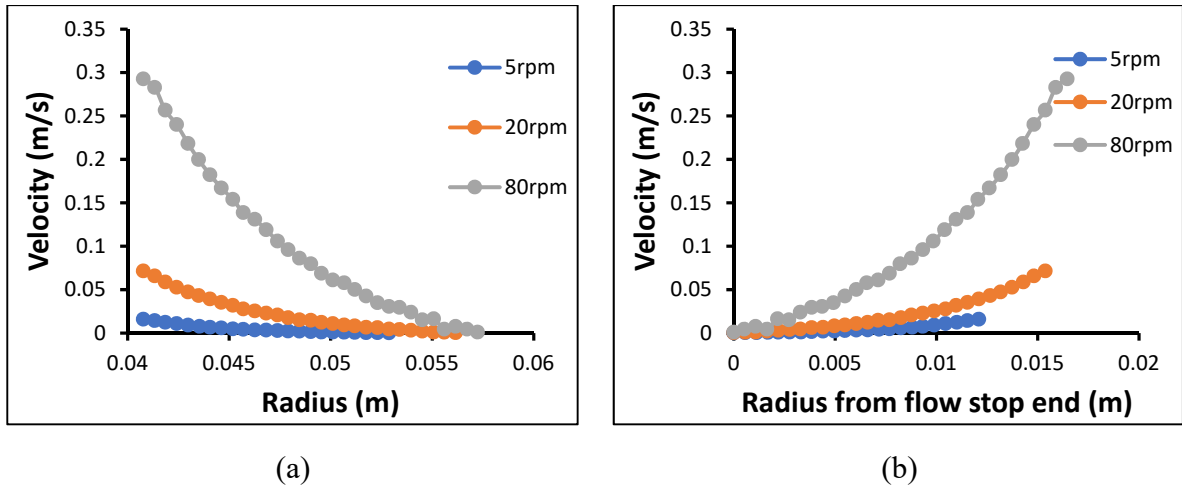


Fig. 4.45: Velocity Profiles (a) From the rotor end (b) From the flow stop end

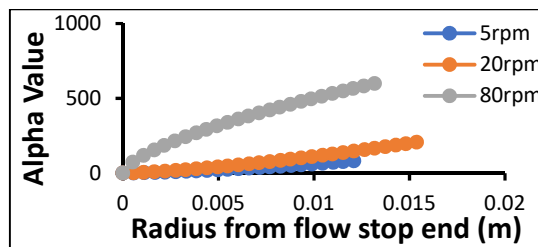
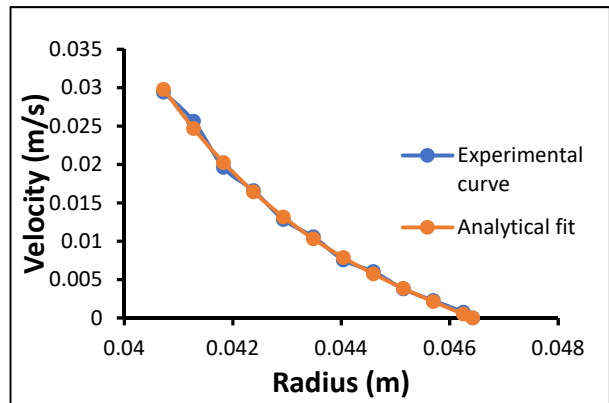
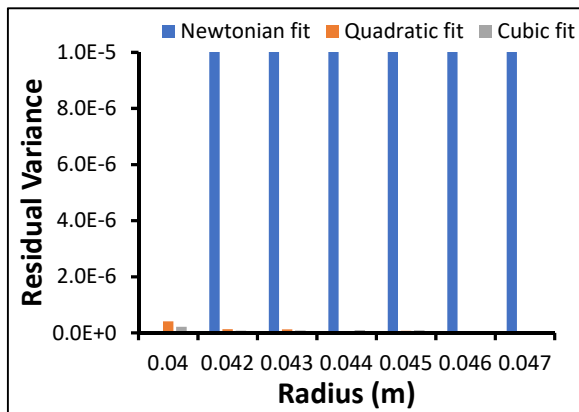


Fig. 4.46: Alpha value variation of Mayonnaise

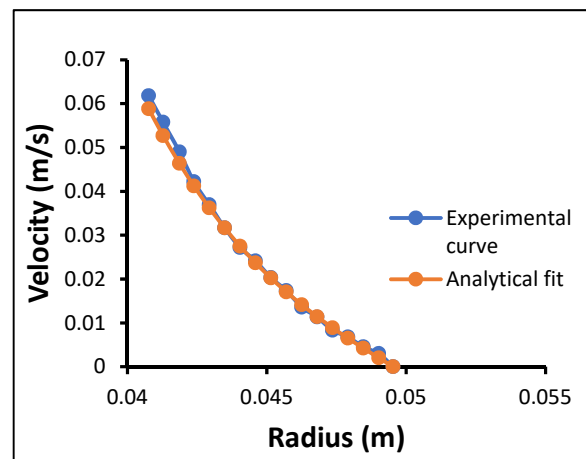
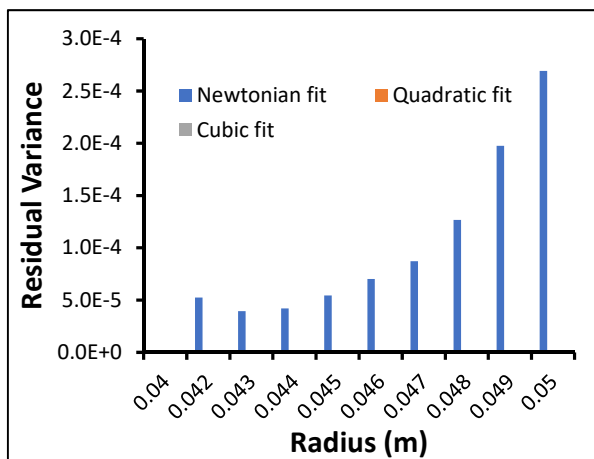




(a)

(b)

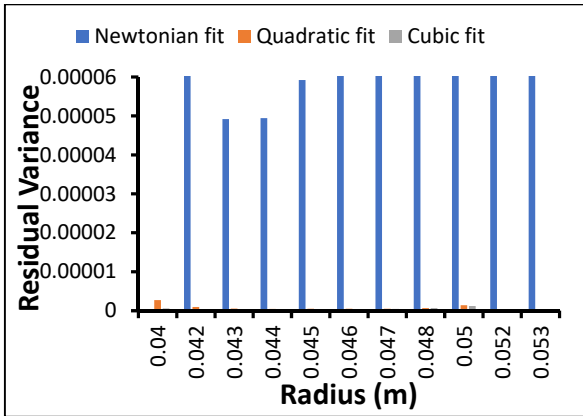
Fig. 4.47: Bentonite 10RPM (a) Residual variance (b) Analytical fit of Non-Newtonian Region



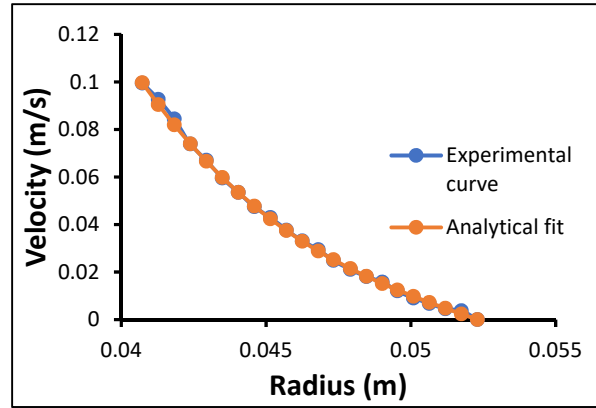
(a)

(b)

Fig. 4.48: Bentonite 20RPM (a) Residual variance (b) Analytical fit of Non-Newtonian Region

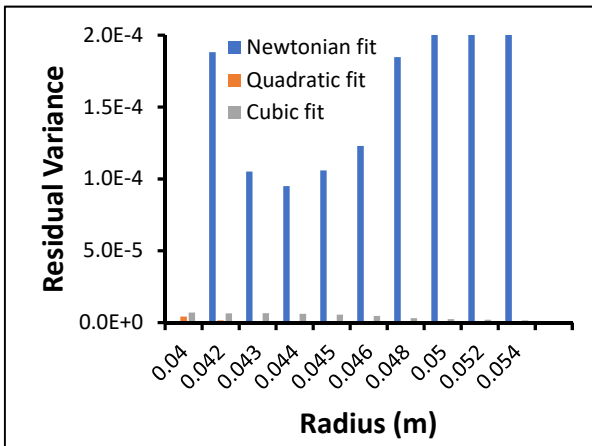


(a)

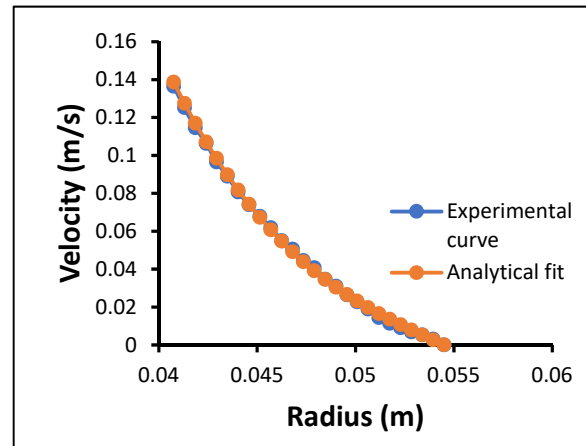


(b)

Fig. 4.49: Bentonite 30RPM (a) Residual variance (b) Analytical fit of Non-Newtonian Region

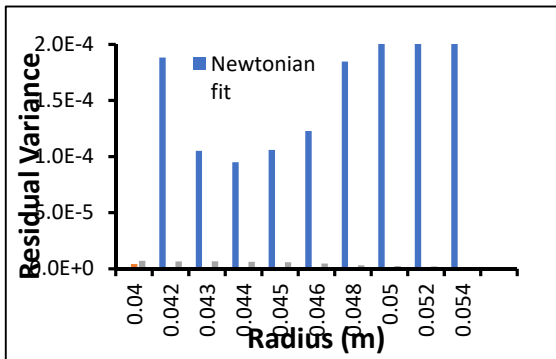


(a)

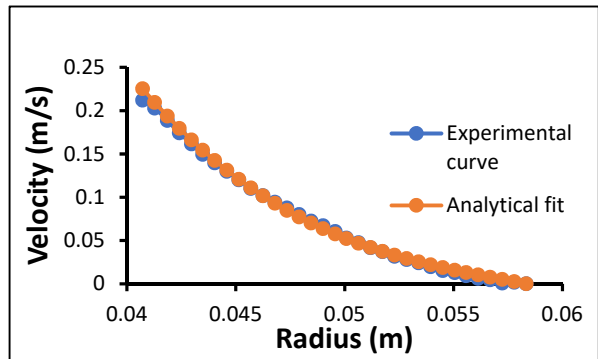


(b)

Fig. 4.50: Bentonite 40RPM (a) Residual variance (b) Analytical fit of Non-Newtonian Region

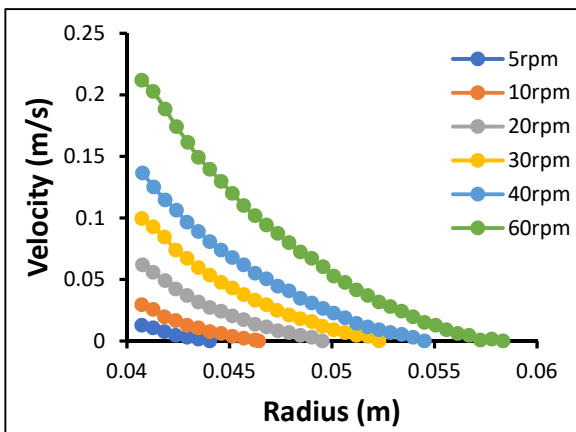


(a)

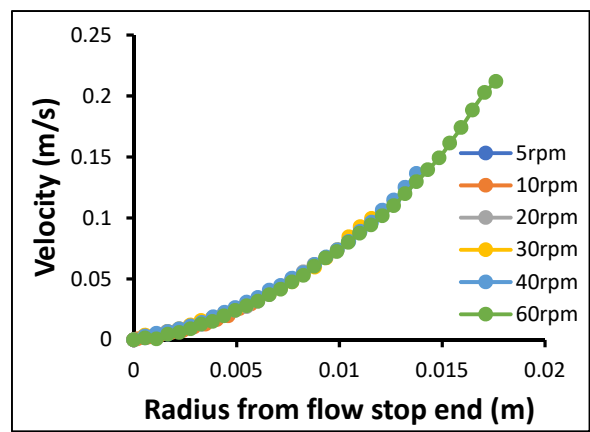


(b)

Fig. 4.51: Bentonite 60RPM (a) Residual variance (b) Analytical fit of Non-Newtonian Region



(a)



(b)

Fig. 4.52: Velocity Profiles Bentonite (a) From the rotor end (b) From the flow stop end

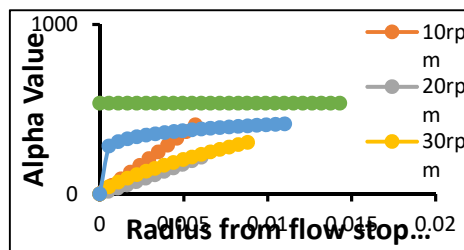
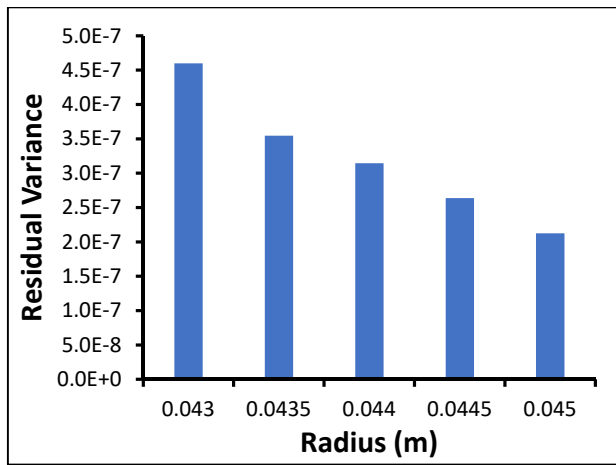
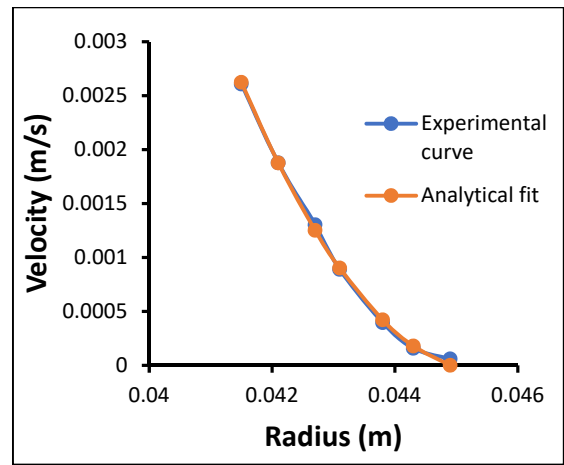


Fig. 4.53: Alpha value variation of Bentonite

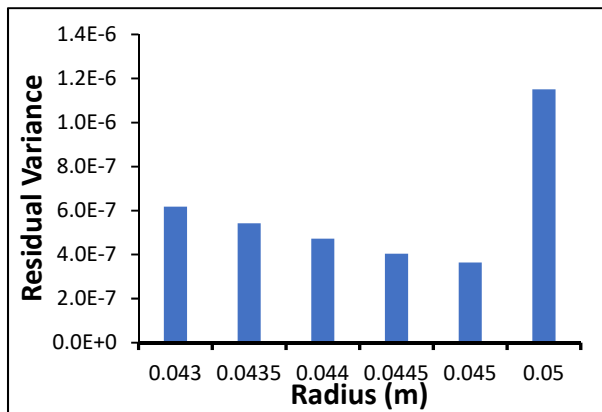


(a)

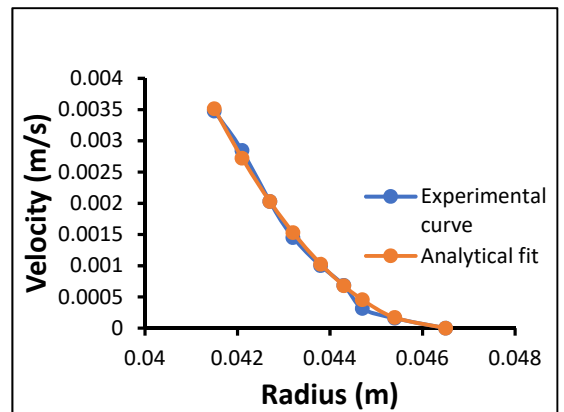


(b)

Fig. 4.54: Cornstarch2 0.6RPM (a) Residual variance (b) Analytical fit of Non-Newtonian Region

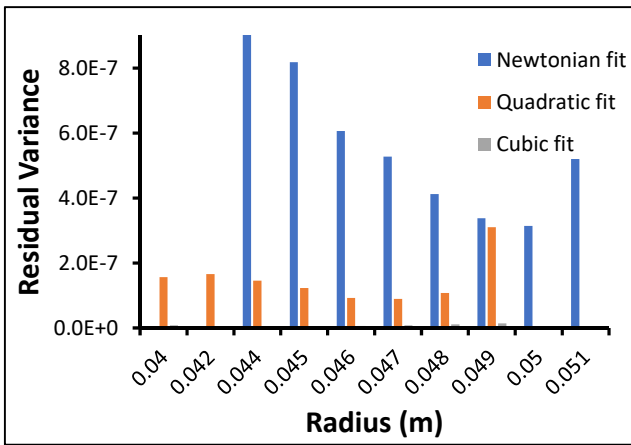


(a)

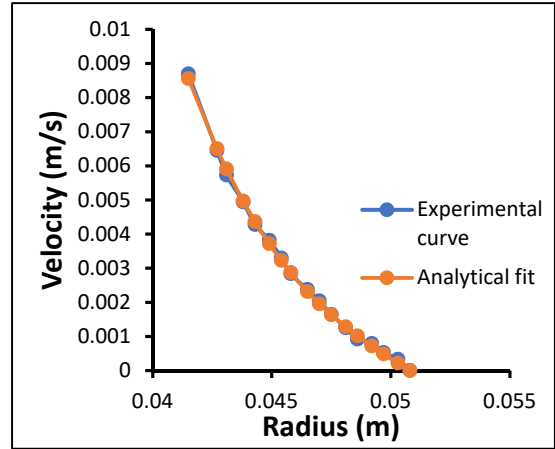


(b)

Fig. 4.55: Cornstarch2 0.8RPM (a) Residual variance (b) Analytical fit of Non-Newtonian Region

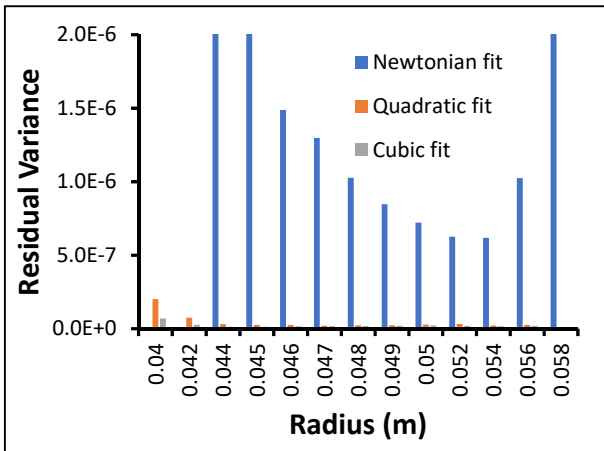


(a)

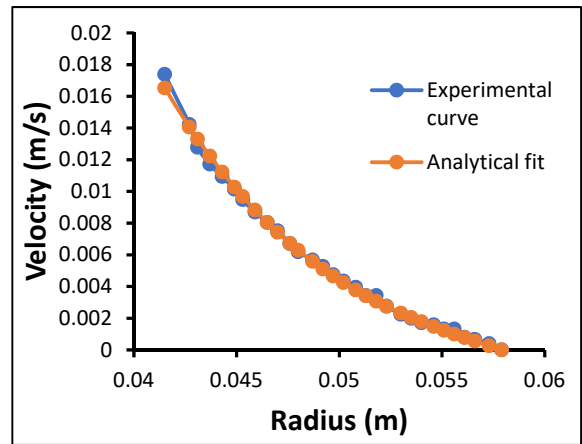


(b)

Fig. 4.56: Cornstarch2 2RPM (a) Residual variance (b) Analytical fit of Non-Newtonian Region

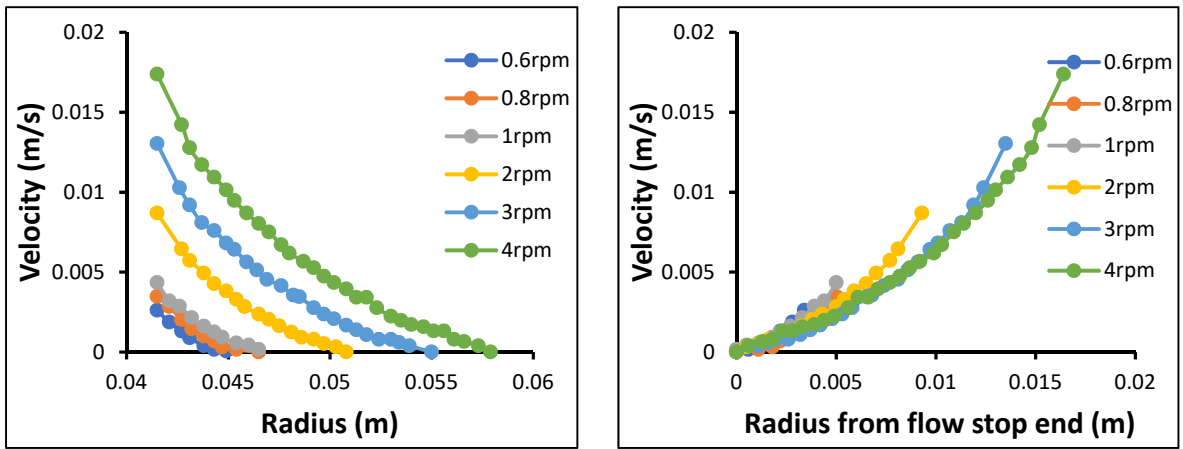


(a)



(b)

Fig. 4.57: Cornstarch2 4RPM (a) Residual Variance (b) Division of Newtonian and Non-Newtonian region



(a)

(b)

Fig. 4.58: Velocity Profiles Cornstarch2(a) From the rotor end (b) From the flow stop end

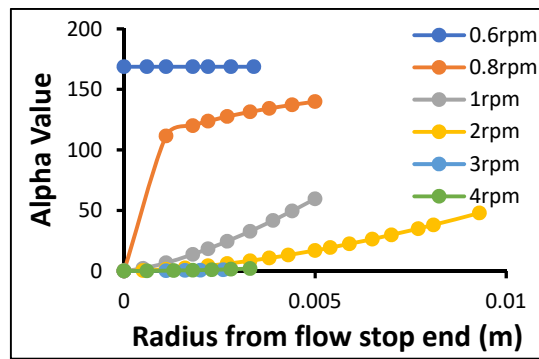
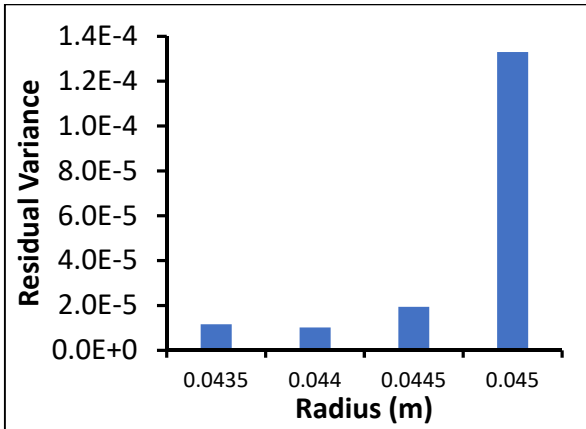
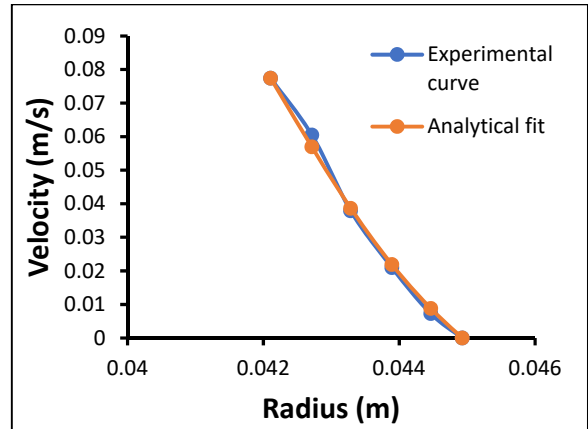


Fig. 4.59: Alpha value variation Cornstarch2

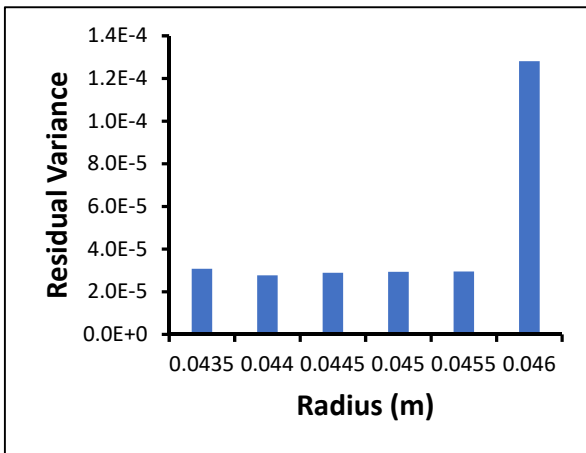


(a)

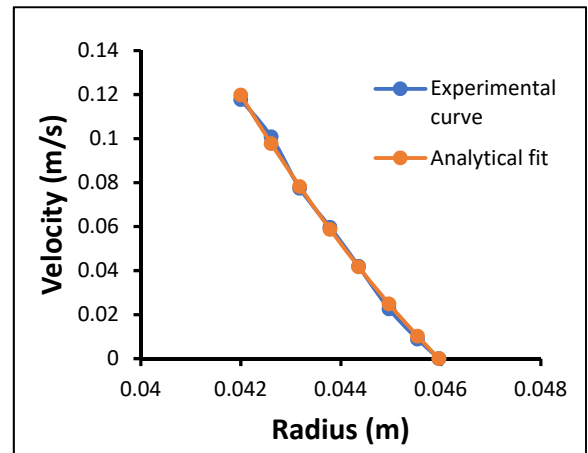


(b)

Fig. 4.60: Cement Paste (CCR2008) 30.9RPM (a) Residual variance (b) Analytical fit of Non-Newtonian Region

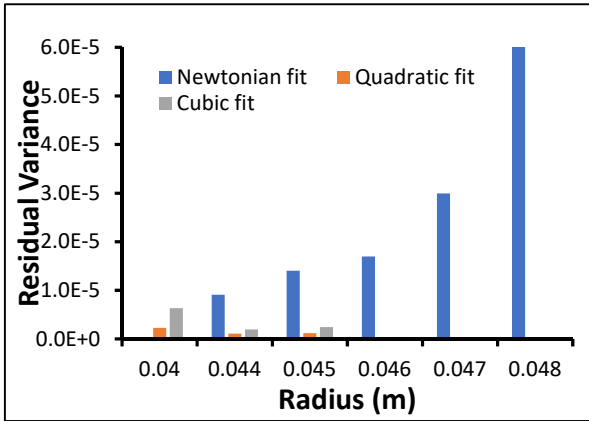


(a)

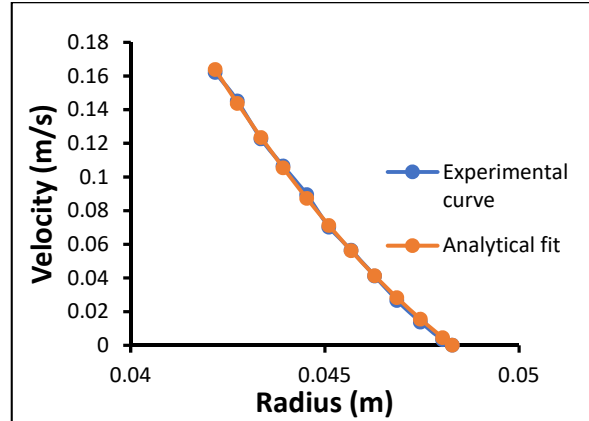


(b)

Fig. 4.61: Cement Paste (CCR2008) 41.2RPM (a) Residual variance (b) Analytical fit of Non-Newtonian Region

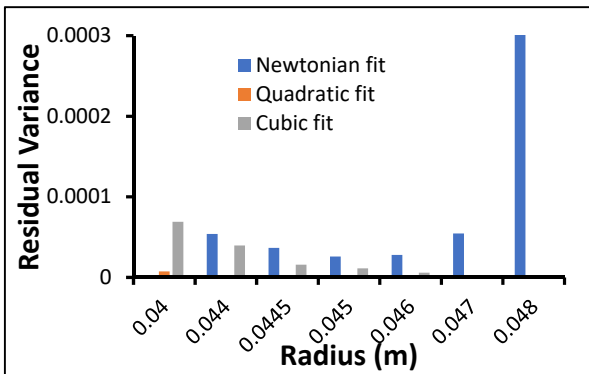


(a)

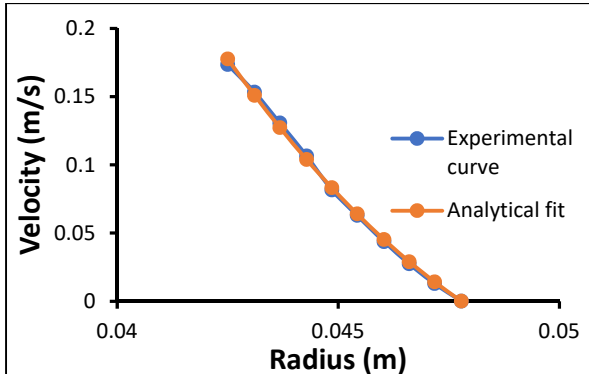


(b)

Fig. 4.62: Cement Paste (CCR2008) 51.5RPM (a) Residual variance (b) Analytical fit of Non-Newtonian Region



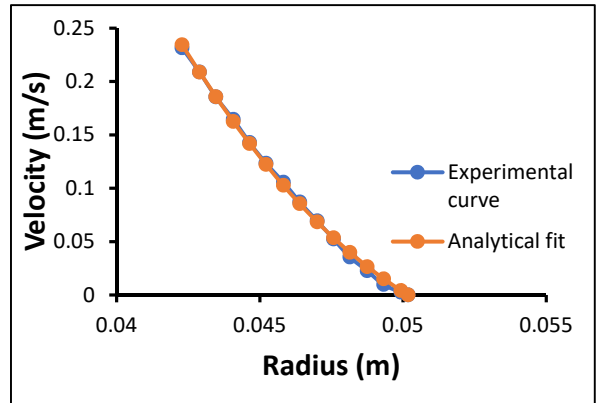
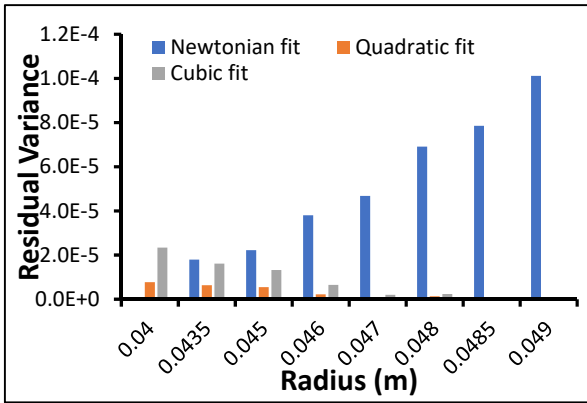
(a)



(b)

Fig. 4.63: Cement Paste (CCR2008) 61.8RPM (a) Residual variance (b) Analytical fit of Non-Newtonian Region

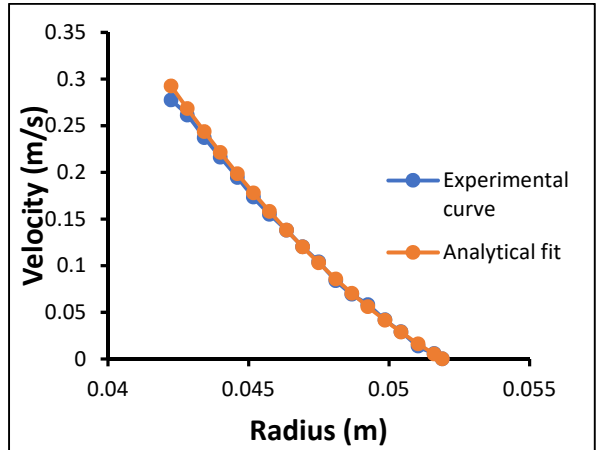
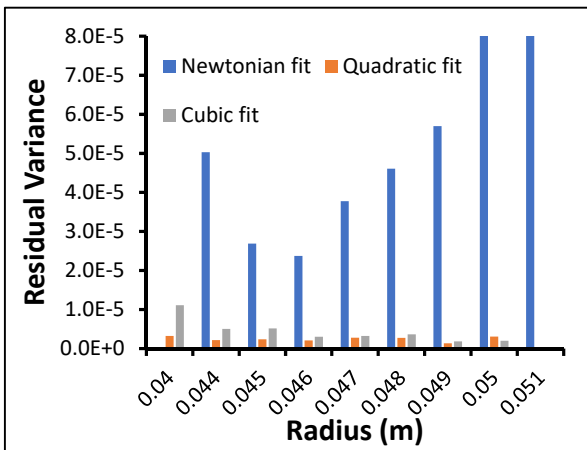




(a)

(b)

Fig. 4.64: Cement Paste (CCR2008) 72.1RPM (a) Residual variance (b) Analytical fit of Non-Newtonian Region



(a)

(b)

Fig. 4.65: Cement Paste (CCR2008) 82.4RPM (a) Residual variance (b) Analytical fit of Non-Newtonian Region

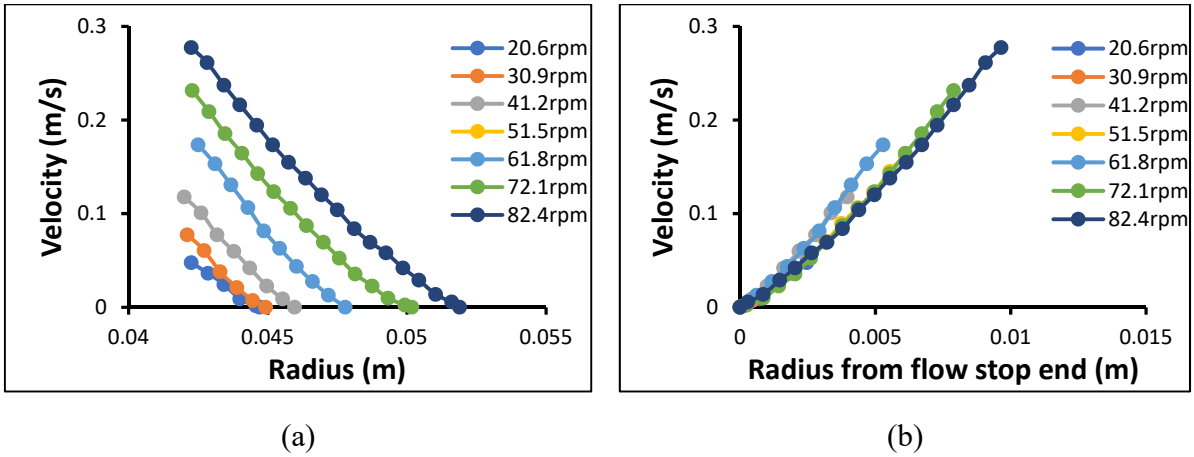


Fig. 4.66: Velocity Profiles Cement paste (CCR2008) (a) From the rotor end (b) From the flow stop end

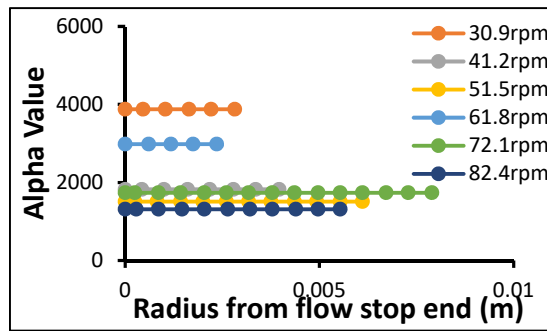


Fig. 4.67: Alpha value variation Cement paste (CCR 2008)

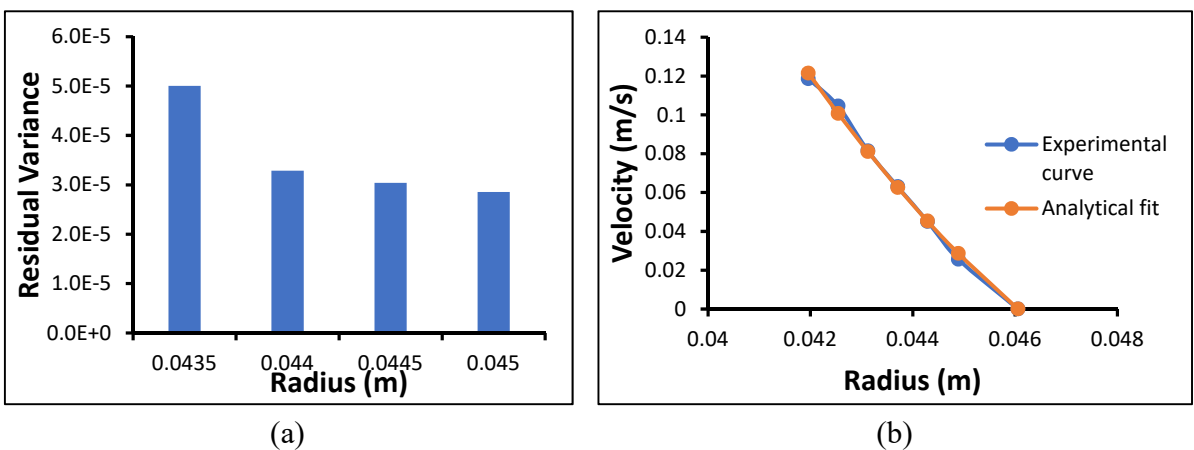
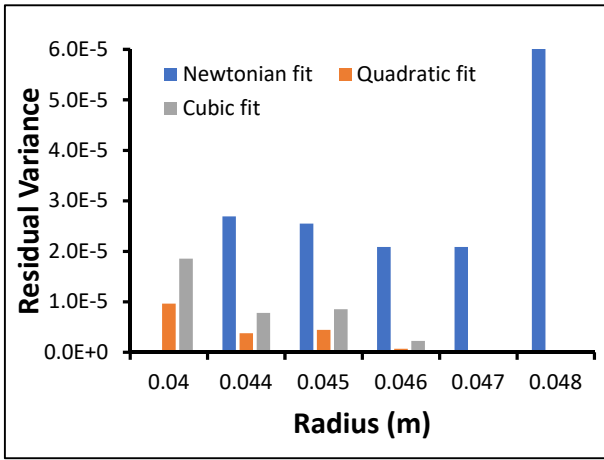
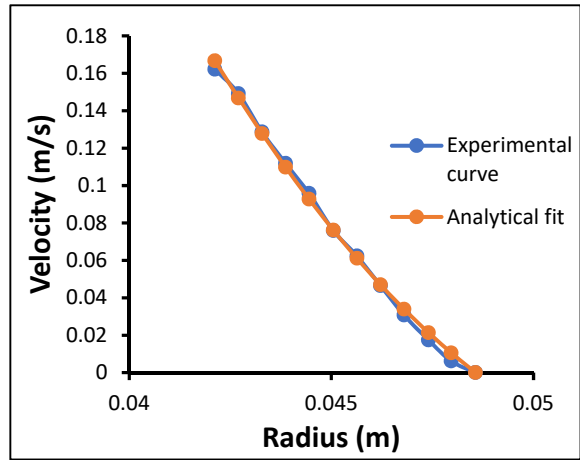


Fig. 4.68: Cement Paste (CCR2005) 41.2RPM (a) Residual variance (b) Analytical fit of Non-Newtonian Region

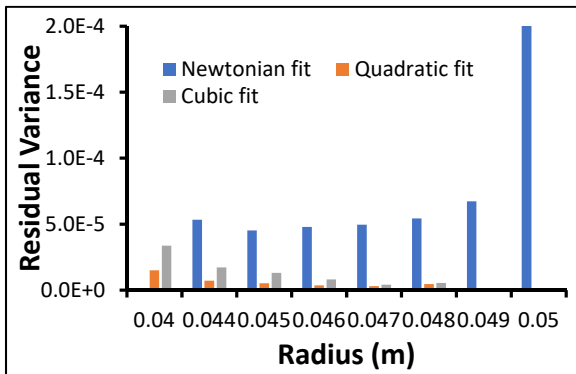


(a)

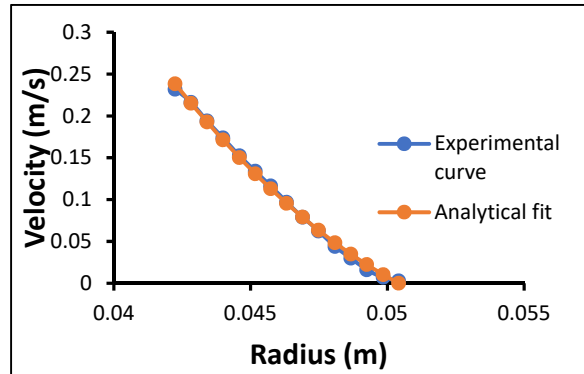


(b)

Fig. 4.69: Cement Paste (CCR2005) 51.5RPM (a) Residual variance (b) Analytical fit of Non-Newtonian Region

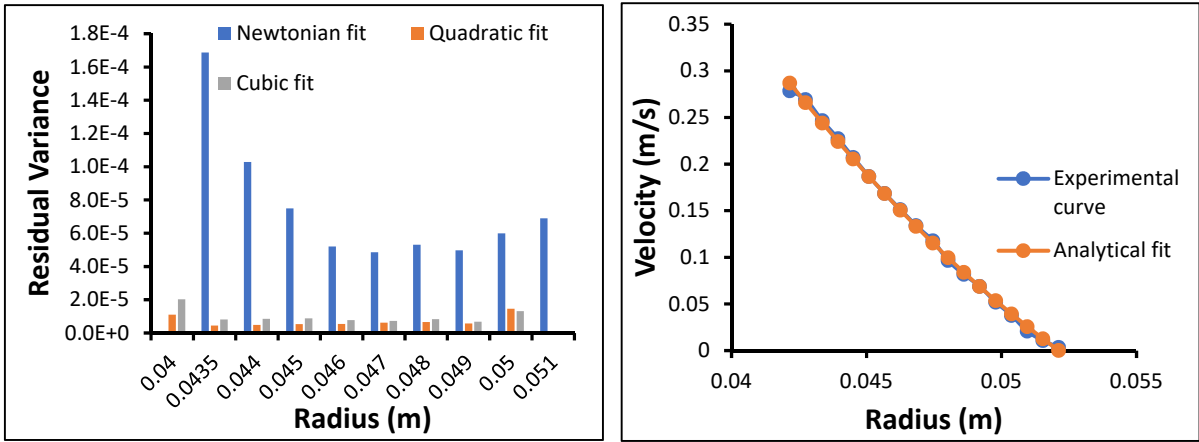


(a)



(b)

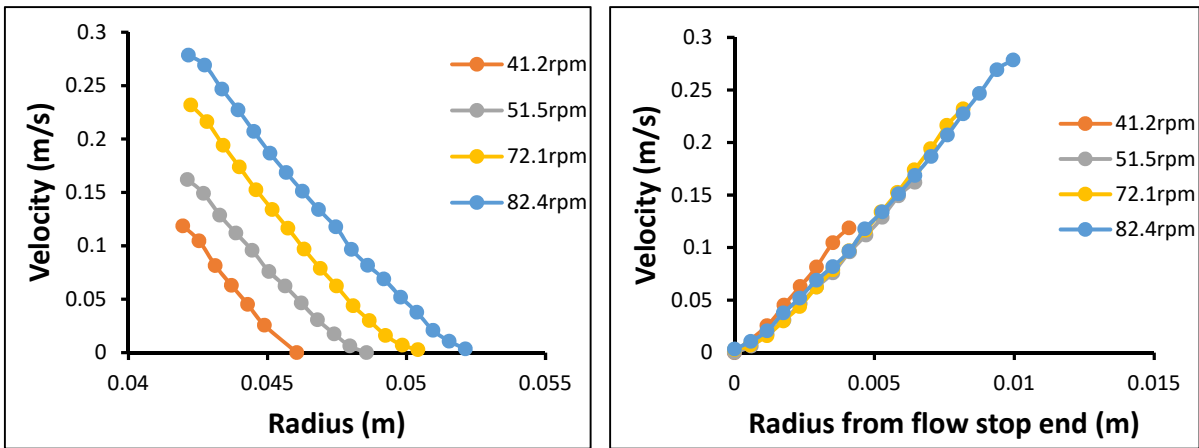
Fig. 4.70: Cement Paste (CCR2005) 72.1RPM (a) Residual variance (b) Analytical fit of Non-Newtonian Region



(a)

(b)

Fig. 4.71: Cement Paste (CCR2005) 82.4RPM (a) Residual variance (b) Analytical fit of Non-Newtonian Region



(a)

(b)

Fig. 4.72: Velocity Profiles Cement Paste (2005) (a) From the rotor end (b) From the flow stop end

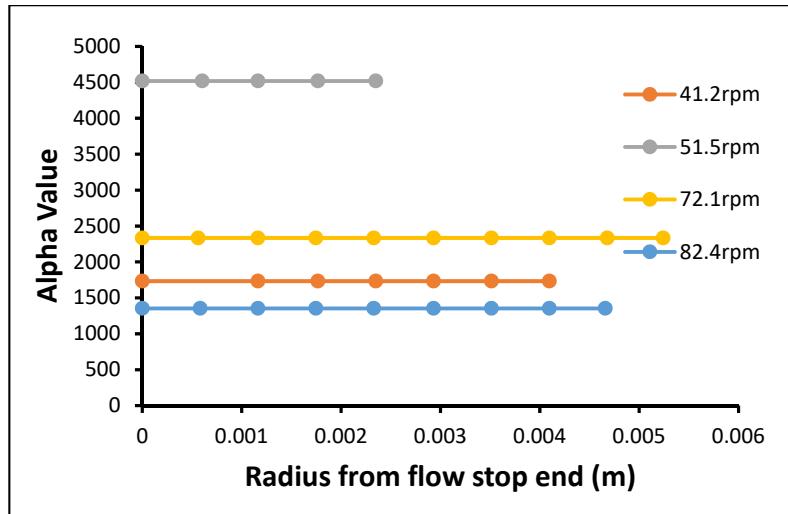


Fig. 4.73: Alpha Value variation Cement Paste (CCR 2005)

**Chapter 5. NEW THEORY FOR  
UNDERSTANDING THE FLUID  
FLOW BEHAVIOR**

### **5.1 Purpose of New hypothesis**

The experimental results obtained by the water flow tests and the results of the analytical analysis can be connected based on the behavior of the fluid particles. Flow tests were conducted using water which is a Newtonian liquid. The analytical analysis of velocity profiles is conducted for the Non-Newtonian fluids. So, there is a large disparity in the type of fluids considered for experimental and analytical analysis. However, the relation can be established based on the universal understanding of the Non-Newtonian fluids and extending it to the Newtonian fluids. A hypothesis is proposed in the current section to understand the Newtonian and Non-Newtonian fluids.

Currently available equations and numerical simulations are based on the Navier-stokes equations which consider only the frictional force between the particles as the major driving force in the flow of fluids. This consideration is very much valid in wide channels, but it is incapable of understanding some of the mechanisms which occur inside the narrow gaps. Some of them include the braking mechanism of the air-water interface [1], [2], Non-Newtonian or yielding behavior of water in narrow gaps, water stagnation phenomena [3], [4]. These observations led to the proposal of a new hypothesis which can explain based on the consideration of rotation of the fluid particles and cohesive forces between the particles.

### **5.2 Fluid Simulations using particles**

Simulations of the complex behavior of the fluids based on the smooth particle hydrodynamics method (SPH) is achieved by Muller [5], [6]. Considering SPH, to approximate the continuous fluid, information everywhere is required and obtained based on the weighted sum of the values from nearby particles. The particles have been assumed to have mass, position and velocity, body forces, density, viscosity, stiffness, and temperature. By discretizing the fluids and applying Navier-stokes forces to particles, the pressure obtained is not symmetric. So, enforcing perfect symmetry is hard, and hence mild compressibility is assumed. However, forces can be determined based on the Navier stokes equation, and velocities are updated. By storing fluid attributes with individual particles, modeling of a variety of fluid-fluid interaction phenomena is executed. Some of them are lava lamp, pouring of liquid into a container considering the buoyancy, diffusion, trapped air.

Based on this concept of SPH, dynamics, and behavior of bubbles, froth inside the fluid are simulated [7]–[9]. Additional considerations are also included in the SPH to understand the gas transfer to discrete air bubbles, buoyancy, drag force. The coalescence of air bubbles is an important consideration and is understood based on the cohesive force between the bubbles. Bubble flow, bubble generation, froth formation in the beer are simulated in real-time conditions. Moreover, simulations using different shapes of the particles have also been carried out successfully [10]. This understanding has been extended to the fluid-solid interactions too [11].

Understanding the fluid-fluid interactions in narrow spaces like pores is the most interesting aspect of the simulations. Fluid flow in porous media is altogether a different scenario especially because of the scale and it has been simulated [12] by defining porosity and permeability. Three different

cases for fluid transportation in the presence of porous materials is considered. The first one is within the porous object fluid mass is diffused at a macro scale between the porous particles. The second one is fluid particles near the porous material are treated as porous particles and mass is taken away from them if fluid is absorbed by the porous material. The final one is when the porous material emits fluid, mass is added to neighboring fluid particles, which are again treated as porous particles. The porous flow model is based on the macroscopic approach in which porous particles represent a volume of solid mass and empty space. The representation of the porous particles and the fluid particles is similar. Based on this particle representation, fluid can move from one particle to another but flow inside the particle is lost in representation. So, flow is stalled in porous particles, and the desired wet flow is achieved instead of usual diffusion. In this case, the multiphase flow (formation of bubbles) is not considered in the simulations.

Even though the real-time simulations of fluid flow were executed based on the SPH particle for different behavior and flows, some forces are not included in understanding fluid behavior. For example, the cohesion of forces is considered in the bubble coalescence to understand the bubble behavior, but this force is ignored in the normal flow of fluids. Though they are not necessary for the macroscopic behavior of fluids, a pivotal role is played by these forces in the narrow gaps like pores. Consideration of these kinds of forces gives an insight into the understanding of new types of mechanisms occurring in different fluids.

### **5.3 Background of Hypothesis**

The work done by Daniel [13] using mustard seeds to obtain the velocity profiles showed slip and rotation behavior. Velocity profiles for the mustard seeds are obtained by combining magnetic resonance imaging, X-ray tomography, and high-speed video particle tracking to obtain the local steady-state particle velocity. Rotation and packing density for shear flow in three dimensional Couette flow. The velocity profiles obtained by this experiment not only contain the information about the particle translation but also about particle spin as shown in Fig. This velocity profile showed slip behavior at integral multiples of  $r/d$  values starting from the rotor and is eventually lost after a certain distance. But after this, we can observe that there is an increase in the rotation of the particle as shown in the inset of the Fig. 5.1. There is no rotation or negligible rotation of the particles when slip occurs, and no-slip is observed when there is no rotation of the particles. Thus, two different zones namely slip dominant zone and a rotation dominant zone can be observed.

There is an appearance of two different zones in the velocity profiles observed in mustard seeds case. This understanding can be extended to the behavior of different fluids. But the behavior of fluids and granular media is different from each other. The major difference is the size or scale of understanding for the granular media and the fluid particles. Fluid behavior can be understood based on the continuum media, but granular media knowledge is based on the behavior of the individual particles. Similarity or like behavior between these materials can be achieved only by comparing the overall behavior of the materials. Akin to that several is the research is available mentioning the behavior of granular media and fluids.



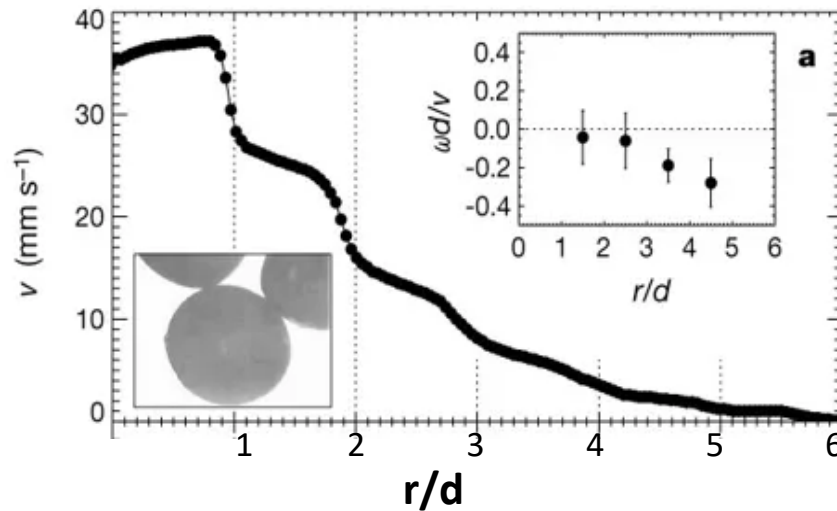


Fig. 5.1 : Velocity profile of the mustard seeds considering slip and rotation behavior [13]

Much research is present to understand the behavior of granular media like fluid behavior. Granular media can behave like a fluid when a sufficient amount of shear rate is applied as mentioned in [14]. Slow relaxations can be found in the vibrated sand piles. Fluid like behavior can be induced in these kinds of materials which can resemble the conventional liquids mentioned by [15]–[20]. As such, the understanding of the granular media like the mustard seeds can be extended to the fluid particles also. Recent research by [21] indicated that the granular materials behave like complex fluids which include foams, suspensions, emulsions, etc. The shape of the granular media considered are the prolate ellipsoids with an aspect ratio of 1.5. These particles are poured in a cyclic box which can impose a shear rate on the particles. Translational mean square displacements calculated for the particles have no plateau at intermediate times even if there is no driving force indicating unusual behavior of granular media. The rotational behavior of the particles also depicted this kind of behavior. It indicates that the material has a normal diffusive behavior. Usually, granular materials have two-step relaxation, but the observed phenomena are quite different. The relaxation dynamics observations indicate the presence of small-scaled relaxation events and friction during the cycle giving rise to a distribution of the displacements. These results suggest that the granular materials are like complex fluids.

### 5.3.1 Umeya Rheology

Flow patterns of disperse systems can be classified into six fundamental patterns describing flow behavior. These include

- (a) Linear relationship between shear stress and shear rate (Newtonian behavior).
- (b) Non-linear relationship with inclination decreasing (Pseudo-plastic behavior).
- (c) Non-Linear relationship with inclination increasing (Dilatant behavior).

- (d) Non-linear relation having an intercept on stress axis and asymptotic to Newtonian (Bingham fluid).
- (e) A non-linear relationship having an intercept on the stress axis and asymptotic to pseudoplastic.
- (f) A non-Linear relationship having an intercept on the stress axis and asymptotic to Dilatant behavior.

After the famous works reported by Ostwald, it was observed that these flow patterns do not exist independently but are present mutually when investigated over an extremely wide shearing range shown in Fig. 5.2. These flow patterns were observed in emulsions, suspensions, and polymer dispersions [22], [23]. The apparent viscosity in the Ostwald flow pattern decreases from a constant value in the 1<sup>st</sup> Newtonian region to the 2<sup>nd</sup> Newtonian region. On the other hand, when the plastic viscosity decreases the flow is Pseudo-plastic, and when it increases the flow of the Dilatant. The initiation of the Ostwald flow depends on the particle orientation to the streamlines of dispersing constituents, agglomeration of disperse system, adsorbability of solvents, or deformability of dispersing high polymer molecules. Solvent molecules can form the adsorbed layers on the surfaces of dispersing particles named as inner and outer Helmholtz or diffused layers. These layers can alter their shapes when exposed to a shearing force, and more-over are stripped off partially from outside. These molecules correspond to the non-Newtonian part of Ostwald flow, and when all the changeable components have been changed completely the 2<sup>nd</sup> Newtonian part occurs.

Experiments conducted on Titanium dioxide-water system, clay-water system, benzene water system exhibited flow patterns as observed by Ostwald. Flow curves of higher

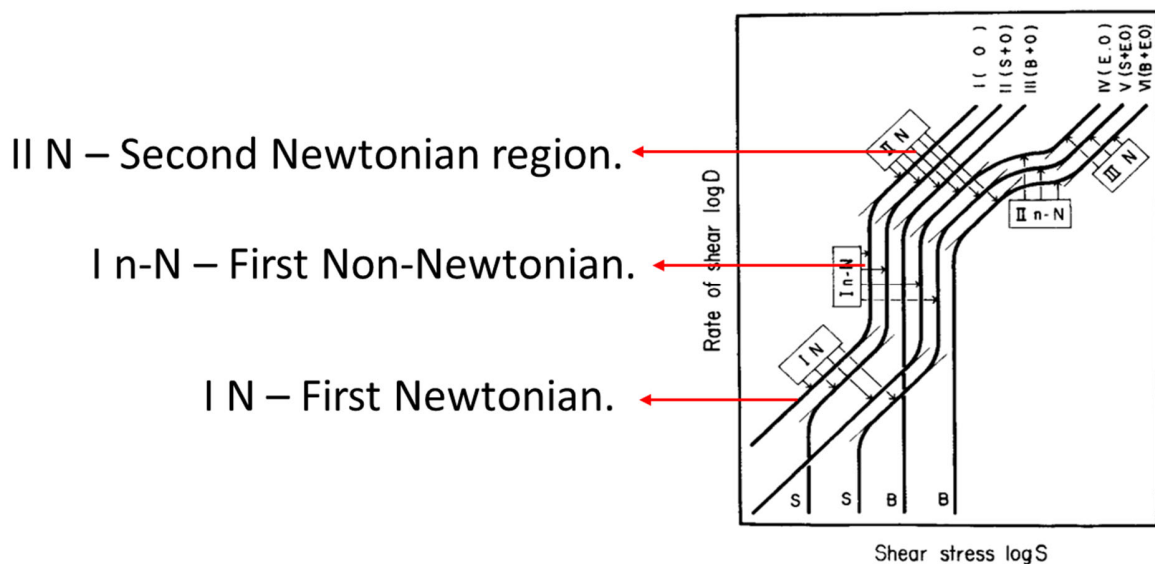


Fig. 5.2: Presence of both Newtonian and Non-Newtonian materials within the same material of laminar flow over a wide range of shear stress. [23]

concentrations of suspensions shift to lower locations and have wider Non-Newtonian regions. The presence of the second Newtonian region was observed for these materials for a wide shearing range. Yielding materials are identified based on Casson’s viscosity relationship for high shearing rates and at low shearing rates, the yield does not occur. We observe that there is a presence of both the Newtonian and Non-Newtonian regions within the same material over an applied wide shear rate range. The Presence of Newtonian and Non-Newtonian regions depends on the applied shear rate. Higher shear rates and Lower shear rates can be divided for the Newtonian and Non-Newtonian behavior, respectively.

#### 5.4 General theory of fluid particles

Understanding of particle behavior in fluids appears in many applications like fluid mechanics, rheology, food processing industries. Industrial processes like sedimentation, water treatment plants, pneumatic transport require the understanding of the behavior of a granular bed with the fluid. The hydrodynamic processes of such phenomena are complex and involve the behavior at a particle level making it difficult to interpret. Numerical models and simulations like computational fluid dynamics, molecular dynamic simulations help in understanding the particle behavior based on the common understanding of the fluids.

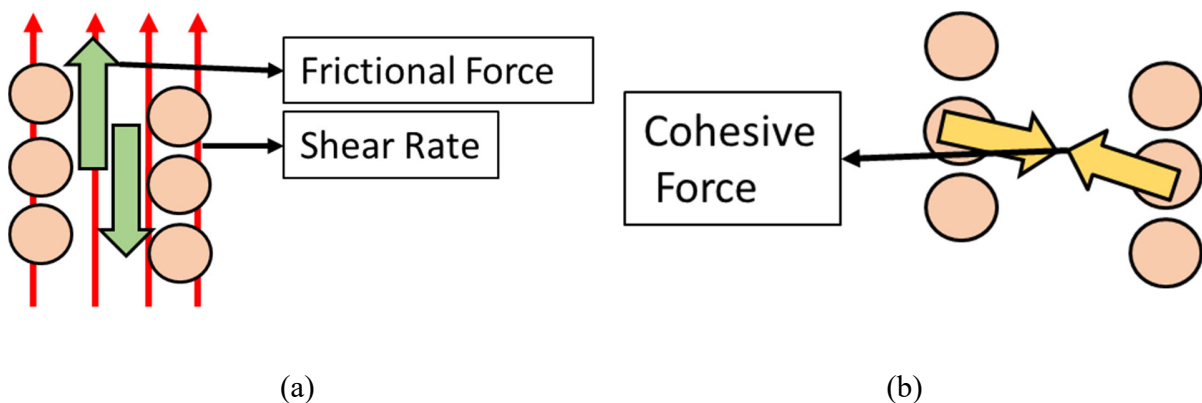


Fig. 5.3: Forces developed within the fluid particles when (a) there is a presence of applied shear rate (b) applied shear rate is 0.

Fluid particles are considered as discrete objects (based on granular materials) [24]–[27]. The particle behavior and path are calculated through the Newtonian equations and collisions. Gravitational force, Collision force and the hydrodynamic force are the major forces acting on the fluid particle shown in Fig. 5.3. Collision force includes the normal and tangential components called elastic and frictional force, respectively. Forces acting on the particle are developed and explained based on the equations of motion. Fluid flow, momentum transfer based on the

hydrodynamic force, and velocity distribution were obtained based on the forces considered. Fluid transport in the porous

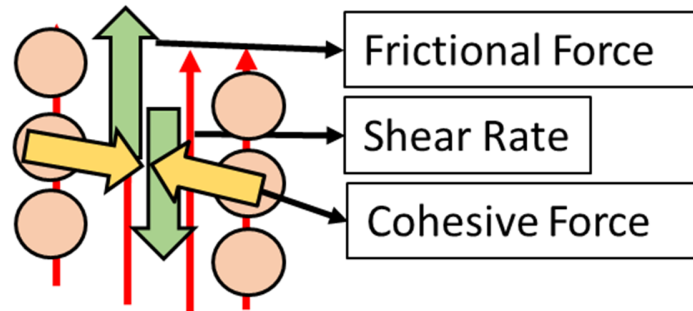


Fig. 5.4: Actual consideration of forces between the particles when the shear rate is applied.

media (restricted to low Reynolds number to ensure laminar viscous regime), phenomena of filtration, mechanism of saltation, quicksand condition were understood based on the behavior of fluid particles.

The presence of both Newtonian and Non-Newtonian behavior in the same material, zones in the velocity profile, and motion of the particles in the porous media cannot be explained easily considering only the Gravitational force, Collision force and the Hydrodynamic forces. However, there is one force that is unaddressed during the flow of the fluid. When fluid is in a static condition, the presence of cohesive force between the particles is of potential importance. As this force is equal in all directions in the material, it helps the material to be together. The interaction at the solid surface and the fluid is discussed a lot for understanding the slip behavior [28], [29]. Different theories explain the behavior of slip phenomena at the fluid-solid interface and corresponding models are also developed [30]. The interactions of fluid-fluid particles within the flow of the fluid are not much considered in past research. So, in this study particle interaction within the same fluid is considered to understand the overall behavior of Newtonian and Non-Newtonian fluids. During the shear flow of the fluid, the behavior of the particles in Newtonian and Non-Newtonian region is hypothesized based on the unconsidered force between the particles during the shear flow. This unaddressed force is the Cohesive force between the particles depicted in Fig. 5.4.

#### 5.4.1 Importance of cohesion

Fluid-solid and fluid-fluid interaction are mainly responsible for the slip behavior. Several factors like viscosity, wettability of the surface, yield-stress, elastic modulus, density, electric charge, and polarity affect the fluid-solid interaction. When a shear rate is applied to the fluid, frictional forces are developed between the particles, and its intensity differs based on the applied shear rate. At low shear rates, the frictional forces are developed between the particles, but the consideration of cohesive forces is also important in these cases. In the static condition, the consideration of cohesive forces between the particles is common but it should be taken into consideration during

the dynamic (flow) condition also. The cause for the rotation of the particles in the experiments conducted by Daniel was not mentioned. Moreover, it is understood that the granular media also behave like complex fluids. So, the behaviors of the granular media can be considered for the fluid particles also. Rotation of the fluid particles also takes place in the fluid and the cause for this rotation is the unaddressed force called Cohesive force.

Consider the experiments conducted on different types of materials using Couette flows [31]–[35]. In these experiments, When the applied RPM value is higher, the fluid is fully sheared within the gap of Couette flow and if the applied RPM value is lower, we observe a static region present in all the materials within the narrow of Couette flows numbered 1 in Fig. 5.5. The existence of the static region in the Couette flow is due to the presence of Cohesive force between the particles. So, at very low shear rates also cohesive force is important to understand the material behavior. This cohesive force between the particles is responsible for the rotation of the particles. We observed the presence of rotation behavior of mustard seeds at a low shear rate and slip behavior at high shear rates. So, in fluids also we observe the rotation of particles at low shear rates due to cohesion between the particles. The existence of solid-like stress transfer mechanism to far static region from the rotor, the existence of small critical shear stress near the flow stop end also shows the importance of cohesive force in understanding the behavior of materials as number 2,3 in Fig. 5.5.

The zonal division for the slip and rotation behavior for the fluids is dependent on this cohesive force only. In slip zone or at high shear rates, slip behavior is observed and the influence of cohesive force is less, but the frictional force is higher. Due to this, the rotation of the particles is negligible at high shear rates and slip behavior of the particles is observed. However, at low shear rates, the cohesive force between the particles comes into the picture due to which the rotation of the particles takes place. The slip behavior of the particles is diminished after a certain distance from the rotor and rotation behavior of the particles is observed numbered 4 and 5 in Fig. 5.5.

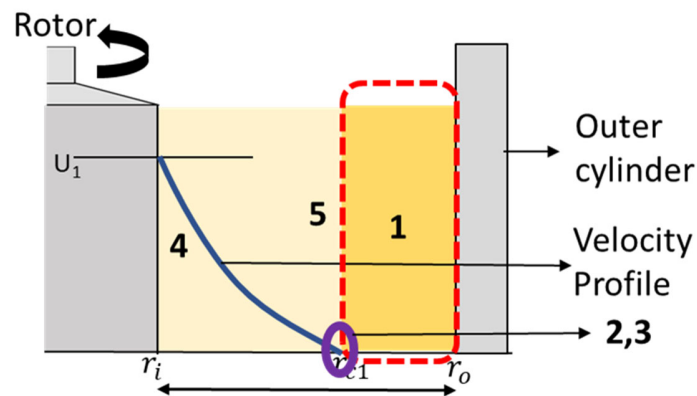
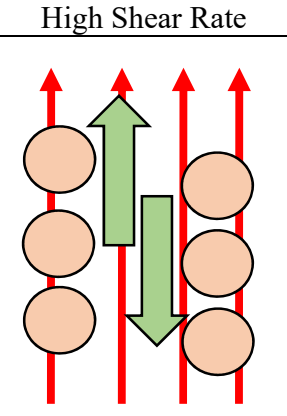
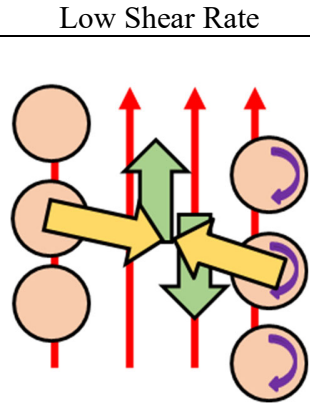
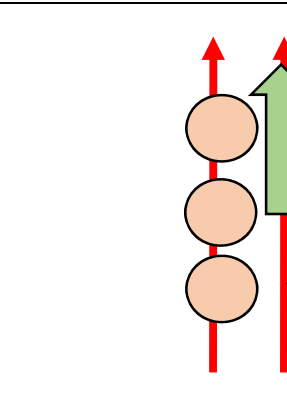
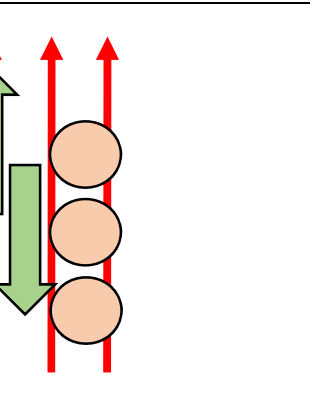
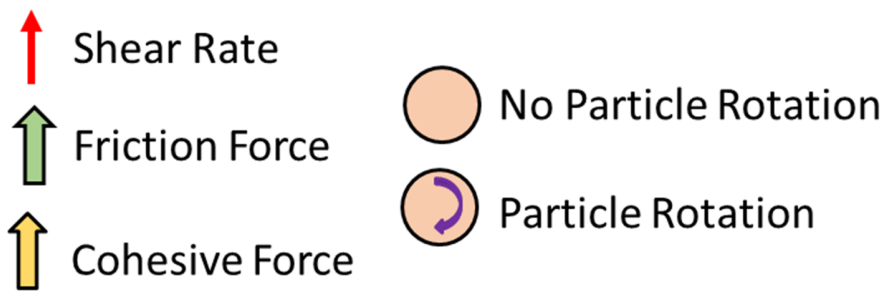


Fig. 5.5: Couette flow showing the presence of different regions and importance of cohesive force

## 5.5 Newtonian and Non-Newtonian Behavior

Table 5.1: Forces present between the fluid particles based on the applied shear rate for different fluids.

	High Shear Rate	Low Shear Rate	Very Low Shear Rate
Non-Newtonian Fluids			N/A
Newtonian Fluids			
			

Based on the understandings of the fluid particle behavior at different shear rates, an overall understanding of fluid during the shear flow is explained. A new understanding of the Newtonian and Non-Newtonian fluids based on the fluid particle is hypothesized as given in Table 5.1. The region close to the rotor is a high shear zone, due to which the frictional forces are much stronger and hence cohesive forces are not much dominant in Non-Newtonian fluids. So, in this region, we observe only the slip behavior of the particles. The energy loss in this region takes place only due to the

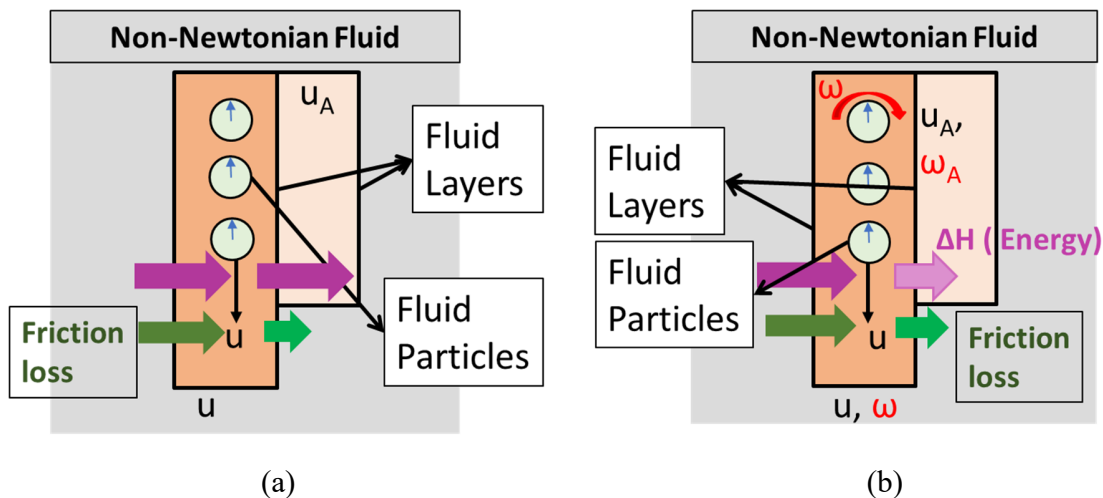


Fig. 5.6: Behavior of Non-Newtonian fluids at (a) High shear rate (b) Low shear rate

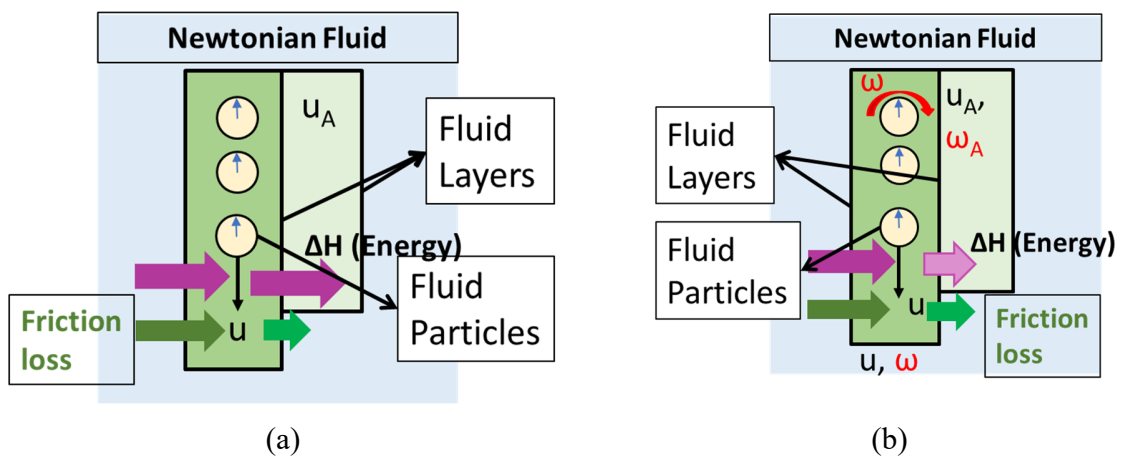


Fig. 5.7: Behavior of Newtonian fluids at (a) High/Low shear rate (b) Very Low shear rate

frictional forces between the layers. The presence of this region is dependent on the applied RPM values, type of particles and the type of material. In Non-Newtonian fluids, the rotation of the particles takes place only at far away from the rotor. The shear rate in this region is low and hence the effect of cohesive force can be visualized in the form of rotation of the particles. The energy loss in this region takes place not only due to friction between the layers but also due to the rotation of the particles.

In Newtonian fluids, the rotation of the particles is restrained or is not dominant as the conservation of momentum is satisfied. As there is no rotation of the particles, there is no energy loss between

the layers of the particles in Newtonian fluids. Energy input is completely transferred to the subsequent layer without any losses. But, because of the friction between the particles, there will be frictional losses occurring between the layers. This is the reason for the reduction in the velocity along with the fluid flow due to the application of shear on the fluid. Moreover, the cohesive force between the particles is negligible at high shear rates. Due to this, the rotation of the particles is restrained, which means there is no rotation of the particles or it is not the major behavior of the particles. So, in Newtonian fluids, rotation of the particles does not take place but the greater influence of frictional force between the layers of fluids which helps in transferring the energy input or shear applied. Slip behavior is observed majorly during this applied shear rate. This is the major behavior of particles in the Newtonian fluids.

At very low shear rates, the cohesive force between the fluid particles in the Newtonian fluids is to be considered. This cohesive force is responsible for the rotation of the fluid particles during the flow. So, particles are rotated at very low shear rates even for Newtonian fluids. However, this region is usually ignored by the researchers. This region can be observed only in very narrow gaps like in concrete pores. This is a very new understanding of the Newtonian fluids and clarifies fluid stagnation behavior in the narrow pores.

## **5.6 Chapter Summary**

In this chapter, a new understanding of the hypothesis for the flow behavior of the fluids in both in microchannels as well as Couette flows is hypothesized. The hypothesis is based on the fluid particle behavior considering the unaddressed forces. Based on the current theories of the flow of fluids and the obtained results, a universal understanding for the fluid particle behavior of Non-Newtonian fluids is hypothesized which can be extended to Newtonian fluids also. A new region called very low shear rate region is identified in Newtonian fluids based on new hypothesis.

Overall, in this chapter, plenty of research supporting the existence of the braking mechanism in the microchannels and the presence of Newtonian and Non-Newtonian regions in same material for a wide shear rate range has been reviewed. These research support well to our inferred understanding of the overall microscopic understanding of the fluid particles. Moreover, major improvements and validations have been presented to understand the phenomena of braking mechanism due to the air-water interface. This is also helpful in understanding the macroscopic behavior of the materials like the pseudo-plastic or dilatant materials.

Overall, a different understanding of the fluid particle in the shear flow is explained to understand the behavior of the braking mechanism leading to the water flow reduction in microchannels and Non-Newtonian behavior of sheared Couette flows.

## **5.7 References**

- [1] M. K. Muzafalu, "Experimental study on the effect of the air-water interface created at wall surface on water flow in narrow gaps," 2017.



- [2] H. Ikomaa, T. Kishib, Y. Sakaib, and M. Kayondoa, “Elucidation of rapid reduction of water flow through concrete crack regarded as self-healing phenomenon,” *J. Ceram. Process. Res.*, vol. 16, pp. 22–27, 2015.
- [3] M. SHIMURA, T. KISHI, and T. KAMADA, “Experimental Study on Stagnation Having Influence on Chloride Ion Penetration in Concrete,” *Cem. Sci. Concr. Technol.*, vol. 69, no. 1, pp. 478–483, 2015, doi: 10.14250/cement.69.478.
- [4] T. KAMADA and T. KISHI, “the Effect of Pore Structure and Moisture State of Concrete on Chloride Ingressコンクリートの含水状態および空隙構造が塩分浸透に与える影響,” *Cem. Sci. Concr. Technol.*, vol. 71, no. 1, pp. 367–372, 2017, doi: 10.14250/cement.71.367.
- [5] M. Müller, B. Solenthaler, R. Keiser, and M. Gross, “Particle-Based Fluid-Fluid Interaction,” in *Eurographics/ACM SIGGRAPH Symposium on Computer Animation*, 2005, no. July, pp. 29–31.
- [6] M. Müller, D. Charypar, and M. Gross, “Particle-based fluid simulation for interactive applications,” *Proc. 2003 ACM SIGGRAPH/Eurographics Symp. Comput. Animat. SCA 2003*, 2003.
- [7] J. M. Hong, H. Y. Lee, J. C. Yoon, and C. H. Kim, “Bubbles alive,” *ACM Trans. Graph.*, vol. 27, no. 3, 2008, doi: 10.1145/1360612.1360647.
- [8] P. W. Cleary, S. H. Pyo, M. Prakash, and B. K. Koo, “Bubbling and frothing liquids,” *ACM SIGGRAPH 2007 Pap. - Int. Conf. Comput. Graph. Interact. Tech.*, vol. 26, no. 3, pp. 1–6, 2007, doi: 10.1145/1239451.1239548.
- [9] M. Ihmsen, J. Bader, G. Akinci, and M. Teschner, “Animation of air bubbles with SPH,” in *GRAPP 2011 - Proceedings of the International Conference on Computer Graphics Theory and Applications*, 2011, pp. 225–234.
- [10] T. Harada, S. Koshizuka, and Y. Kawaguchi, “Smoothed particle hydrodynamics in complex shapes,” in *Proceedings - SCCG 2007: 23rd Spring Conference on Computer Graphics*, 2007, pp. 191–198, doi: 10.1145/2614348.2614375.
- [11] B. Solenthaler, J. Schläfli, and R. Pajarola, “A unified particle model for fluid–solid interactions,” *Comput. Animat. Virtual Worlds*, vol. 18, pp. 69–82, 2007, doi: 10.1002/cav.
- [12] T. Lenaerts, B. Adams, and P. Dutré, “Porous flow in particle-based fluid simulations,” *ACM Trans. Graph.*, vol. 27, no. 3, pp. 1–8, 2008, doi: 10.1145/1360612.1360648.
- [13] D. M. Mueth, G. F. Debregeas, P. J. Eng, S. R. Nagel, and H. M. Jaeger, “Signatures of granular microstructure in dense shear flows,” *Nature*, vol. 3, pp. 385–389, 2000.
- [14] H. M. Jaeger, S. R. Nagel, and R. P. Behringer, “Granular solids, liquids, and gases,” *Rev. Mod. Phys.*, vol. 68, no. 4, pp. 1259–, 1996.
- [15] C. Laroche, S. Douady, and S. Fauve, “Convective flow of granular masses under vertical vibrations Convective flow of granular masses under vertical vibrations,” *J. Phys.*, vol. 50, no. 7, 1989, doi: 10.1051/jphys:01989005007069900i.

- [16] O. Zik and J. Stavans, “Self-Diffusion in Granular Flows,” *EPL (Europhysics Lett.)*, vol. 16, no. 3, p. 255, 1991, doi: 10.1209/0295-5075/16/3/006.
- [17] F. Melo, P. Umbanhowar, and H. L. Swinney, “Transition to parametric wave patterns in a vertically oscillated granular layer,” *Phys. Rev. Lett.*, vol. 72, no. 1, pp. 172–175, Jan. 1994, doi: 10.1103/PhysRevLett.72.172.
- [18] H. K. Pak and P. R. Behringer, “Bubbling in vertically vibrated granular materials,” *Nature*, vol. 371, no. 6494, pp. 231–233, Sep. 1994, doi: 10.1038/371231a0.
- [19] H. K. Pak, E. Van Doorn, and R. P. Behringer, “Effects of ambient gases on granular materials under vertical vibration,” *Phys. Rev. Lett.*, vol. 74, no. 23, pp. 4643–4646, Jun. 1995, doi: 10.1103/PhysRevLett.74.4643.
- [20] H. K. Pak and R. P. Behringer, “Surface waves in vertically vibrated granular materials,” *Phys. Rev. Lett.*, vol. 71, no. 12, pp. 1832–1835, Sep. 1993, doi: 10.1103/PhysRevLett.71.1832.
- [21] B. Kou *et al.*, “Granular materials flow like complex fluids,” *Nature*, vol. 551, no. 7680, pp. 360–363, 2017, doi: 10.1038/nature24062.
- [22] K. Umeya, T. Isoda, T. Ishii, and K. Sawamura, “Some observations on the flow properties of disperse systems,” *Powder Technol.*, vol. 3, no. 1, pp. 259–266, 1969, doi: 10.1016/0032-5910(69)80093-8.
- [23] K. Umeya and S. Tanifuji, “Flow properties of some suspending systems,” *Rheol. Acta*, vol. 13, no. 4, pp. 681–688, 1974.
- [24] H. J. Herrmann, J. S. Andrade, A. D. Araújo, and M. P. Almeida, “Particles in fluids,” *Eur. Phys. J. Spec. Top.*, vol. 143, pp. 181–189, 2007, doi: 10.1140/epjst/e2007-00086-x.
- [25] H.J.Herrmann and J.S.Andrade, “Particles in Fluids,” *Societ`a Italiana di Fisica*, pp. 1–49, 2003.
- [26] B. C. Burman, P. A. Cundall, and O. D. L. Strack, “A discrete numerical model for granular assemblies,” *Geotechnique*, vol. 30, no. 3, pp. 331–336, 1980, doi: 10.1680/geot.1980.30.3.331.
- [27] G. H. Ristow and H. J. Herrmann, “Forces on the walls and stagnation zones in a hopper filled with granular material,” *Phys. A Stat. Mech. its Appl.*, vol. 213, no. 4, pp. 474–481, 1995, doi: 10.1016/0378-4371(94)00249-S.
- [28] T. Sochi, “Slip at fluid-solid interface,” *Polym. Rev.*, vol. 51, no. 4, pp. 309–340, 2011, doi: 10.1080/15583724.2011.615961.
- [29] H. J. Walls, S. B. Caines, A. M. Sanchez, and S. A. Khan, “Yield stress and wall slip phenomena in colloidal silica gels,” *J. Rheol. (N. Y. N. Y.)*, vol. 47, no. 4, pp. 847–868, 2003, doi: 10.1122/1.1574023.
- [30] M. Cloitre and R. T. Bonnecaze, “A review on wall slip in high solid dispersions,” *Rheol. Acta*, vol. 56, no. 3, pp. 283–305, 2017, doi: 10.1007/s00397-017-1002-7.
- [31] A. Fall *et al.*, “Macroscopic discontinuous shear thickening versus local shear jamming in

- cornstarch,” *Phys. Rev. Lett.*, vol. 114, no. 9, pp. 1–5, 2015, doi: 10.1103/PhysRevLett.114.098301.
- [32] A. Fall, N. Huang, F. Bertrand, G. Ovarlez, and D. Bonn, “Shear thickening of cornstarch suspensions as a reentrant jamming transition,” *Phys. Rev. Lett.*, vol. 100, no. 1, 2008, doi: 10.1103/PhysRevLett.100.018301.
- [33] S. Jarny, N. Roussel, R. Le Roy, and P. Coussot, “Modelling thixotropic behavior of fresh cement pastes from MRI measurements,” *Cem. Concr. Res.*, vol. 38, no. 5, pp. 616–623, 2008, doi: 10.1016/j.cemconres.2008.01.001.
- [34] J. Drappier, D. Bonn, J. Meunier, S. Lerouge, J. P. Decruppe, and F. Bertrand, “Correlation between birefringent bands and shear bands in surfactant solutions,” *J. Stat. Mech. Theory Exp.*, no. 4, 2006, doi: 10.1088/1742-5468/2006/04/P04003.
- [35] S. Rodts, J. C. Baudez, and P. Coussot, “From ‘discrete’ to ‘continuum’ flow in foams,” *Europhys. Lett.*, vol. 69, no. 4, pp. 636–642, 2005, doi: 10.1209/epl/i2004-10374-3.

## **Chapter 6. ANALYSIS AND DISCUSSION**

## 6.1 Analysis of Water Flow Tests

The results of water flow tests conducted using the microchannels with crevices have shown water flow reduction in narrow hydrophilic channels only when equilibrated water is used but not in the hydrophobic channels even when equilibrated water is used. In the NMC, with hydrophilic nature of surfaces and without crevices, there is not much decrease in the water flow rate even though equilibrated water ( $DO > 95\%$ ) is used as shown in Fig. 4.4. The decrease in the water flow is considered due to the presence of invisible air bubbles in the path of the water flow. High water flow reduction is observed in the microchannels with a greater number of crevices (54) and then a smaller number of crevices (27). The decrease is supposed to cause due to the formation of small micro air bubbles at the location of crevices due to the equilibrated water. Appreciable water flow reduction was not observed in the microchannels with no crevices even when equilibrated water is used. This is due to the inability of the formation of air bubbles on the surfaces of microchannels without crevices.

When water is flown through microchannels containing crevices, air bubbles are formed on these locations due to the presence of high levels of dissolved oxygen ( $DO > 95\%$ ) present in equilibrated water. Crevices act as initiation points for the formation of air bubbles. These potential points or crevices helpful in the formation of air bubbles are absent in the microchannels with no crevices. So, it is difficult to form air bubbles on these surfaces easily and hence no decrease in the water flow rate. Degassed water has lower levels of dissolved oxygen ( $DO < 40\%$ ) and this makes it more difficult to form micro air bubbles on the hydrophilic surface microchannels with crevices. As there are fewer oxygen levels in the water the ability to form air bubbles is reduced to a greater extent even when there are crevices on the surface. Hence, degassed water with crevices also showed less water flow reduction because of the less or no formation of bubbles. Hydrophobic surfaces are repellent to water due to which the bubble formation is easier. This immediate formation was observed by using the luminescence powder in the hydrophobic microchannels. But a drastic reduction in the water flow rate is not observed due to the formation of micro air bubbles in the flow path.

To understand the formation of air bubbles at the crevices, WMC is used. In these channels, water flow reduction occurs in both hydrophilic and hydrophobic surfaces. The decrease in water flow in hydrophobic surface microchannels is due to the increase in the air bubble size and thus decreasing the effective cross-sectional area of flow and it can be observed in Fig. 4.9. The bubble size increases continuously from the initial 1hr to the final 7hr. The bubble finally reaches the path of water reducing the effective flow of cross-sectional area and the water flow rate. The increase in the bubble volume at each bubble location with respect to the initial volume of the bubble is shown in Table 4.3. There is an increase of around 85% in the volume of the bubble from the initial hour of the start of the test. The decrease in water flow rate in hydrophilic surface microchannels is shown in Fig. 4.7. It is observed that even when there is a decrease in the volume of the bubble as can be observed from Fig. 4.8. The percentage of decrease in the volume of the bubble on hydrophilic surfaces is shown in Table 4.2. The decrease in water flow rate in hydrophilic WMC can be understood based on the slip and drag force behavior. The slip behavior of the water molecules on the hydrophobic surface can be understood based on the arrangement of the

molecules near the surface. Drag force on the water molecules due to the surface depends on the adhesive force between them.

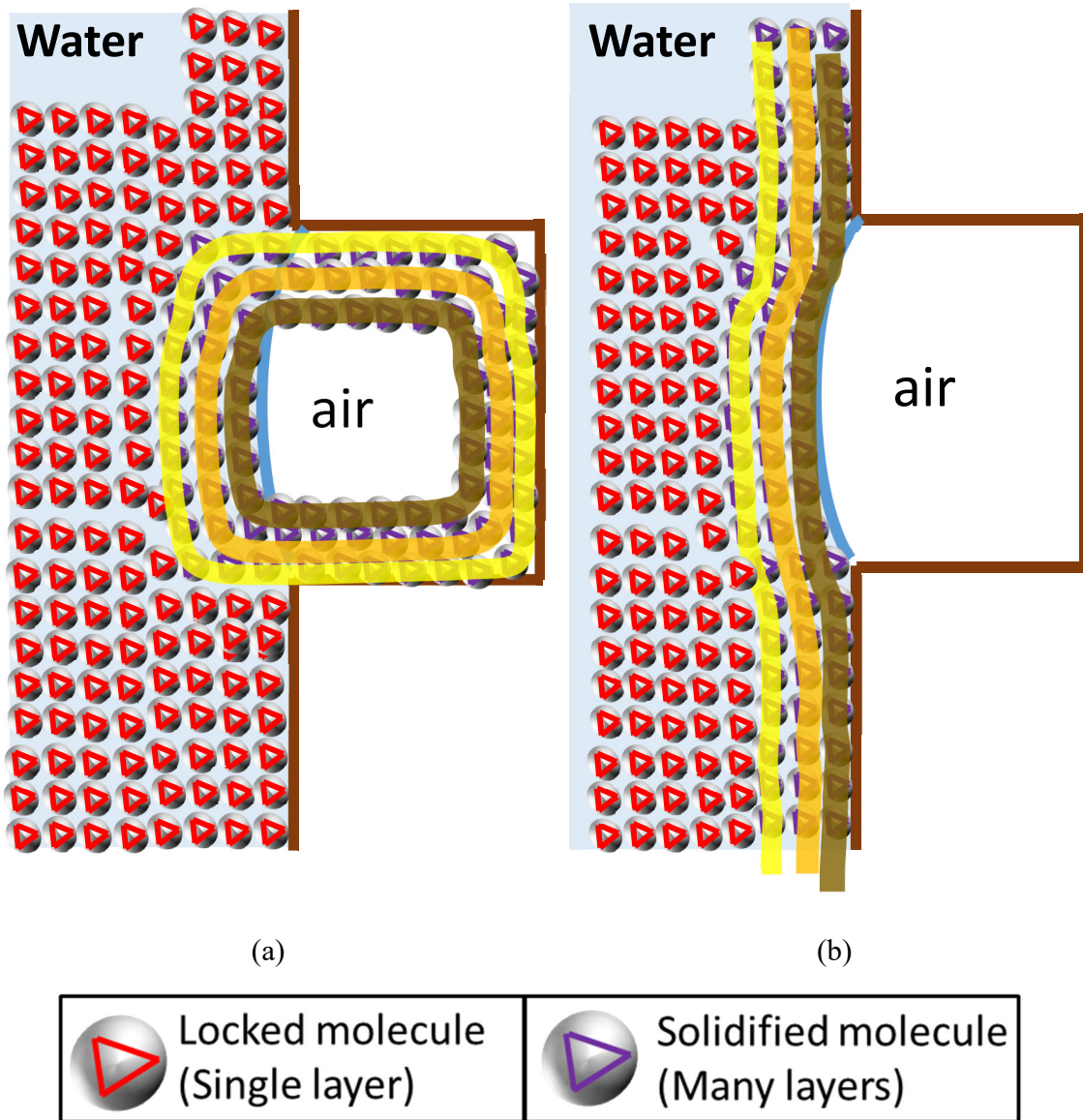


Fig. 6.1: Showing the interaction of particles at (a) Hydrophilic Surface (b) Hydrophobic Surface

Initially, we understand the behavior of water molecules at different types of surfaces based on literature and use an energy loss mechanism to support this behavior.

Slip behavior at the surfaces of hydrophobic and hydrophilic surfaces is studied by many researchers [1]–[6]. In all the research mentioned, it has been summarized that slip flow occurs

majorly in the hydrophobic surfaces in comparison to the hydrophilic surfaces. It majorly occurs due to the formation of nano air bubbles on the hydrophobic surfaces. Hydrophobic surfaces can easily form the air bubbles as there is no strong adhesion between the water and the hydrophobic

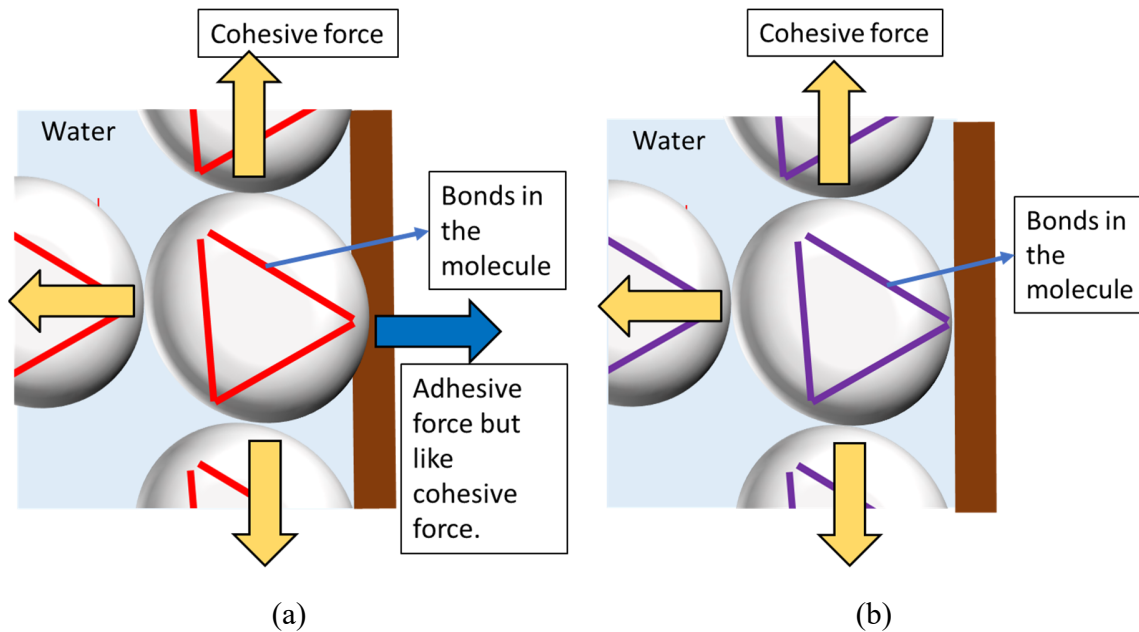


Fig. 6.2: Showing the presence of isotropic and non-isotropic nature in (a) Hydrophilic Surface (b) Hydrophobic Surface.

surface. The extent of slip length depends on the degree of wettability of the surface (contact angle), shear rate flow of fluid. If the contact angle is higher and the applied shear rate is higher bubbles can be formed easily on the surfaces which are responsible for the slip behavior of the flow at the surface. Hydrophobic surfaces, which can easily form air bubbles on the surface have more slip behavior of flow than the Hydrophilic channels.

Now based on the previous research understandings, we observe that the water molecules are more stable at the hydrophobic surface and exhibit more slip flow behavior. In hydrophilic channels, slip flow behavior is less but there is an adhesive force between the water molecules and the surface which is responsible for the drag force. In this study, an attempt is made to understand the stability and slip type behavior based on the energy loss mechanisms due to the viscous forces present in the fluid. A detailed explanation of the theory and the assumptions, formulations are given in Chapter Chapter 5. The linear velocity of the particle is used to describe the stability in the flow while the rotational motion of a particle is used to understand the slip behavior of the particles.

The decrease in the water flow rate in the WMC of hydrophilic surfaces due to the decrease in the air bubble can be understood based on the slip behavior and the anchorage of fluid particles acting on the fluid. This similar kind of behavior may also be present in the NMC of hydrophilic surfaces but is not visible to the naked eye. We observed water flow reduction in these channels even when

there is no presence of the formation of air bubbles visible to the naked eye. The constant water flow rate in the hydrophobic NMC is due to the no appreciable increase in the air bubble formation and presence of constant slip behavior at the interface along the hydrophobic surface and air-water interface. The particles at the hydrophobic surface have more slip behavior and less rotation of particles and in hydrophilic surface particles have less slip behavior and more rotation of particles based on the theory of energy loss mechanism.

### **6.1.1 Discussion of Hydrophobic and Hydrophilic Surface Behavior of Molecules.**

After hypothesizing the Newtonian and Non-Newtonian behavior of the fluid particles, we understand the fluid behavior on Hydrophobic and Hydrophilic surfaces. In the experimental setup, water is used as a fluid to understand the flow rate behavior in the microchannels. Water is a Newtonian fluid, so the molecules are locked or restrained to the rotation. In the bulk water molecules, cohesive force exists between the water molecules as a Hydrogen bond and is equal in all the directions. Thus, in bulk water molecules cohesive force is isotropic in nature, and molecules are locked. These molecules are present in only a single layer. At the hydrophobic surface, the water molecules are not attached to the surface. So, there are no adhesive forces present between the water molecules and the surface. But cohesive forces are present between the surrounding water molecules. As there is no force present in one direction of the water molecule at the hydrophobic surface, the resultant cohesive force is directed in a certain direction. Thus, the isotropic nature of the cohesive force in the water molecules is lost at the hydrophobic surface. The cohesive forces are rearranged between the water molecules near the surface due to the non-isotropic nature of cohesive forces in the water molecules present at the surface. This rearrangement of the cohesive forces is spread to a certain distance of molecular layers till the isotropic nature of cohesive force is restored. Molecules with non-isotropic nature of the cohesive forces are considered as solidified molecules. So, these solidified molecules form many layers to rearrange the cohesive force between themselves and attain the isotropic nature of the cohesive force. Many layers of the solidified molecules form a continuous sheet of a layer on the Hydrophobic surface, causing the slip behavior. Because of this behavior, water slips along the surface and there is no decrease in the water flow rate. The air-water interface also behaves as the Hydrophobic surface as mentioned by [7]. So, the presence of an air-water interface along with the hydrophobic surface does not have any influence on the water flow rate. The continuous sheet of the layer is also present at the air-water interface and hence slip behavior occurs. This was observed in the experimental results as well. The water flow rate in the Hydrophobic surface is not decreased at the end of 6hrs. The water flow rate calculated at the end of the microchannel is unchanged at every time interval. This is due to the slip behavior of the water molecules forming a continuous sheet of layer near the air-water interface and hydrophobic surface.

In contrast, the water molecules behavior at the Hydrophilic surface is different from the hydrophobic surface. It was already mentioned that the cohesive force in bulk water molecules is isotropic in nature (as it is equal in all the directions). At the hydrophilic surface, the adhesive force between the water molecules and surface is stronger. So, water molecules get easily attracted to the surface. For the water molecule at the surface, the cohesive force is present in all the directions except in the direction where the hydrophilic surface is present. However, adhesive force is present in this direction, which can be regarded as the cohesive force between the water molecule



and the surface. The presence of this force is responsible for restoring the isotropic nature of cohesive forces between the molecules near the surface as well as molecules and surfaces. When water flows in the hydrophilic surface drag force is experienced by the water molecules because of the attraction between the molecules and the surface. But when an air-water interface is present in the path of water flow of a hydrophilic channel, the adhesive force between the molecules and the interface is lost. A thin film layer of water is present around the crevice even if the air bubble is present due to the stronger attraction of hydrophilic surfaces to the water molecules. The behavior of the molecules at the air-water interface is like the hydrophobic surface. So, the nature of the cohesive force between the molecules is non-isotropic in nature around the air-water interface. These molecules are present in layers around the air-water interface and form an anchorage layer. When water flows, the anchorage layer hinders the water flow rate causing a reduction in the water flow rate.

The behavior of the same nature of the molecules (solidified molecules) is different on different surfaces. In a hydrophobic case, the solidified molecules form a continuous sheet of layer causing the slip behavior. While in hydrophilic channels, these molecules form an anchorage layer around the crevice which hinders the water flow causing the reduction in the water flow rate.

## 6.2 Analysis of Analytical Results

Velocity profile data obtained for different materials from the previous research is plotted and shown in the results section. Partially sheared flows are considered to understand the actual material behavior and hence the velocity profile does not reach the outer end of the radius. These velocity profiles are rearranged and plotted based on the radius of flow stop end (the radius at which velocity of the material becomes zero after the application of shear force is called the radius of flow stop end). When the velocity profiles are plotted in this way, they overlap each other for different RPM values as shown in different figures Fig. 4.14, Fig. 4.18, Fig. 4.23, Fig. 4.25 and others. This suggests that the rate of shear rate decrease in the velocity profile is the same in each material irrespective of the RPM applied. However, there is an upward shift or downshift of the velocity profiles at a specific RPM after which it reaches the next velocity profile reaches the outer end of the rotor. It means that whenever an upward shift or downward shift of the velocity profile at an RPM value, the velocity profile obtained by the application of a next RPM value, higher than the previous value, reaches the outer rotor end.

The Non-Newtonian regions obtained after identifying them in each profile are either fit using the quadratic or cubic equation. This is required to understand the shear rate behavior in the Non-Newtonian region. Theoretically, either quadratic or cubic equation is chosen to understand the variation of shear rate behavior as well as the non-linearity in velocity. In some cases, if only a portion of the Non-Newtonian profile is fit then the whole region is automatically got fit in the entire region as shown in Fig. 4.40. The material parameter alpha ( $\alpha$ ) played an important role in identifying the type (linear or non-linear) of shear rate decrease in the velocity profile. The material parameter alpha is a coefficient of quadratic term in the velocity equation. If the variation of alpha is constant, then the assumed variation of non-linearity of the quadratic profile is sufficient for the

velocity profile. If there is a variation in the parameter alpha, then assumed quadratic non-linearity is insufficient

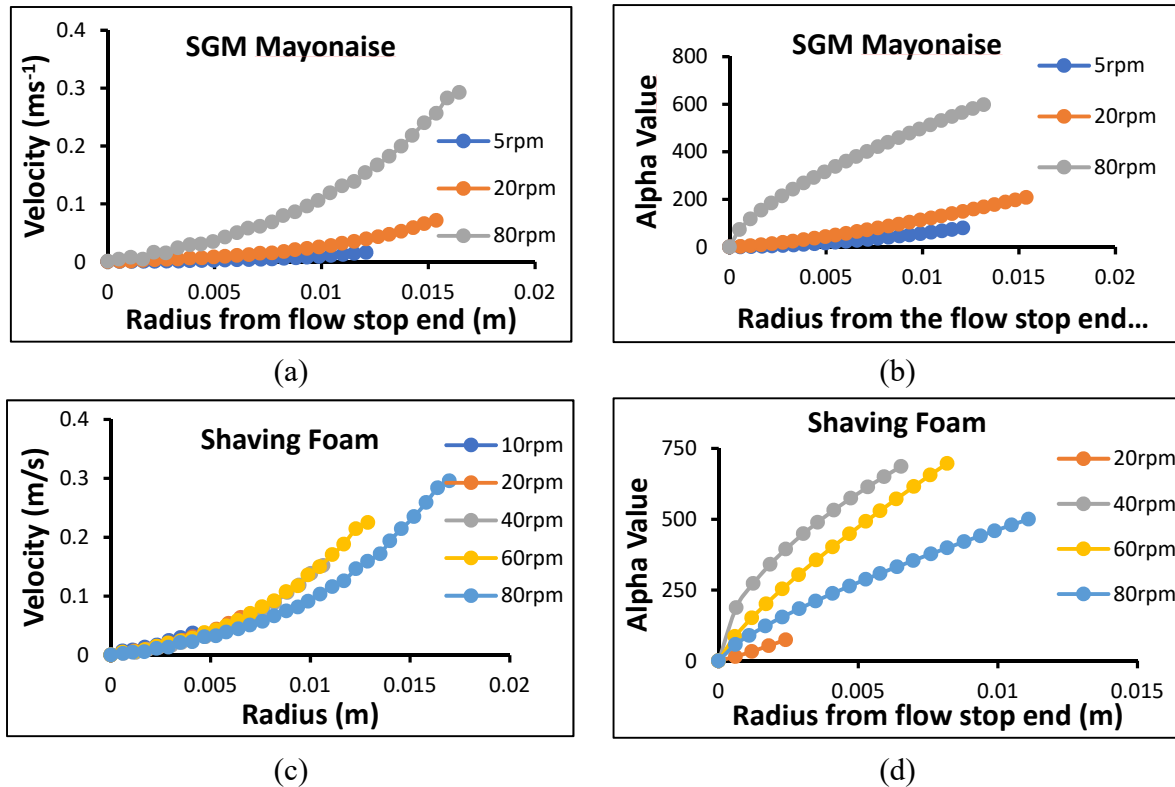


Fig. 6.3: Comparison of the shift in velocity profile and alpha value variation (a) PMMA upward shift of velocity profiles (b) PMMA increase of alpha value variation (c) Shaving Foam downward shift of velocity profile (d) Shaving Foam decrease of alpha value variation

and hence cubic equation is used for fitting the velocity profile and understanding the shear rate behavior. Alpha ( $\alpha$ ) value variation showed an increase in behavior with an increase in RPM value when there is an upward shift of the velocity profiles and decrease behavior with an increase in RPM value when the velocity profile is shifted downwards This is clearly shown in Fig. 6.3. We observe that the classification of the velocity profiles for the macroscopic behavior can be achieved based on the shift in the velocity profiles and the variation of material parameter alpha with respect to the increase in RPM value.

Results of the shift in the velocity profiles and the alpha value variation with respect to RPM value increase are tabulated in Table 6.1. For materials PMMA, Drilling Mud, Cornstarch 1, Silicon Oil Emulsion and Cacl<sub>2</sub> solution the velocity profiles shift upwards and the alpha value variation also increases majorly (“increases majorly” indicates that for most RPM values the trend is increasing) with an increase in the RPM value. Velocity profiles of materials like Bentonite, Surfactant, Cement Paste, and Shaving foam shift downwards, and the alpha value variation also decreases majorly with an increase in the RPM value. We clearly observe two distinct trends or behavior being followed by the materials. This distinct trend can be attributed to the macroscopic behavior

Table 6.1: Summary of the analysis of velocity profiles

S. No.	Material	RPM Value	Shift of velocity profiles	Variation of alpha	Quadratic or Cubic fit
1.	PMMA	Increase	Upward shift	Increase	Cubic
2.	Drilling Mud	Increase	Upward shift	Increase	Quadratic
3.	Mayonnaise	Increase	Upward shift	Increase	Cubic
4.	Silicon Oil Emulsion	Increase	Upward shift	Increase and decrease	Cubic
5.	Cacl <sub>2</sub>	Increase	Upward shift	Increase and decrease	Cubic
6.	Cornstarch 1	Increase	Overlapped (No shift)	Increase and decrease	Cubic
7.	Bentonite	Increase	Overlapped (No shift)	Decrease and increase	Cubic
8.	Cement Paste (CCR 2008)	Increase	Overlapped (No shift)	Decrease and increase	Quadratic
9.	Cement Paste (CCR 2005)	Increase	Overlapped (No shift)	Decreases	Quadratic
10.	Surfactant	Increase	Downward shift	Decreases	Quadratic
11.	Shaving Foam	Increase	Downward shift	Decreases	Cubic
12.	Cornstarch 2	Increase	Downward shift	Decreases	Cubic

of the materials usually described as pseudoplastic or dilatant materials. Currently, the shear rate attenuation mechanism, slip, and rotation of the particle behavior in the fluids due to the

application of shear force in Couette flow are understood by considering the cohesive between the particles. Slip behavior for emulsions as well as other complex fluids is mentioned by [8] along with the numerical models. These models assume the presence of an adsorbed layer on the solid surface and this layer is depleted causing the slip behavior.

### **6.2.1 Discussion of Macroscopic Material Behavior**

Non-Newtonian velocity profiles in the Couette flow are fitted by either quadratic or cubic equation. The slope of the velocity profile is shear rate and the double differential is shear rate attenuation. For quadratic equation, the double differential is constant hence the rotation rate of the fluid particles for these velocity profiles is constant irrespective of the applied shear rate. On the other hand, for the velocity profiles fit by using cubic equation, the double differential is a linear term. So, the rotation rate of the fluid particles is changed with respect to the applied RPM values. In both quadratic and cubic equations there is a parameter  $\beta$  which is the coefficient of the constant term. It represents the minimum shear stress to start the motion from the solid-like fluid in the steady static region.

The velocity profiles obtained from the past research are plotted from the flow stop end to understand characteristic behavior of the materials. These velocity profiles showed different behavior for different materials. Some of the materials have showed upward shift in the velocity profiles with respect to the applied RPM values while others depicted the downward shift of the velocity profiles with respect to the applied RPM values. Moreover, the  $\alpha$  value variation (quadratic equation parameter) for upward shift velocity profiles is increasing with increase in applied RPM values and decreasing with increase in RPM values for downward shift of velocity profiles. Some velocity profiles are perfectly overlapped irrespective of the applied RPM values. No upward or downward shift of the velocity profiles is observed. But in this case, the  $\alpha$  value variation is either decrease and increase or increase and decrease with respect to the applied RPM values. This difference in the behavior of the analysis results can be related to the macroscopic understanding of the materials. Upward, downward and overlapped velocity profiles can be categorized into three different macroscopic materials viz Pseudo-plastic, Dilatant and Bingham fluids, respectively.

Upward shift of the velocity profiles is the representative of Pseudo-Plastic behavior materials. Considering the proposed hypothesis, it can be viewed that, in these materials the ease of rotation of the particles is higher. Hence the viscosity of the material decreases with increase in the applied RPM values. When a shear force is applied on these materials, the frictional forces are increased but cohesive forces between the fluid particles are decreased at a rate higher than frictional forces. In contrast, downward shift of the velocity profiles is representative of Dilatant materials. The ease of rotation of the particles showing this kind of behavior is lower due to which the viscosity of the material increases with increase in the shear rate. When an increasing shear force is applied to these kinds of materials, the frictional forces increase is very much higher compared to the decrease in the cohesive forces between the particles.

Overlapped velocity profiles is a special case, in which there is not upward or downward shift of velocity profiles, but all of them perfectly overlap irrespective of the applied RPM. So, the ease of rotation of the fluid particles in these materials is also constant and the viscosity too. When an increasing shear rate is applied to these materials, the frictional force increases and cohesive force decreases. Both increase of frictional force and the decrease of cohesive force have balanced each other. So, these materials are considered as Bingham fluids having a yield stress required to start the flow of material.

### **6.3 Key findings of New Hypothesis**

#### **6.3.1 Improvements and Highlights of the Hypothesis**

The theory proposed by Kayondo et al (2017) mentioned about the presence of braking mechanism due to the air-water interface. In the current hypothesis, the validation of braking mechanism is achieved based on the consideration of the cohesive forces between the molecules and the rotation of the molecules. The braking effect is present only in hydrophilic microchannel surfaces with crevices due to which water flow rate reduction is observed. However, in hydrophobic channels, this type of braking mechanism is not observed as the hydrophobic surface and air-water interface behave similarly. Secondly, the presence of restrained molecules on the air-water interface was hypothesized but the mechanism involved in obtaining the restrained molecules is not clearly mentioned. The molecules around the air water interface are regarded to be solidified molecules, which are present in layers. This solidified molecular layer forms an anchorage layer around the crevice in the hydrophilic surfaces causing the braking mechanism.

#### **6.3.2 Major Contributions of the Hypothesis**

The major contributions of the hypothesis include

- a. Consideration of cohesive force between the fluid particles along with the frictional forces in the flow of fluids.
- b. Identifying the significance of very low shear rate region in Newtonian fluids in very narrow gaps.
- c. Distinguishing the macroscopic rheological material behavior based on the forces acting between the particles and interactions between them.
- d. Energy loss mechanisms occur not only due to the frictional losses between the layers but also due to the rotation of the particles within the layer itself.

### **6.4 Chapter Summary**

In this chapter, based on the proposed hypothesis, the mechanism of the water flow reduction in the hydrophilic microchannels is explained. The presence of anchorage around the crevice is responsible for the braking mechanism which leads to the water flow reduction. The nature of the cohesive force between the water molecules clarifies this kind of phenomena. But in hydrophobic channels this kind of anchorage is not present due to which slip behavior is observed in these microchannels. So, no water flow reduction is observed.

The analysis of velocity profiles clarifies that either quadratic or cubic equations are necessary to understand the shear rate attenuation behavior of the velocity profiles. The categorization of the velocity profiles is done based on the understanding of the analytical analysis. Further, the macroscopic behavior is established for various velocity profiles and the mechanism of the behavior of the materials is explained based on the current hypothesis. The analytical parameters of the theoretical non-linear equations used for understanding the velocity profiles is explained based on the ease of rotation of the fluid particles.

Overall, there are sufficient improvements in understanding the and visualizing the hypothesis. Foremost is the consideration of the cohesive forces also along with frictional forces between the fluid particles. Others include the rotation of the particles and the molecules behavior at different nature of surfaces.

## 6.5 References

- [1] C.-H. Choi, K. J. A. Westin, and K. S. Breuer, "To slip or not to slip-Water flows in hydrophilic and hydrophobic microchannels," *Proc. IMECE2002 ASME Int. Mech. Eng. Congr. Expo.*, pp. 557–564, 2002.
- [2] Y. Kurotani and H. Tanaka, "A novel physical mechanism of liquid flow slippage on a solid surface," 2020.
- [3] D. C. Tretheway, X. Liu, and C. D. Meinhart, "Analysis of Slip Flow in Microchannels," *Proceedings of 11th International Symposium on Applications of Laser Techniques to Fluid Mechanics*, no. 1, p. (pp. 8-11).
- [4] A. Sunarso, T. Yamamoto, and N. Mori, "Numerical analysis of wall slip effects on flow of newtonian and non-newtonian fluids in macro and micro contraction channels," *J. Fluids Eng. Trans. ASME*, vol. 129, no. 1, pp. 23–30, 2007, doi: 10.1115/1.2375127.
- [5] E. Schnell, "Slippage of Water over Nonwetable Surfaces," *J. Appl. Phys.*, vol. 27, no. 10, pp. 1149–1152, 1956, doi: 10.1063/1.1722220.
- [6] C.-H. Choi, K. J. A. Westin, and K. S. Breuer, "Apparent slip flows in hydrophilic and hydrophobic microchannels," *Phys. Fluids*, vol. 15(10), no. April 2003, pp. 2897–2902, 2003, doi: 10.1063/1.1605425.
- [7] J. Israelachvili, *Intermolecular and Surface Forces*. 2011.
- [8] T. Sochi, "Slip at fluid-solid interface," *Polym. Rev.*, vol. 51, no. 4, pp. 309–340, 2011, doi: 10.1080/15583724.2011.615961.

**Chapter 7. CONCLUSIONS AND FUTURE  
RECOMMENDATIONS**

To understand the mechanism of the shear flow of fluid, different phenomena have been considered. The first one is water flow in microchannels in the presence of crevices or surface deformations. The second phenomenon is the Couette flow of suspensions or slurries in the gaps of concentric cylinders. Individually, both the phenomena are studied to understand the behavior of fluid in each case. Experimentally, water flow reduction in the microchannels due to the presence of crevices is known. Analytically, the shear rate reduction along with velocity profile behavior in the Couette flow is understood. The conclusions of each phenomenon are summarized below.

### **7.1 Conclusions of Water Flow Tests**

Water flow tests have been conducted using different types of microchannels. Different results obtained based on the type of microchannel and the surface used are given below.

- a. Water flow reduction is observed in the hydrophilic surface of microchannels when equilibrated water ( $DO > 95\%$ ) is used because of the decrease in the bubble area due to which there is an increase in the drag force in the microchannel and decrease of slip behavior too. Drag force and slip behavior have a substantial effect on the water flow rate, especially in microchannels.
- b. The water flow rate decrease is dependent on the number of crevices present. Higher water flow reduction is present in the microchannel with a larger number of crevices and lesser water flow reduction in the microchannel with fewer crevices. However, very less water flow reduction or negligible reduction is observed in the microchannel with no crevices.
- c. A quantitative understanding of the water flow tests is visualized by wide microchannels. Water flow reduction in hydrophilic channels is observed to cause due to the reduction in the bubble area. A higher reduction is achieved when there is a higher reduction in the area of the bubble. In hydrophobic cases, water flow reduction was observed only when there is a larger increase in the area of the bubble obstructing the flow path of the water.
- d. In hydrophobic channels, the water molecules at the surface behave differently compared to the bulk water molecules. In the bulk water molecules, cohesive forces between the molecules are isotropic but at the surface, this nature of cohesive is lost. The behavior of the air-water interface and the hydrophobic surface are similar due to which the molecules form a continuous sheet of layer causing the slip behavior. So, no reduction in the water flow is observed in the hydrophobic microchannels.
- e. In hydrophilic microchannels, the molecules at the surface are like the bulk water molecules due to the isotropic nature of the cohesive force between the particles. But when an air bubble is present due to the crevice the water molecules surrounding it behave like the molecules at the hydrophobic surface. In this case, these kinds of molecules form an anchorage around the crevice portion causing the braking mechanism and eventually reducing the water flow rate.

### **7.2 Conclusions of Analytical Analysis of Velocity Profiles**

Analytical analysis of the velocity profiles in Couette flow by differentiating Newtonian and Non-Newtonian regions clarified the shear rate as well as the velocity behavior of each material. The conclusions of the analysis are given below.



- a. Velocity profile plotted from the rotor end does not show any regularity in the flow behavior but when these profiles are plotted from the flow stop end (radius at which the velocity is 0 and it is considered as a starting point for velocity calculation). These velocity profiles showed the same rate of decrease in the shear rate irrespective of the RPM applied for each specific material.
- b. Non-linear velocity profiles are either fit by theoretical quadratic or cubic equations by considering the variation of the material parameter alpha ( $\alpha$ ).
- c. Classification of the macroscopic behavior of the materials based on the analysis is done by considering two different criteria.
  - i. The shift of the velocity profile just before the subsequent RPM applied velocity profile reaches the outer end of the radius.
  - ii. Variation of the material parameter alpha ( $\alpha$ ) with respect to the applied RPM.
- d. If the shift in of the velocity profile is upwards and the alpha value variation is increasing with respect to the increase in applied RPM, the macroscopic behavior is considered as Pseudoplastic and dilatant if the shift in velocity profile is downward and there is a decrease in the alpha value variation with respect to the applied RPM. The velocity profiles in which there is no either upward shift or downward shift, i.e., perfectly overlapped velocity profiles are regarded as Bingham fluid having a certain yield stress value.
- e. In Pseudoplastic materials, the ease of rotation of the particles is difficult due to which there is a decrease in the viscosity as shear rate increases. When a shear rate is applied to these materials, the increase in the frictional force is lesser than the decrease of the cohesive force between the particles.
- f. In Dilatant materials, the ease of rotation of the particles is easier due to which there is an increase in the viscosity as shear rate increases. When a shear rate is applied to these materials, the increase in the frictional force is much higher than the decrease of the cohesive force between the particles.
- g. In Bingham fluid materials, the ease of rotation of the particles is constant irrespective of the shear rate applied as such a constant viscosity is observed. When a shear rate is applied to these materials, the increase of frictional force and decrease of the cohesive force between the particles have balanced each other.
- h. In the Non-Newtonian region, the rotation of the particles seems to take place due to a stronger cohesive force between the particles. Rotation of the particles is an important characteristic of Non-Newtonian materials.

### 7.3 Future Recommendations

Based on the water flow tests conducted and the analytical analysis performed to understand the shear rate attenuation behavior in Couette flow following recommendations can be stated

- The effects of various other different parameters like the height of microchannel, the diameter of the crevice on the water flow rate can be investigated quantitatively.
- The consideration of the classification of materials may be identified by conducting the experiments of viscometer using two different types of materials (pseudoplastic and dilatant).

- The practical application of the findings has not been deeply investigated in this research. The pressure-driven flows, in the microchannel, can be emulated to the flow in micro-cracks of concrete surface. The nature of the surface considered in this research affects the water flow rate due to the slip behavior at the interface.
- The mechanism of water flow reduction in pressure-driven flows and shear rate attenuation in shear driven Couette flows is understood by the common understanding of the rotation of particles and cohesive force between the particles. The hypothesis used in this research is strengthened by the previous literature but the consideration of rotation of particle/molecule is to be examined in fluid flow.
- The proposed hypothesis can be useful in understanding the stagnation phenomena of water inside the narrow gaps of concrete pores. Most interesting applications are related to the transport and storage of materials including powders and suspensions. Finally, the hypothesis can be used in microfluidics where one of the boundaries is exposed to air.